5-8-2019 10:30 AM

A comparison of different carrier media for biofilm formation and performance in aerobic inverse fluidized bed bioreactor

Haoran Xu, *The University of Western Ontario*

Supervisor: Zhu, Jingxu, *The University of Western Ontario*
: Nakhla, George, *The University of Western Ontario*
A thesis submitted in partial fulfillment of the requirements for the Master of Engineering Science degree in Chemical and Biochemical Engineering

Follow this and additional works at: https://ir.lib.uwo.ca/etd

Recommended Citation

Abstract

In three parallel aerobic inverse fluidized bed bioreactors (AFBBR), the attachment rate and biofilm quantity during the startup stage and the biofilm characteristics and nutrient removal efficiency at steady-state were analyzed to evaluate the characteristics of three different particle carriers, polyethylene (PE), polypropylene (PP) and activated carbon-coated polyethylene (PEC) under various operating conditions. In addition, the effects of other factors, such as hydraulic retention time (HRT) and carbon-nitrogen (C/N) ratio were also tested to optimize the startup method and to accelerate the biofilm attachment process for the particles. The results showed that under a favourable startup condition of 4h HRT and 300 mg/L influent COD, PE had reached the best attachment in 14 days and PEC came in second, using 20 days, whereas PP failed to achieve attachment due to serious shear force. The peak attached biomass were 9.4 mg VSS/g media for PE and 10.7 mg VSS/g media for PEC respectively. Additionally, PEC had the lowest suspended biomass fraction and detachment rate.

Keywords

Aerobic inverse fluidized bed bioreactor, Carrier particles, Attached biomass.

Acknowledgments

I would like to express my gratitude to my supervisors Dr. Zhu and Dr. Nakhla for their guidance through whole research and support including providing experimental equipment and reagents. Besides, I have to thank Michael Nelson who helped me a lot on thesis work.

I also want to thank my parents Fei Xu and Min Xu, for their encouragement and perpetual support. Besides, I have to say thanks to my girlfriend, Lu Chen for taking care of me for a long period.

Thank you,

Haoran

Table of Contents

List of Tables

List of Figures

List of Appendices

Chapter 1

1 Introduction and literature review

1.1 Background

Since ancient times, water quality for daily consumption is found to be at the crux of urban population development. Accessing high quality water corresponds to the health and success of a civilization. The importance of developed sanitation was initially realized by modern cities in the nineteenth century due to its strong correlation with public health. With industrial developments and population increase, untreated wastewater significantly changed from a single source of daily municipal wastewater, which can be treated using more passive treatment methods, to multi-source wastewater which has more complex constituents and has to be treated using engineered processes to meet health requirements. During the transformation process of wastewater characteristics, pollutants detection and analyzation methods were improved. There has been increasing concerns of water quality from the public as well. The motivation of developing new techniques was stemmed from urgent requirements of solving health related issues caused by polluted water. There are several stages in the enrichment of wastewater treatment processes (Figure 1.1).

Urban wastewater generally refers to a mixture of municipal wastewater, industrial wastewater and storm runoff. Their properties differ based on city scale, industry category and scale, climate factors and sanitation system (Yu et al., 2004). The largest proportion of pollution is organic pollutants. Exceeding COD discharge limits, containing a lot undegradable organics and toxic organics are typical of organic wastewaters. In addition to organic contaminants, nitrogen and phosphorus in the wastewater effluent could cause eutrophication.

Traditionally, there are three kinds of treatment processes: physical, chemical and biological processes. The main objective of physical processes is removing insoluble suspended substances, while chemical processes make soluble pollutants sedimented or nontoxic. Toxic materials could restrict normal cellular activities and poison cells to

destroy the cellular biological structure, such as enzyme protein denaturation. Heavy metals, such as As, Pb, Cr, Cd and Cu, are commonly found as toxic materials in industial wastewaters. Physical processes are typically used as pre-treatment with the help of flocculants or gravity. For biological processes, microorganisms are acclimated and fed under certain circumstances to oxidize or decompose soluble organic pollutants and remove nitrogen and phosphorous. Next, a bacteria floc adsorbs suspended pollutants and then is separated using physical processes (Yu et al., 2004). Generally, nitrogen and phosphorus removal processes are combined with COD removal processes.
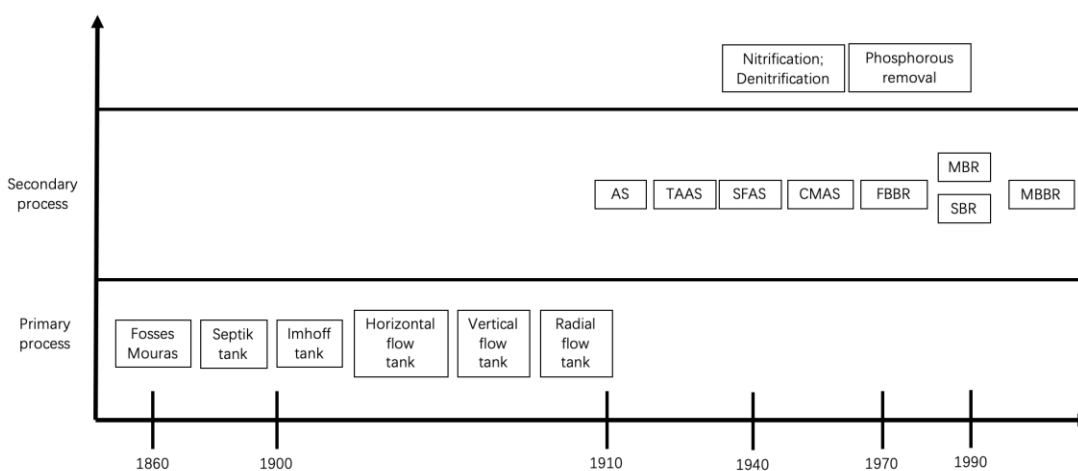
Figure 1.1 Evolution of wastewater treatment. AS - Activated sludge; TAAS - Tapered aerobic activated sludge; SFAS - Step-feed activated sludge; CMAS - Completely mixed activated sludge; FBBR - Fluidized bed biofilm reactors; MBR - Membrane biological reactors; SBR - Sequencing batch reactors; MBBR - Moving bed biofilm reactors (Lofrano & Brown, 2010).

Primary treatment is also considered as preliminary treatment which is usually placed ahead of major treatment processes (secondary process), using physical methods to remove insoluble solids to avoid clogging and decrease unnecessarily high organic loadings on downstream processes. Initially, trenches and pits were basic forms of primary treatment processes. In 1860, the Fosses Mouras was designed by L.H. Mouras as a prototype of a modern sedimentation tank (Lofrano & Brown, 2010). In 1895, Donald Cameron retrofitted the Fosses Mouras, creating the septic tank (Lofrano & Brown, 2010). Karl Imhoff designed the Imhoff tank which is similar to present

sedimentation tanks (Lofrano & Brown, 2010). At present, various primary processes exist, such as sedimentation tanks, rotating belt filters and rotary drum filters.

Because primary processes cannot meet secondary requirements, secondary processes were created to further treat wastewater. Based on different growth forms, biological processes are divided into the suspended growth process, attached growth process and hybrid process.

Since Arden and Lockett created the activated sludge process (AS) in 1914, AS has been researched and developed using aeration methods, operational conditions and reactor structures. Through 100 years of development, the activated sludge process has become a world-wide used process. However, the disadvantages of the activated sludge process, such as huge footprints, large amount of excess sludge and low organic loading, has yet to be solved.

The basic principle for attached growth processes is similar to suspended growth processes, which utilizes microorganisms for treatment. Specifically, for the attached growth process, pollutants are transported into a biofilm, grown on a carrier media by mass transfer and are oxidized to be purified. Prominent advantages of the attached process include higher nitrogen removal efficiency, higher treatment capability due to high biomass concentrations, less excess sludge, convenient operation without return sludge and greater stability under dynamic volumetric loadings. In the 1960s, new synthetic materials were developed to drive the progress of attached biofilm processes. Then in the 1970s, fluidized beds were introduced in wastewater treatment to enhance liquid solid mass transfer (Yu et al., 2004). In recent years, biofilm reactors have received attention from researchers and engineers because of unique advantages. Furthermore, many new reactors emerged, including the membrane biofilm reactor (MBR) (Zhang et al., 2017), airlift biofilm reactor (Tijhuis et al., 1994), moving bed biofilm reactor (MBBR) (Leyva-Díaz et al., 2017), hybrid activated sludge biofilm reactor (Gebara, 1999), sequencing batch biofilm reactor (Jiang et al., 2016), biological aerated filter (Ahmed et al., 2012) and various forms of fluidized bed bioreactors (Lu et al., 2015).

1.2 Attached growth processes

Immobilized biomass processes provide a solution for overcoming the problems happening in activated sludge processes, such as high biomass production, short sludge age and space requirement for treatment plants (Tijhuis et al., 1994). Meanwhile, short sludge age causes the limitation of slowly growing species, such as nitrifiers. As a result of high biomass concentration, low biomass production, short hydraulic retention time and operation stability are main features of the attached growth processes.

Airlift biofilm reactor

The airlift bioreactor could be considered to be a special version of the fluidized bed bioreactor, because the basic principle for both is fluidizing particles in columns. But for the airlift bioreactor, there is an internal loop tube inside the column for the upflow liquid which is dragged by the gas. The gas escapes from the top of the inner tube, and liquid will spill from the top with speed as well. The pushed liquid carries bioparticles in the downcomer so that bioparticles begin to fluidize in the column (Tijhuis et al., 1994). The design of the internal loop tube has an advantage of that bioparticles are easily fluidized in a certain region. Therefore, the phenomenon of bioparticles washout rarely occurs, even under high liquid velocity. Furthermore, due to the gas only existing in the internal loop tube, bioparticles suffer from low gas shear force and biofilm is protected from detachment.
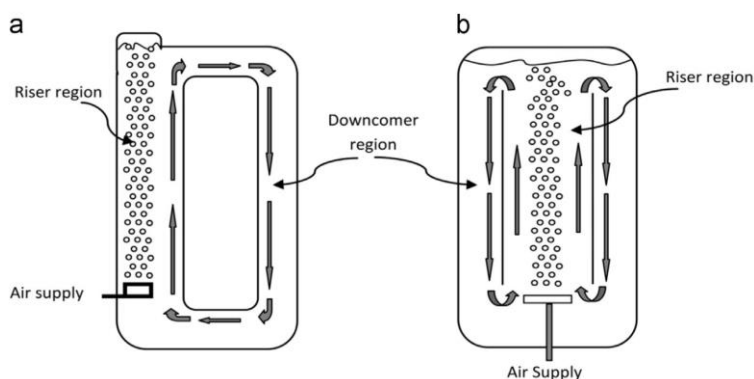
Figure 1.2 Schematic of airlift bioreactor with (a) external recirculation and (b) internal recirculation (AL-Mashhadani et al., 2015).

Moving bed biofilm reactor

Support media in the moving bed bioreactor is quite different from the carriers in fluidization and air lift bioreactors, which has an unique three-dimensional structure, cylindrical with external fins, in constrast to the spherical particles. The MBBR support media has a larger specific surface area and its structure could shelter the growing biofilm inside from abrasion. Support mediums are agitated by gas flow or being mechanically stirred. Although the support media movement within the bed bioreactor is less turbulent than the movement within the fluidized bed bioreactor, slow movement is still necessary to improve mass transfer. Using the moving bed bioreactor as an attached biomass process has advantages such as high biomass concentration, high organic loading, strong tolerance for dynamic loading and occupies a smaller area. Sludge is stable without sludge bulking, and long sludge age leads to low sludge production. The whole system operates easily with low head loss and without frequent backwash (Barwal & Chaudhary, 2014). Support carriers subsist under a stable circumstance. This causes a large amount of biomass to be resistant to high loading and hydraulic shocks. Additionally, when biofilm extends to a level high of thickness, different biofilm layers could appear, an aerobic outer layer and anoxic/anaerobic inner layer, based on the dissolved oxygen concentration. This means reactions that normally happen in different conditions, such as nitrification and denitrification, could take place simultaneously in same column.
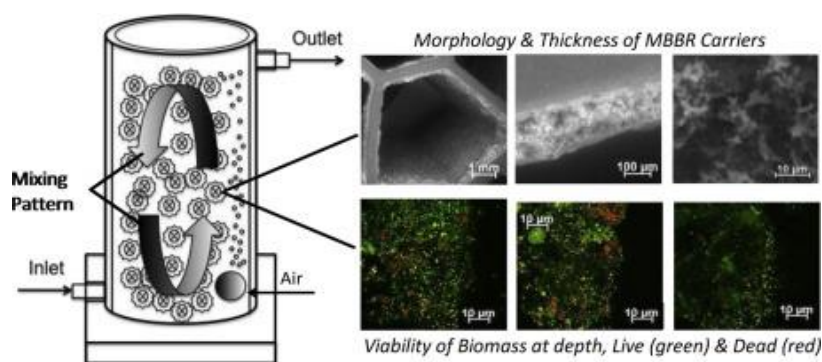
Figure 1.3 Schematic of moving bed bioreactor (Hoang et al., 2014).

Circulating fluidized bed bioreactor (CFBBR)

A typical circulating fluidized bed bioreactor consists of two relatively independent columns, a downer and a riser. The name of the column reflects the bioparticles movement direction. Based on different functions, there is an aerobic column and an anoxic column. Circulating fluidized beds have several advantages, such as improved interphase contact efficiency and significantly enhanced mass and heat transfer (Zhu et al., 2000). Therefore, temperature and substance concentrations will be homogenous to provide a stable environment for microorganisms. In addition to the typical circulating form, a twin circulating fluidized bed is also tested as a novel fluidized bed bioreactor (Andalib et al., 2010; Nelson et al., 2017).

When compared with the circulating fluidized bed bioreactor, the bed expansion direction for the inverse fluidized bed bioreactor (FBBR) is opposite. Basically, expansion direction is the result of particle densities. For heavy particles (generally particle densities heavier than water), gas flow is not sufficient to fluidize them completely, as there are always dead zones where particles agglomerate together. Therefore, circulating liquid at certain recycle ratios is used to fluidize particles. For light particles (less dense than water), upflow gas fluidizes those particles and the expansion direction of light particles is opposite of heavy particles. Though system configuration differences exist, the inverse fluidized bed bioreactor possesses similar advantages, homogenous conditions and high mass and heat transfer efficiency. Meanwhile, the IFBBR also possesses the same advantages as an attached biomass process, including high biomass concentration, low biomass production and short hydraulic retention time (Sokół & Korpal, 2006; Sokół et al., 2009).
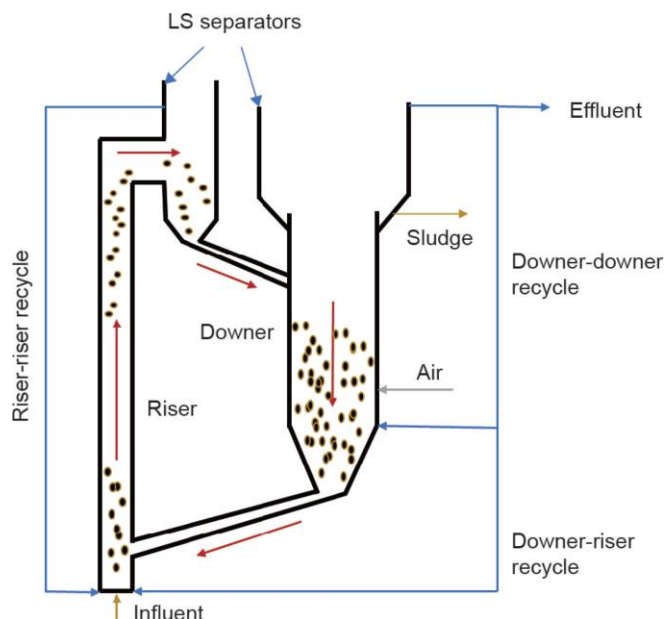
Figure 1.4 Schematic of circulating fluidized bed bioreactor (Nelson et al., 2017).

1.3   Biofilm

1.3.1   Background

Wastewater treatment plays an important role in protecting the ecosystem and water resource. Biofilm processes are well suited to degrade pollutants, such as organics and toxic elements. In addition, biofilm also acts as a producer in microbial food chains (Anderson-Glena et al., 2008). It also contributes to nature carbon and nutrient cycles (Davey and O'Toole, 2000) and immobilizing energy in organics through photosynthetic activity (Underwood et al., 2005). In wastewater treatment, the functions of biodegradation and bioremediation are utilized to remove pollutants.

The definition for biofilm is changeable based on biofilm structures, surrounding conditions and microorganism composition. The definition which is commonly accepted is that microorganisms are in the form of multicellular aggregates on the support media surface. Various microorganisms could take up substrates, grow and multiply with help of extracellular enzymes inside the polymer matrix (Golladay and Sin-sabaugh, 1991). Polymer matrix is composed of polysaccharides which provide mechanical support and

build a polymer network which could fix and interconnect biofilm cells (Wingender and Flemming, 2011; Decho, 2000; Gerbersdorf et al., 2008). The polymer matrix, acting as a barrier could protect internal contents from toxic material and physical penetration.

As biofilm structure research continuously advances, new discoveries, such as biofilm structure inhomogeneities, enrich original biofilm structure theory and new models are presented as well. Biofilm structure is influenced by microorganism categories, growth surface, liquid flow, system structure and biofilm sloughing (Gjaltema et al., 1994). Furthermore, there are cavities, void and channels existing in both aerobic and anaerobic biofilm (de Beer et al., 1994). Hence, directions of mass transfer in biofilm should not be confined to the direction perpendicular to the carrier surface only. With the development of scanning microscope, parameters which describe the biofilm structure could be measured. Textual entropy, areal porosity, fractal dimension and maximum diffusion distance were measured through experiments (Jackson et al., 2001). All these parameters could contribute greatly to building novel models, such as the cluster model (Bishop, 1997).

The target pollutants of wastewater treatment processes depend on the metabolic functions of different microbes. Hence, attaining detailed information about fraction, categories and specific functions of the microorganism community is quite valuable. In recent years, molecular technologies, such as clone library, microarray and polymerase chain reaction were widely used for microorganism community analyzation (Noble et al., 2016; Naz et al., 2018).

1.3.2   Basic growth principles

Biofilm development

In general, there are five stages of biofilm development, initial attachment, extracellular polymeric substances (EPS) enhanced attachment, early biofilm architecture, mature biofilm architecture and cells dispersion (Stoodley et al., 2002).
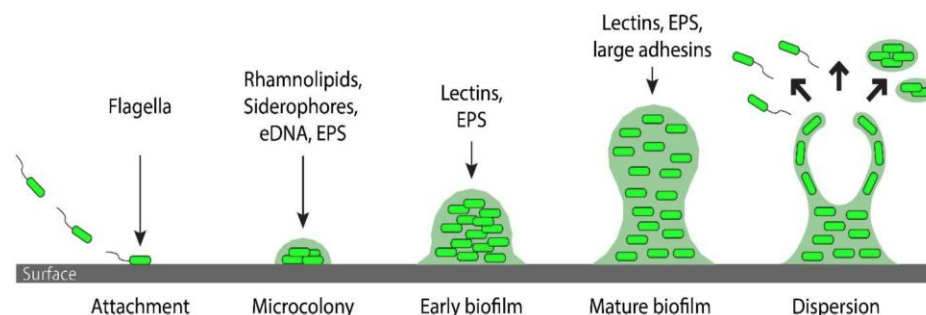
Figure 1.5 Five stages for biofilm development (Passos da Silva et al., 2017).

Initial attachment

In this stage, microorganisms utilize extracellular accessories, such as flagella, fimbriae, pili and extracellular membrane protein to detect the existence of a possible surface for attachment (Thomas et al., 2004), and those structures could help the initial attaching of microorganisms onto surfaces.

EPS enhanced attachment

Microorganisms start to secrete EPS to enhance the attachment between microorganisms and attached surfaces. Attachment with EPS becomes irreversible and EPS become a skeletal frame to support the biofilm structure.

Early biofilm architecture

In this stage, microorganisms begin to reproduce, becoming bacterial colonies and secrete more EPS to reinforce the biofilm structure. Based on research, quorum sensing plays an important role in early biofilm formation, because it can adjust and control the microbial community's growth, attachment and migration (Klausen et al., 2006).

Mature biofilm architecture

Early biofilm develops with microorganisms reproducing persistently to become a mature biofilm with a complete three-dimensional structure (Stoodley et al., 2002). In addition, a mature biofilm could provide necessary structural support and assistance to microorganisms to grow and metabolize (Stewart, 2002).

Cells dispersion

Aging biofilm splits gradually and microorganisms living in the biofilm begin to disperse from the decomposed biofilm. After microorganisms leave the original biofilm, they will search for new possible surfaces and attach to form a new biofilm.

1.3.3 Aerobic biodegradation

Aerobic biological oxidation treatment

Aerobic biological oxidation is the process by which aerobic microorganisms utilize oxygen to metabolize organic pollutants. Organic pollutants are oxidized to harmless inorganic small molecules, such as H_2O and CO_2, and energy is released. Processes for aerobic oxidation are described in Figure 1.6. After being absorbed, typically, one third of organics will be decomposed to provide energy for life activities and two third of organics are utilized for synthesizing cells themselves (Gao, 1999). The reaction rate for aerobic oxidization is high. Therefore, aerobic biological oxidation is an effective and environmentally friendly method for the removal of organics from wastewater.

$$3C_6H_{12}O_6 + 8O_2 + 2NH_3 \rightarrow 2C_5H_7NO_2 + 8CO_2 + 14H_2O + energy \qquad (1)$$
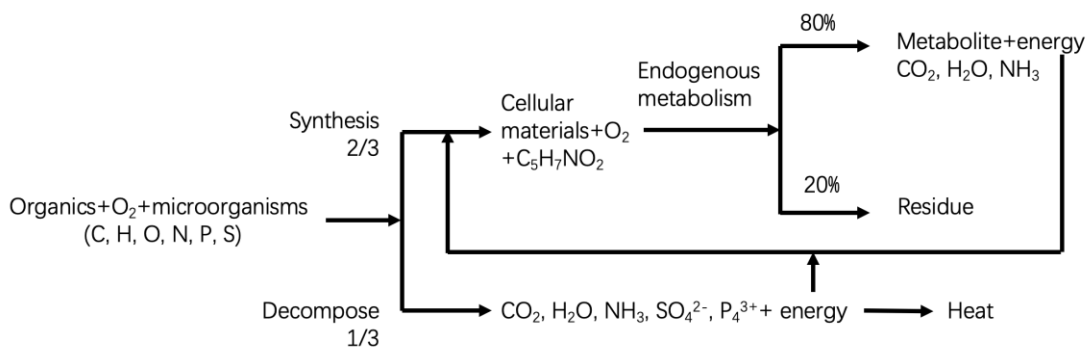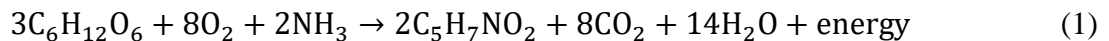
Figure 1.6 Organics transformation of aerobic metabolism (Gao, 1999).

Nitrogen removal

NH_4-N is removed using nitrification, in that ammonia is oxidized to NO_X with oxygen. Based on the reaction equations shown below (Tchobanoglous et al., 2014), for nitrification, 4.57g O_2 (2×32/14 g) are consumed to oxidized one gram of NH_4^+-N to NO_3^--N and 7.14g alkalinity as $CaCO_3$ (100/14 g) are consumed for one gram of NH_4^+-N to NO_3^--N. Similarly, NO_X-N is removed through denitrification, in which nitrate and nitrite are reduced to nitrogen using COD. Electron acceptor in denitrification is NO_X, versus oxygen in the nitrification process. In the denitrification reaction, 3.57g alkalinity is recovered for both one gram of NO_3^--N or NO_2^--N to N_2.

$$NH_4^+ + 2HCO_3^- + 2O_2 \rightarrow NO_3^- + 2CO_2 + 3H_2O \tag{2}$$

$$5CH_3COOH + 8NO_3^- \rightarrow 4N_2 + 10CO_2 + 6H_2O + 8OH^- \tag{3}$$

$$3CH_3COOH + 8NO_2^- \rightarrow 4N_2 + 6CO_2 + 2H_2O + 8OH^- \tag{4}$$
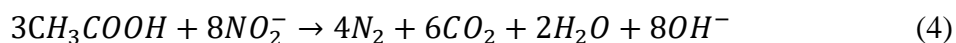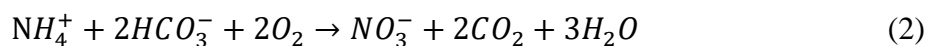
In addition to nitrification and denitrification, assimilation also removes nitrogen from wastewater. Removed nitrogen is used to synthesize cells and collected in the form of effluent biomass.

Enhanced biological phosphorous removal

The basic principal for biological phosphorous removal is that phosphorus accumulating organisms release phosphorous in an anaerobic condition and excessively absorb phosphorous in an aerobic condition. Phosphorus accumulating organisms take oxygen as an electron accepter to oxidize poly-b-hydroxybutyrate (PHB) and polyhydroxyvalerate (PHV) to produce energy which is stored in the ATP and used to form polyphosphate bonds. (Gao, 1999; Tchobanoglous et al., 2014) Finally, biomass with high phosphorous concentrations will be removed as waste sludge.

1.3.4   Suspended growth kinetics

Organics in wastewater are recognized as pollutants but they are also basic nutrients for biomass growth. The substrate utilization rate which is derived from the Monod equation, reflects the ability of biomass to remove organic substances. When the biomass concentration is constant, the substrate utilization rate will rise with the substrate concentration increase in the solution.

$$r_{su} = \frac{kXS}{K_s + S} \tag{5}$$

r_{su} = substrate utilization rate per unit of reactor volume, $g/m^3 \cdot d$

k = maximum specific substrate utilization rate, g substrate/g microorganisms$\cdot$d

X = biomass (microorganism) concentration, g/m^3

S = growth-limiting substrate concentration in the solution, g/m^3

K_s = half-velocity constant, substrate concentration at one-half the maximum specific substrate utilization rate, g/m^3

After taking in nutrients from the wastewater, microorganisms will grow with time. The equation of the substrate utilization rate could be transformed to describe bacteria growth rate.

$$r_g = \frac{\mu_m XS}{K_s + S} \tag{6}$$

r_g = bacteria growth rate from substrate utilization, $g/m^3 \cdot d$

μ_m = maximum specific bacteria growth rate, g biomass/g biomass$\cdot$d

Combined with Eq. 5 and Eq. 6, bacteria absorbs nutrients to synthesize biomass and multiply. Therefore, the synthesis yield coefficient, which is also called true yield, is equal to the bacteria growth rate divided by the substrate utilization rate. From Eq. 5, Eq. 6 and Eq. 7, there is a relation between the maximum specific bacteria growth rate and maximum specific substrate utilization rate.

$$r_g = Y r_{su} \qquad (7)$$

Y = synthesis yield coefficient, g biomass/g substrate used

$$\mu_m = Y k \qquad (8)$$

Net biomass growth rate is that bacteria growth rate minus decay rate of endogenous respiration.

$$r_X = Y r_{su} - bX \qquad (9)$$

r_X = net biomass growth rate per unit reactor volume, g VSS/m^3·d

b = specific endogenous decay coefficient, g VSS/g VSS·d

Total VSS production rate consists of three parts, net biomass growth rate, rate of cell debris production and nondegradable influent biomass. Rate of cell debris production comes from non-biodegradable parts of dead microorganisms. After dead cells lysis, 10% to 15% of the weight of those cells can not be reused by other cells, such as the cell wall (Tchobanoglous et al., 2014), and those parts will keep existing in the solution. In this case, influent is the synthetic wastewater and the third part should be neglected.

$$r_{X_T,VSS} = Y r_{su} - bX + f_d(b)X + Q X_{o,i}/V \qquad (10)$$

$r_{X_T,VSS}$ = total VSS production rate, g/m^3·d

Q = influent flowrate, m^3/d

$X_{o,i}$ = influent nbVSS concentration, g/m^3

f_d = fraction of biomass that remains as cell debris, 0.10 – 0.15 g VSS/g biomass VSS depleted by decay

V = volume of reactor, m^3

1.3.5   Biofilm kinetics

The biofilm structure influences the microbial kinetics inside the biofilm (Bishop, 1997). For most biofilm kinetics models, their basic hypothesis is that biofilm is

homogeneous and continuous, so substrates concentration difference only exists in the direction which is vertical to the carrier surface in a mix-culture biofilm (Bishop, 1997). Based on that assumption, substrate utilization rate in biofilm is described using Eq. 11 which is also derived from the Monod equation: (Rittmann et al., 1980)

$$\left(\frac{\partial S_f}{\partial t}\right)_{rx} = -\frac{kX_f S_f}{K_s + S_f} \tag{11}$$

X_f = cell density

S_f = the rate-limiting substrate concentration in the biofilm

K_s = the half-velocity coefficient

k = the maximum specific rate of substrate utilization

t = time

Molecular diffusion as the only transport method in biofilm is describe as Eq. 12 which is based on Fick's law: (Rittmann et al., 1980)

$$\left(\frac{\partial S_f}{\partial t}\right)_{diff} = D_f \frac{\partial^2 S_f}{\partial z^2} \tag{12}$$

D_f = the molecular diffusivity of the substrate in the biofilm

z = diffusion position at z direction

Therefore, combing Eq. 11 and Eq. 12, substrate utilization rate could be written as Eq.13:

$$\frac{kX_f S_f}{K_s + S_f} = D_f \frac{\partial^2 S_f}{\partial z^2} \tag{13}$$

Similar to activated sludge kinetics, net growth rate was described as Eq. 14: (Rittmann et al., 1980; Herbert et al., 1956)

$$\frac{\partial AS_f dz}{\partial t} = Y \frac{AX_f kS_f dz}{K_s + S_f} - bAX_f dz \tag{14}$$

Y = the true yield

b = the specific decay coefficient

A = the cross-sectional area of the biofilm section

dz = the thickness of the biofilm section

Except for the above typical kinetic model, there are other models such as the Capdeville biofilm growth kinetics model (Capdeville & Nguyen, 1990) and cellular automaton model (Colasanti, 1992). The Capdeville kinetic model uses the Logistic equation to describe the accumulation of active bacteria and showed the interaction between M_a, M_i, M_b. Furthermore, this model could calculate the exponential growth rate, the accumulation rate and the maximum quantity of active bacteria (Capdeville & Nguyen, 1990).

$$M_b = M_a + M_i \tag{15}$$

M_a = active bacteria

M_i = inert bacteria

M_b = total biofilm dry matter

1.3.6 True yield

The value of the observed yield could be attained by total the VSS production rate divided by the substrate utilization rate. Observed yield under a steady state could be written as Eq. 16.

$$Y_{obs} = r_{X_T,VSS}/r_{su} \tag{16}$$

Y_{obs} = observed yield, g VSS produced/g substrate removed

$$Y_{obs} = \frac{Y}{1+b(SRT)} + \frac{f_d(b)(Y)SRT}{1+b(SRT)} + \frac{X_{o,i}}{S_0-S} \tag{17}$$

Though all above equations were claimed to describe biomass growth kinetics for many years, the value of true yield was not yet ascertained. 0.42 mg VSS/mg COD was mentioned in 1965 by McCarty and the typical value given in Table 1.1 is 0.45 mg VSS/mg COD with a range from 0.4 to 0.6 mg VSS/mg COD. Additionally, different carbon and nitrogen sources could cause diversity of the true yield value. According to the expanded thermodynamic true yield prediction model, the estimated true yield value with acetate as a carbon source, ammonia as a nitrogen source at pH 7, is 0.446 mol-C cells($C_5H_7O_2N$) /mol-C acetate, compared with the average experimental value 0.420 mol-C cells($C_5H_7O_2N$) /mol-C acetate (Xiao & VanBriesen, 2008). The average experimental value was obtained from an average of 0.406, 0.456, 0.41, 0.44, 0.389, 0.471 and 0.368 (Rutger, 1990; Verduyn et al., 1991; Heijnen & Van Dijken, 1992; Andrews, 1993; Linton & Stephenson, 1978; Birou et al., 1987; von Stockar & Liu, 1999). Comprehensively considering the model prediction value and experimental value, the average of these two values which is 0.433 mol-C cells($C_5H_7O_2N$) /mol-C acetate. After unit conversion (0.433×22.6/32), true yield is 0.31 mg VSS/mg COD.

Table 1.1 Typical kinetic coefficients for the activated sludge process for the removal of BOD from domestic wastewater for T = 20°C (Tchobanoglous et al., 2014).

Coefficient	Unit	Value range	Typical value
K	g bsCOD/g VSS·d	4 ~ 12	6
K_s	mg/L bsCOD	5 ~ 30	15
Y	mg VSS/mg COD	0.4 ~ 0.6	0.45
b	g VSS/g VSS·d	0.06 ~ 0.15	0.10

1.4   Support media

1.4.1   Background

For the fluidized bed bioreactor, the characteristics of support particles could significantly affect the performance of reactors. In essence, the following types of cell immobilization were applied: (Schügerl, 1997)

1. Attachment of microorganisms onto the surface of support carriers as a form of biofilm.

2. Colonization of microorganisms in porous carriers.

3. Immobilization in hydrogel or pellet for microorganism cultivation.

The advantages and disadvantages of these categories are listed in Table 1.2.
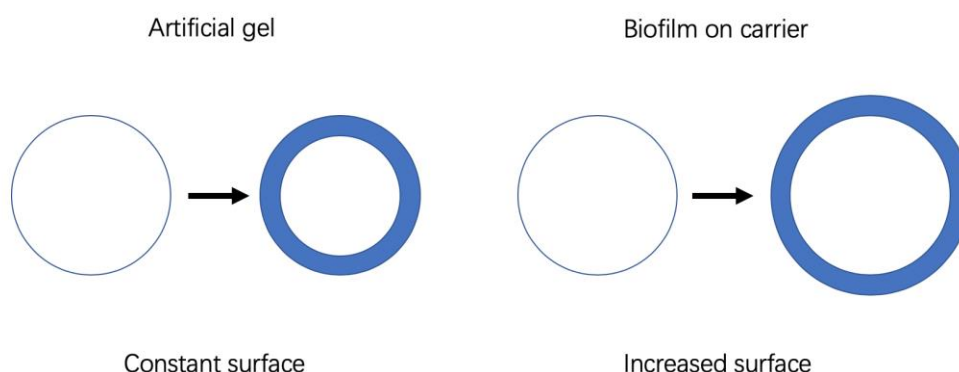
Figure 1.7 Attachment methods for biofilm on support media.

Table 1.2 Advantages and disadvantages for various support media (Schügerl, 1997).

	Advantages	Disadvantages
Attachment	Attached easily	1. Weak under high shear force; 2. High detachment under low shear force, due to limited dissolved oxygen; 3. Clogging caused by excessive thick biofilm under anaerobic
Colonization	Stable yield	1. Poor mass transfer efficiency due to excessive colonization; 2. Thick biofilm that impairs the viability of cells and quality of fluidization
Immobilization	Easily forming encapsulation of cells	1. Expensive; 2. Low mechanical stability; 3. Possibility of breakdown of CO_2 produced inside

1.4.2   Particle surface properties

Several criteria should be considered for selecting materials (Table 1.4). Some features could influence the cells adhesion on support carriers, such as static electrical interaction and Van der Waals's force between support and cell surface, hydrophobicity, free surface energy and the modified functional group (Xiong et al., 2018). Based on the zeta potential measurement research, most microorganisms are covered with a negative charge (Soni et al., 2008). Hence, material which is positively charged on the surface will be attached easily. The overall hydrophobicity of cells and support strongly relates to the microbial attachment as well. With hydrophobicity increasing, bacterial adhesion improves significantly (Liu et al., 2004). Furthermore, it was observed that a hydrophobic surface had higher microbial colonization than the hydrophilic surface. This could be explained by when the total surface free energy for interactions of cells and support surface is negative, adhesion could take place (Dimitrov et al. 2007). This theory could also explain the influence of the roughness of the surface. The roughness of the surface could not only increase the interface area to reduce the influence of shear force, but also lower surface energy to reduce Van der Waals's force (Dimitrov et al. 2007). Other features, such as solubility, biodegradability, mechanical stability, chemical stability and cost will guarantee economical and operational stability in the long term.

In addition, particle properties such as size, shape, density, porosity, roughness, and specific surface area should also be considered. For these criteria, the acceptable ranges can be modified to best suit the given environmental conditions or system requirements. Moreover, like roughness, particles could be modified to meet certain criteria.

Table 1.3 Effects of surface properties on biofilm formation (Xiong et al., 2018).

Material properties	Bacterial strain	Effects	Mechanism	Reference
	P. aeruginosa AK1	Initial adhesion was twice as fast on the positively charged surface than on the negatively charged surface	Electrostatic interaction	Gottenbos et al., 1999

Surface charge	E. coli	E. colicell density on the positively charged surface was 23 times higher than that on the negatively charged surface after 8 h incubation	Electrostatic interaction	Terade et al., 2012
	S. epidermidis	Adhesion to hydrophobic substrata for all strains occurred to a greater extent than that to hydrophilic surfaces.	Interaction between hydrophobic and hydrophilic group	Cerca et al., 2005
Hydrophilicity	E. coli	Biofilm fail to form on superhydrophobic film.	Obstructed by air film on surface	Pernites et al., 2012
	E. coli	Biofilm fail to form on under superoleophobic surface.	Obstructed by water film on surface	Chang et al., 2016
Roughness	E. coli, S. aureus	Bacteria cells showed preferential attachment on rougher samples. But when surface roughness reached certain value, comparatively less bacterial cells attached and no biofilm formation.	Increase interface area and reduce surface free energy	Singh et al., 2011

Table 1.4 Characteristics and selection criteria of support materials (Leenen et al., 1996).

Characteristics	Criteria
Solubility	Low
Biodegradability	Low
Mechanical stability	High
	It is not sensitive to abrasion.
Chemical stability	High
	Resistance of acid and alkali
Electrical property	Positive charge
Hydrophilicity	Hydrophobic
Bio-affinity (attachment)	High
Cost	Low

1.4.3   Experimental media

As shown in Table 1.5, various support carriers in previous works are employed.

Table 1.5 Carrier materials for wastewater treatment in fluidized bed and airlift bioreactors.

Materials	Particle size (mm)	Surface area (m^2/m^3)	Density (kg/m^3)	Reactor process	Reference
Sand	0.5	12000*	2557.7	Fluidized bed	Balaguer et al., 1997
	0.25 – 0.4	20000*	1274.9		
				Fluidized bed	G lli et al., 1987
Sepiolite	0.5	12000*	1977.4	Fluidized bed	Balaguer et al., 1997
Pumice stone	0.5	12000*	1526.4	Fluidized bed	Balaguer et al., 1997
Zeolite	0.6 - 0.85	3200	2496	Fluidized bed	Eldyasti et al., 2012
Lava tock	0.6	10950	2560	Fluidized bed	Chowdhury et al., 2010
	0.6 - 0.85	3500	2685	Fluidized bed	Eldyasti et al., 2012
Quartzite	2.2 - 2.8	2400*	2600	Fluidized bed	Jiang et al., 2009
Resin	2.5 - 4	1846*	1220	Fluidized bed	Saucedo-Terán et al., 2004
Perlite	2.5 - 4	1846*	1710	Fluidized bed	Saucedo-Terán et al., 2004
Kaolinitr bead	3	500	2500	Fluidized bed	Jian et al., 1893
Polypropylene	5	524**	870	Fluidized bed	Haribabu et al., 2016
Activated charcoal	1 - 1.5	4800*	495	Fluidized bed	G lli et al., 1987
Polyethylene	0.6 - 0.85	4600	1230	Fluidized bed	Wang et al., 2019

* the value was calculated by Surface area $= \frac{6}{d}(1 - \varepsilon)$ (Eldyasti et al., 2012).
** unit is mm^2/particle

In this case, three different particles are selected as support carriers, which are polypropylene (PP), polyethylene (PE) and active carbon coated polyethylene (PEC).

Polyethylene (James, 1999)

Polyethylene in this case is low density polyethylene (LLPE) which is polymerized under 100 ~ 300 MPa with oxygen as the catalyst.

Advantages:

1. LLPE is nontoxic and odourless with a density between 0.91 ~ 0.94 g/cm^3 which is the lightest category of PE.

2. LLPE has a low crystallinity (55% ~ 65%) and softening point (90 ~ 100°C).

3. LLPE has great softness, malleability, transparency, cold tolerance (-70°C) and machinability.

4. LLPE has high chemical stability: resistance of acid, alkali and salt solution, and inflammability.

5. LLPE has insulativity, breathability and low hydroscopicity.

Polypropylene (James, 1999)

1. PP has a low relative density of 0.89 ~ 0.91, which is one of the lightest categories of plastics.

2. PP has great mechanical properties, aside from worse shock resistance. It has better strength, rigidity and hardness than PE.

3. PP has higher thermostability which could work 110 ~ 120°C lower than PE and insulativity and higher transparency.

4. PP also has great chemical stability which is nonreactive with most of chemicals.

5. PP is nontoxic, inodorous and low hydroscopicity.

Activated carbon

The great performance of activated carbon as a carrier can be found in many cases (Wright & Raper, 1996), and coating activated carbon on the carrier surface was proved to be an effective way for faster colonization and higher cell concentration (Dimitrov et al. 2007). Activated carbon exists as an amorphous carbon that has an extraordinarily large specific surface area for adsorbing inorganics, organics and colloidal solids in solutions. Therefore, activated carbon is widely applied in various aspects of life and industries as an effective adsorbent. It has great chemical stability with acid and alkali, great mechanical properties and reproducibility. Because the major component is carbon, it has hydrophobicity which means insolubility in water.

Depending on different producing conditions, two forms of activated carbons can be produced. The H-type activated carbons which is produced at 1200°C under vacuum or the CO_2 atmosphere, when exposed to air at room temperature has a positive charge in water and is hydrophobic. The L-type activated carbons which is produced under 200 ~ 400°C in air, has a negative charge in water and is hydrophilic (Corapcioglu & Huang, 1987). For biofilm attachment, the H-type activated carbon should be selected.

Based on previous researches, carbon fiber has less negative potential and no energy barrier for the microorganism attachment process, so when compared with polypropylene and polyethylene fiber, carbon fiber has higher adsorption capacity for microorganism to form biofilm (Matsumoto et al., 2012). In addition, there are several papers introducing surface modifying methods for optimizing carbon carriers for wastewater treatment, such as physical activation by carbon dioxide (Yusof et al., 2012) and by ferrous oxalate (Xu & Jiang, 2018), oxidation etching method including acid etching (Woodhead et al., 2017) and electrochemical oxidation (Jiang et al., 2017), chemical vapor deposition method (Guo et al., 2016), and plasma-mediated modification (Lee et al., 2017).

1.5   Biofilm detachment

Based on previous researches, influencing factors of biofilm detachment could be summarized by shear force and biofilm growth (Xiao et al., 2005). The models in Table 1.6 were reported for describing biofilm detachment.

Table 1.6 Detachment models.

Models	Parameters	Reference
When $L_f < 0.003$ $$R_d = -8.42 \times 10^{-2} X_f L_f \sigma^{0.58}$$ When $L_f > 0.003$	Biofilm density (X_f); Biofilm thickness (L_f); Biofilm shear loss rate (R_d); Bydrodynamic shear force (σ)	Rittmann, 1982

R_d $= -8.42 \times 10^{-2} X_f L_f \left(\dfrac{\sigma}{1 + 433.2(L_f - 0.003)}\right)^{0.58}$		
$R_d = -\text{b}X_f L_f$	Biofilm loss rate (R_d); Specific biomass decay coefficient (b)	Rittmann, 1982
$R_d = b_s X_f A L_f - b_s' X_f A Y k \displaystyle\int_0^{L_f} \dfrac{S_f}{K_s + S_f} dz$	Media surface area (A); maximum substrate Utilization rate (k); Monod half-saturation coefficient (K_s); Substrate concentration (S_f); Biofilm shearing coefficient (b_s); A dimensionless Parameter describing the biological aspects of shearing (b_s')	Speitel & DiGiano, 1987
$R_{di} = K_{d1}\rho_i \displaystyle\int_0^{L_f} \mu(z)(L_f - z)dz + \dfrac{1}{2} K_{d2}\rho_i L_f{}^2$	Detachment rate of component i (R_{di}); Detachment rate coefficient (K_d); Density of component i in the biofilm (ρ_i); Growth rate (μ)	Stewart, 1993
$P_6 = 1.95 \times 10^{-10} P_1^{1.49} P_2^{2.67}$ $P_1 = \dfrac{\rho_l d_c u}{\mu} \quad P_2 = \dfrac{d_e}{d_c} \quad P_6 = \dfrac{d_c b_s}{\mu}$	Dimensionless parameters (P);	Nicolella et al., 1996
$P_{ds} = K_{ds}\Delta t \left(\dfrac{h_i}{h_{max}}\right)^2$ $P_{dn} = K_{dn}\Delta t \left(1 - \dfrac{S_i}{S_{bulk}}\right)$ $P_{de} = K_{de}\Delta t \left(\dfrac{NB_{free,i}}{NB_{total}}\right)$	Detachment probability caused by shear (P_{ds}); Detachment coefficient (K_{ds}); Simulation time step (Δt); Distance between the cell i and the attached surface (h_i); Maximum biofilm thickness (h_{max}); Detachment probability caused by nutrient-limited (P_{dn}); Detachment coefficient (K_{dn});	Li et al., 2015

	Substrate concentration at the location of the bacterium i (S_i); Bulk nutrient concentration (S_{bulk}); Detachment probability caused by weak interactions (P_{de}); Detachment coefficient (K_{de}); Number of neighbor grids free of biomass ($NB_{free,i}$); Total number of neighbor grids (NB_{total})	
$$\frac{dB}{dt} = G - D = \mu_{max}\frac{1}{1+K_{inv}B} - C_{det}QB$$	Epilithic biofilm biomass (B); Time (t); Maximum specific growth rate (μ_{max}); Inverse half-saturation constant for biomass (K_{inv}) Empirical detachment coefficient (C_{det}); Flow discharge (Q)	Graba et al., 2010
$$F_{det} = \frac{k_{det}x^2}{\rho(x)}$$	Detachment speed function (F_{det}); Distance to the solid substratum (x); Detachment speed coefficient (k_{det}); Local biofilm density (ρ)	Xavier et al., 2005

1.5.1   Sloughing and erosion

Sloughing and erosion occur together causing biofilm detachment, with erosion causing more detachment than sloughing. Erosion results in small particles which could flow away with effluent, but sloughing causes large biomass pieces which became sediments at the reactor bottom (Telgmann et al., 2004). Therefore, sloughing could greatly influence biofilm morphology. Possible reasons for the sloughing phenomenon are lacking dissolved oxygen due to thick biofilm (M C M van Loosdrecht et al., 1995) and nutrients starvation which is triggered by metabolic product accumulation and metabolic substances depletion (Hunt et al., 2004). Sloughing and erosion happen

spontaneously when the biofilm structure is not stable. However, biofilm detachment caused by shear force is more acute and is influenced by external factors and occurs passively.

1.5.2   Shear force

Shear force has two opposite effects on biofilm. On one hand, appropriate shear force could keep biofilm thickness within healthy value to avoid low oxygen and nutrient transfer efficiency. On the other hand, uncontrollable shear force will become the main limiting factor for biofilm growth and lead to high detachment rate. In the a fluidized bed bioreactor, shear force consists of hydrodynamic shear force, attrition shear force and gas shear force.

Hydrodynamic shear force

The hydrodynamic shear stress could be calculated under different conditions for a single particle size. When the Re number is smaller than 10 which means equation reflects the shear force for fixed bed reactors, shear force could then be calculated by Eq. 19. Additionally, specific surface area for the biofilm carrier is simplified to the specific surface area of bare particle which is easier to calculated by Eq. 20. When Re is more than 100 which frequently appears under fluidized bed conditions, shear force could be calculated by Eq. 22 (Rittman, 1982).

$$\text{Re}' = \frac{d_p u \rho_w}{\mu} \leq 10 \tag{18}$$

$$\sigma = \frac{100 \mu u (1-\varepsilon)^3}{d_p \varepsilon^3 a (7.46 \times 10^9)} \tag{19}$$

ε = the total bed voidage, %

d_p = the steady state bioparticle diameter, cm

μ = liquid viscosity, gm/cm·day

u = the liquid superficial velocities, cm/day

a = specific surface area of the biofilm carrier, cm^{-1}

σ = hydrodynamic shear force, dyn/cm^2

$$a = \frac{A}{V} \tag{20}$$

A= surface area of particle, cm^2

V = particle volume, cm^3

$$Re' = \frac{d_p u \rho_w}{\mu} > 100 \tag{21}$$

$$\sigma = \frac{1.4 u^2 \rho \omega^4 (1-\varepsilon)^3}{d_p \varepsilon^3 a} \tag{22}$$

For the fluidized bed, there is another equation to describe the shear force. However, it only represents the minimum shear force for the fluidized bed startup. If particles could be fluidized, shear force must be bigger than, at least equal to, the value calculated by Eq. 23.

$$\sigma = \frac{(\rho_P - \rho_W)(1-\varepsilon_0)g}{a} \tag{23}$$

ρ_p = particle density, g/cm^3

ρ_w = water density, g/cm^3

g = the gravitational acceleration, 980 cm/s^2

ε_0 = initial bed porosity (compact bed of bare particles)

After obtaining the shear force, the specific shear force loss coefficient can be calculated using the shear force and biofilm thickness. The definition of the specific shear force loss coefficient is the percentage of biomass lost per day. Similarly, based on different biofilm thickness, a different equation is selected. For $L_f > 0.003$ cm, Eq. 24 demonstrates specific shear force loss coefficient. When $L_f < 0.003$ cm, Eq. 25 is selected (Rittman, 1982).

$$b_s = 8.42 \times 10^{-2}(\frac{\sigma}{1+443.2(L_f-0.003)})^{0.58} \qquad (24)$$

L_f = biofilm thickness, cm

b_s = specific shear force loss coefficient, day^{-1}

$$b_s = 8.42 \times 10^{-2}\sigma^{0.58} \qquad (25)$$

All above equations are fit for hydrodynamic shear force in a liquid solid fluidized bed, because those experimental equations are summarised from an annular biofilm reactor which uses an external gas diffuser.

Attrition force

Based on the hydrodynamic shear force, a novel model which considers the influence of hydrodynamic shear force and particle to particle attrition is provided. However, Eq. 26 is derived from former results. It has same limitation in which it only works for the liquid solid fluidized bed (Chang et al., 1991).

$$b_s = -3.14 + 0.335C_p + 19.3Re - 3.46\sigma \qquad (26)$$

C_p = the bare particle concentration, g/cm^3

Re = the Reynolds number

$$Re = \frac{d_b u \rho_w}{\mu} \qquad (27)$$

d_b = the diameter of bioparticles, cm, which equals 2(r_p+L_f)

$$\sigma = \frac{(\rho_b - \rho_W)(r_p + L_f)g}{3} \qquad (28)$$

ρ_b = the effective density of a biofilm-covered particle, g/cm^3

r_p = the radius of clean particle, cm

Gas shear force

Until now, there is no accurate models or equations used to predict the gas shear force in a gas liquid solid three phase fluidized bed. According to previous research, biomass detachment caused by gas shear force is 10 to 100 times higher than in liquid solid fluidized beds (Trinet et al., 1991). In addition, superficial gas velocity being closely related to biofilm attachment in a fluidized bed bioreactor was confirmedn (Tavares et al., 1995). It can be concluded that in a three-phase fluidized bed, the gas shear force occupies a large portion of the total shear force, even the hydrodynamic shear and particles attrition could be neglected.

1.6   Operational factors

1.6.1   pH and temperature

The relationship between specific the substrate utilization rate of ammonium and nitrite oxidations and pH is given as Eq. 29 (Park et al., 2007). Furthermore, others also gave out some models focused on ammonium oxidizing bacteria, but those models still needed to be optimized (Siegrist & Gujer, 1987).

$$\hat{q}_{pH} = \frac{\hat{q}_{max}}{2}\left\{1 + \cos\left[\frac{\pi}{w}(pH - pH_{opt})\right]\right\} \tag{29}$$

$$(pH_{opt} - w \leq pH \leq pH_{opt} + w)$$

$\hat{q}_{pH}$ = the maximum specific substrate utilization rate at given pH, mg/mg VSS·d

$\hat{q}_{max}$ = the greatest maximum specific substrate utilization rate under the optimal pH, mg/mg VSS·d

w = a pH range within which the maximum specific substrate utilization rate is larger than a half of the $\hat{q}_{max}$

pH_{opt} = the optimal pH

Similar to pH, temperature influences metabolic activities extraordinarily. Therefore, identifying the temperature dependence for microorganism life activities is significant for accurately predicting and calculating the biological reaction rate. Accredited value for θ varies from 1.02 to 1.25 (Tchobanoglous et al., 2014).

$$k_T = k_{20}\theta^{T-20} \tag{30}$$

k_T = reaction-rate coefficient at temperature T, °C

k_{20} = reaction-rate coefficient at 20°C

θ = temperature-activity coefficient

T = temperature, °C

1.6.2   Dissolved oxygen

Dissolved oxygen concentration directly influences the removal efficiency. If aerobic microorganisms can not access sufficient oxygen, the metabolism activities will be restricted. Next, some species that can live with low oxygen demand will become of greater importance and replace the original microorganisms, so that the nutrient removal efficiency will be inferior. For aerobic columns, DO should be controlled to be around 2 mg/L.

Despite providing the necessary drag force to fluidize particles, gas in the fluidized bed bioreactor has another function of meeting the oxygen requirement. Maintaining a certain dissolved oxygen concentration is vital for microorganism respiration in an aerobic condition. When the biofilm becomes thick, raising the dissolved oxygen concentration could prevent biomass sloughing. The motivation of oxygen transferring from the gas phase to the liquid phase and from the liquid phase to solid (biofilm) phase is the concentration gradient between the two phases. The diffusion flux is determined by concentrations at certain phase thickness which is called Fick's law.

$$J = -D\frac{dC}{d\delta} \qquad (31)$$

J = the diffusion flux, of which the dimension is the amount of substance per unit area per unit time, mol m^{-2} s^{-1}

D = the diffusion coefficient, m^2/s

C = the substances concentration, mol/m^3

δ = the thickness of laminar film, m
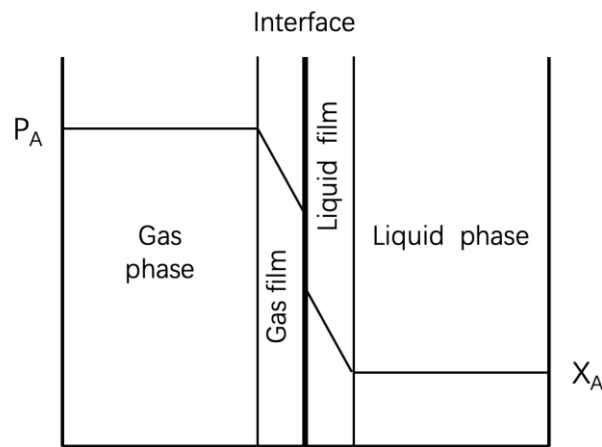
Figure 1.8 The model of two-film theory (Luo et al., 2014).

Generally, two film theory proposed by W.G. Whitman and L.K. Lewis is used to explain the oxygen transfer process between the gas and liquid phase. Basic assumptions are: (Gao, 1999)

1. Laminar films exist on both sides of the interface.

2. Concentrations at any position in two phases do not change with time. All the transfer resistance exists in two laminar films.

3. Concentration gradient is the motivation of oxygen mass transfer. Equilibrium exists at the interface, thus there is no mass transfer resistance across the interface.

4. Due to low solubility of oxygen, mass transfer resistance mainly lies in the liquid laminar film. Therefore, the diffusion flux of liquid laminar film will be limitating the total diffusion flux.

According to the two film model, the oxygen transfer process could be described as Eq. 32. Form Eq. 32, there are several ways to promote oxygen mass transfer, such as increasing the interface area by using fine bubbles and increasing the oxygen partial pressure in the gas phase by using pure oxygen for aeration.

$$\frac{dC}{dt} = \frac{D}{\delta_L}\frac{A}{V}(C_S - C) \tag{32}$$

δ_L = the thickness of liquid laminar film, m

A = interface area, m^2

V = liquid phase volume, m^3

Cs = saturated dissolved oxygen concentration in gas phase, kg O_2/m^3

C = dissolved oxygen concentration in liquid phase, kg O_2/m^3

However, a more restricting process for oxygen diffusion is oxygen diffusing within the biofilm. Generally, due to the complex biofilm structure, oxygen distribution inside the biofilm is hard to determine. Qiu (2009) claimed a model to estimate oxygen distribution in biofilms and model parameters q_{max} and k_o are 10 mg O_2/g VSS h and 1.2 mg/L respectively.

$$D_{eff}\frac{d^2C}{dx^2} = q_{max}\frac{C}{K_o+C}X_f \tag{33}$$

D_{eff} = effective diffusion coefficient of oxygen inside biofilm, mm^2/h

C = oxygen concentration, mg/L

x = biofilm depth, mm

K_o = Oxygen half saturation coefficient, mg/L

X_f = biofilm density, mg/L

q_{max} = μ_{max}/Y, mg O_2/g VSS h

1.6.3   Hydraulic retention time

The hydraulic retention time is a measure of the average length of time that a soluble compound remains in a constructed bioreactor, which is calculated by dividing the volume of the aeration tank by the influent flowrate. Heijnen (1984) announced a hypothesis that the only condition possible for biofilm to attach onto particles is that hydraulic retention time is smaller than the inverse of maximum growth rate, or it can be expressed as the dilution rate is larger than the maximum growth rate.

$$D = \frac{1}{HRT} > \mu_{max} \tag{34}$$

When the system is under long HRT, suspended biomass will not be washed out of the system with effluent, so that they could remain in reactor. Because of the higher nutrient concentration in the liquid, mass transfer efficiency for suspended biomass is much higher than the attached biomass (Tijhuis et al., 1994). The result of the nutrients competition between suspended and attached biomass is evident, that the suspended biomass stays at the dominant place. Therefore, the growth of attached biomass will be restricted. On the contrary, for short HRT, suspended biomass barely has the opportunity to stay in the system, owing to the entrainment of suspended biomass in the effluent. Attached biomass could develop due to less nutrient competition, but extremely low HRT could also impede growth of attached biomass, due to the serious hydrodynamic shear force. Therefore, an appropriate HRT should be short enough to guarantee that most of the suspended biomass leaves the system, but not be excessively short to enhance attached biomass detachment.

To prove this theory, there are several biofilm formation tests in the internal loop fluidized bed bioreactor under various HRT (Zhou et al., 1998). In that research, the attached VSS reached 3.4 g VSS/L for HRT 0.55h, while for HRT 2.2h and 5h, attachments failed in the end. Additionally, HRT could also influence nitrogen and phosphorous removal efficiencies. When HRT is too short, low removal efficiency is attained, and when HRT is too long, the system became unstable (Yin et al., 2014).

1.6.4   Organic concentration

In line with Eq. 5, the substrate utilization rate will increase with the substrate concentration when the biomass amount is constant. Similarly, the biomass growth rate will increase as well when the organic concentration increases. For the startup test, the main point is to determine the biofilm attachment rate. Therefore, the influent concentration rather than organic loading should be considered as an influence factor in the startup test, because it could provide a higher growth rate which means less startup time. However, when the system enters a steady state, influent concentration should not be considered as an influence factor, because the main point changes from time to quantity, such as quantity of attached biofilm or quantity of nutrient removed.

1.6.5   Organic loading rate

The definition of organic loading rate is the amount of BOD or COD applied to the aeration tank volume per day. It also demonstrates the ability to treat organics for bioreactors. The value could be calculated through HRT and influent organic concentration. Decreasing HRT or rising influent concentration are optional ways of increasing organic loading. Organic loading was analyzed as an influence factor for biofilm attachment process in many researches, but it was found that the organic loading rate only affected the biomass amount (Tijhuis et al., 1994).

$$OLR = \frac{S_0}{HRT} \tag{35}$$

1.6.6   C/N ratio

The appropriate C/N should be 100:5 (20:1), but typical municipal wastewater C/N is 7-10. C/N ratio might influence the nitrogen removal efficiency by affecting the growth of ammonia oxidizing bacteria and heterotrophic bacteria in an aerobic condition (Mannina et al., 2017). It was reported that the nitrification rate increased with the C/N ratio varying from 9.3 to 5.3 (Fu et al., 2009). Monod kinetics is described using Eq. 36

when substrate limitation is avoided, and dissolved oxygen concentration is the only limiting factor for growth rate in an aerobic condition.

$$\mu = \mu_{max} \frac{c_{O2}}{K_{O2} + c_{O2}} \tag{36}$$

μ = the specific growth rate of the microorganisms, d^{-1}

μ_{max} = the maximum specific growth rate of the microorganisms, d^{-1}

c_{O2} = the concentration of dissolved oxygen, mg/L

K_{O2} = the "half-velocity constant"—the value of S when $\mu/\mu_{max} = 0.5$, mg/L

Table 1.7 Kinetic coefficients for growth rate at T = 20°C (Wiesmann, 1994).

NH_4-oxidation	NO_2-oxidation	Aerobic degradation of organics
μ_{max}= 0.77d^{-1}	μ_{max}= 1.08d^{-1}	μ_{max}= 7.2d^{-1}
K_{O2}= 0.3 mg/L O_2	K_{O2}= 1.1 mg/L O_2	K_{O2}= 0.08 mg/L O_2

The sensitivity of ammonia and nitrite oxidation relative to the organics is reflected by the significantly higher K_{O2} concentration. The following example illustrates this sensitivity.

So when dissolved oxygen concentration is 1 mg/L hypothetically, the values of specific growth rate are:

NH_4-oxidization $\mu = 0.59$ d^{-1}, $\mu/\mu_{max} = 0.77$

aerobic degradation of organics $\mu = 6.67$ d^{-1}, $\mu/\mu_{max} = 0.93$

If μ/μ_{max} of ammonia oxidization bacteria reaches 0.93, dissolved oxygen concentration should be $\frac{0.93}{0.07} \times 0.3 = 3.99$ mg/L (Wiesmann, 1994). Therefore, dissolved oxygen is utilized by the heterotrophic bacteria rather than ammonia oxidization bacteria, so that when C/N is low, the heterotrophic bacteria growth could be restricted by a

relatively limited substrate and ammonia oxidization bacteria could get superiority. Then, nitrification capacity will be enhanced (Fu et al., 2009).

1.7   Knowledge gaps

Fluidized bed bioreactors utilized as one of the attached growth processes were tested in many works (Andalib et al., 2010; Nelson et al., 2017) with advantages, such as improving the interphase contact efficiency and enhancing mass and heat transfer significantly (Zhu et al., 2000). However, most researchers focused on conventional fluidized bed bioreactors. Inverse fluidized bed bioreactors received less attentions and carriers of inverse fluidized bed bioreactor were rarely investigated. Therefore, comprehensively testing various carriers in a inverse fluidized bed bioreactor is significant for selecting carriers and acquiring performance data. Moreover, due to having no equations for shear force in a three-phase fluidized bed, a model based on gas and liquid flow rate could be developed to estimate the detachment rate.

1.8   Thesis objectives

The inverse fluidized bed bioreactor was tested successfully in recent years as a novel fluidized bed bioreactor (Sokół et al., 2009). Support media as a crux part in inverse fluidized bed bioreactor could influence the treatment performance. Therefore, various support particles were tested to select the appropriate media in this research. The specific objectives are listed as following:

1. To evaluate the performance, including attachment rate and biofilm quantity, for different particles under different conditions in a startup stage and to identify influence factors to confirm the best operational conditions to optimize startup procedures.

2. To select the best particle based on steady state performance, including biofilm characteristics and nutrient removal efficiency in incremental organic loading conditions.

1.9   Thesis structure

In addition to the background knowledge of wastewater treatment development history, a comprehensive literature review of biomass kinetics, basic biofilm knowledge, introductions of relevant bioreactors, particle properties and influence factors analyzation are presented in chapter 1. In chapter 2, detailed descriptions of materials and methods of whole research were presented. In chapter 3, three particles were tested under various operational conditions in both the startup stage and steady state. The performances of those particles were analyzed to explain how influence factors affect their performances. Major findings and conclusions of this research were summarized in chapter 4.

<div align="center">Chapter 2</div>

2 Materials and methods

2.1 Sludge and wastewater sources

Activated sludge

The seed active sludge was taken from the Adelaide wastewater treatment plant which is a local treatment plant in London, Ontario. The major treatment process in this plant is activated sludge process. BOD and ammonia are almost completely removed (effluent ammonia about 0.1 mg/L), so sludge in this plant has excellent organic degradation ability and high nitrogen removal. Besides, best pH range for sludge growth is from 7.0 to 7.5. The sludge was taken once from aeration tanks with VSS of 2088 mg/L, because sludge there has higher vitality. After taken, all the sludge was fed by synthetic municipal wastewater for several days to acclimate.

Synthetic municipal wastewater

Based on data from treatment plants, influent characteristics for real wastewater are BOD = 210 mg/L and ammonia = 22 mg/L (Adelaide Pollution Control Plant, 2018). Because of availability of real wastewater and lacking primary treatment processes, such as screening, synthetic municipal wastewater is used instead of real municipal wastewater in this case. Considering the undegradable organics and other impeditive factors in wastewater, characteristics of synthetic municipal wastewater are set as Table 2.1. Additional sources, NH_4Cl for nitrogen and KH_2PO_4 for phosphorous, should be added in wastewater when nitrogen and phosphorous are insufficient. For C/N ratio = 5, the concentration of COD will be half as 150 mg/L.

Table 2.1 Components of synthetic municipal wastewater.

CH_3COONa	384.62 mg/L	COD	300 mg/L
NH_4Cl	114.62 mg/L	Ammonia	30 mg/L
$NaHCO_3$	425 mg/L	ALK	300 mg/L as $CaCO_3$
KH_2PO_4	17.87 mg/L	Phosphorous	4 mg/L
Trace elements solution	1.5 ml/L	15 mg EDTA/L, 0.43 mg $ZnSO_4 \cdot 7H_2O/L$, 0.24 mg $CoCl_2/L$, 0.99 mg $MnCl_2/L$, 0.25 mg $CuSO_4 \cdot H_2O/L$, 0.22 mg $NaNoO_4 \cdot H_2O/L$, 0.19 mg $NiCl \cdot 6H_2O$ /L, and 0.014 mg H_3BO_4/L	

2.2   Particle properties

Three kinds of particles, PP, PE and PEC, were employed as support carriers. The properties of these particles were listed in Table 2.2. All the particles were ground by blender for 1 min to make their surface rough. Specially, powder active carbon was added in during grinding process to mix with PE to make PEC. Therefore, PE and PEC had similar physical properties, such as real density and skeletal density, while they were diverse chemical properties as summarized in particle introduction. After the roughening process, particles were screened and washed to removal tiny and cracked parts.

Table 2.2 Particle properties for PE, PP and PEC.

	PE	PP	PEC
Skeletal density (kg/m^3)	930	906	930
Bulk density (kg/m^3)	560	510	545
Size (mm)	3-4	3-4	3-4
Packing volume (L)	1.1	1.1	1.1
Mass (g)	610	560	600
Sphericity	0.95	0.95	0.95
Specific surface area (m^2/kg)	1.8	1.9	1.8 (1.2×10^6 [a])

[a] 1155 m^2/g is specific surface area for micro-sized activated carbon powder only (Saeidi & Lotfollahi, 2016).

2.3   The aerobic bioreactors

Four identical columns were arranged in parallel comprised the whole system. The fourth column could be used to run more tests simultaneously. All columns were

made by polymethyl methacrylate with total length of 1.2 m and inner diameter of 7 cm corresponding to total volume of 4.6 L. Inlet port was placed on top area with 15 cm away from peak of column and outlet port was on the bottom. Influent was pumped from feeding tank by peristaltic pump (Masterflex I/P; Masterflex, Germany). There was no other pump for effluent, so that barometric pressure was used to push liquid out of column. The end of effluent pipe and liquid level in column were at same height (35 cm away from column peak). Therefore, active volume was 3.3 L corresponding to active height of 85 cm. Aquarium aeration stone (d = 6 cm) was chose as gas distributor which was set at 5 cm from bottom. Air source was liquid pressurised gas transported by supply pipes. Solids hold up for each kind of particles was 30 percent of total volume which was 1.1 L (compact volume). All the particles were fluidized by fine bubbles. DO and pH meter were fixed on the top to monitor the operation conditions.
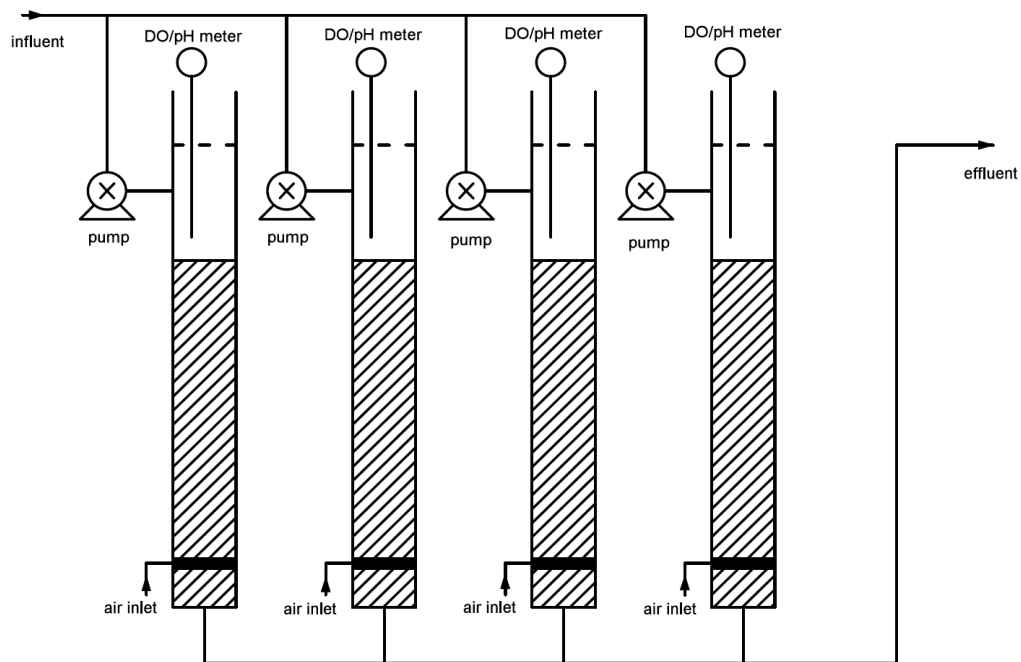
Figure 2.1 Schematic diagram of reactors.

2.4 Experiment start and operational conditions

2.4.1 Startup stage

After acquiring active sludge from wastewater treatment plant and growing them with synthetic wastewater for several days, 2.2 L sludge were put into column with 1.1 L particles. To promote biofilm formation, column was operated under fluidized condition for couple days to mix sludge and carriers completely without influent. Then, started tests with feeding under presupposed flow rates, 6.6 L/d, 9.9 L/d and 19.8 L/d. Because of different particle properties, air flows for fully fluidization which meant that expanded bed height equaled to active height 85 cm, were various from 1.4 L/min to 0.5 L/min. All the tests were shown in Table 2.3. With biofilm development, air flow could probably decrease, because attached bioparticles can be fluidized with less gas. Therefore, air flow was changing all the time with biofilm growing. Each test lasted four weeks to select appropriate operation conditions, and particles were evaluated by their performances in startup stage. SCOD, attached VSS and suspended VSS were measured twice a week to represent the status of biofilm. Once a test was finished, all particles in this column were sonicated for 4 hours, washed by disinfectors and dried under 104°C for 24 hours to eliminate possible microorganisms on particles.

Table 2.3 General operational conditions for startup test.

Materials	HRH (h)	Flow rate (L/d)	Influent COD (mg/L)	Initial air flow (L/min)
PP	12	6.6	300	1.4
PP	8	9.9	300	1.2
PP	4	19.8	300	0.9
PE	12	6.6	300	0.8
PE	8	9.9	300	0.7
PE	4	19.8	300	0.6
PEC	12	6.6	300	0.8
PEC	8	9.9	300	0.6
PEC	4	19.8	300	0.5
PEC	4	19.8	150	0.5

2.4.2   Steady state

Restart system on condition of 4h HRT and COD 300 mg/L. After biocarriers getting attached, feeding with the same synthetic wastewater continued for weeks until biofilm entirely developed. Then, feed under 9.2h HRT until systems were in steady state. Collected data, including SCOD, TCOD, NH_4^+, NO_3^-, alkalinity, DO, pH, attached VSS, suspended VSS and effluent VSS once a week for four weeks. Then followed same procedures under 6.1h and 4.1h HRT. Specific operating conditions were in Table 2.4. Each test lasted four weeks as well. When a test finished, changing of the operating conditions was done directly without cleaning particles.

Table 2.4 General operational conditions in steady state.

Materials	HRH (h)	Organic loading (g/L·d)	C/N ratio
PP	9.2	0.78	10
PP	6.1	1.18	10
PE	9.2	0.78	10
PE	6.1	1.18	10
PE	4.1	1.76	10
PE	4.1	0.88	5
PEC	9.2	0.78	10
PEC	6.1	1.18	10
PEC	4.1	1.76	10
PEC	4.1	0.88	5

2.5   Analytical methods

There were several parameters to be analyzed, SCOD, TCOD, NH_4^+, NO_3^-, alkalinity, DO, pH, alkalinity, attached VSS, suspended VSS and effluent VSS. Influent and final effluent samples were collected in airtight bottles once a week, refrigerated at 4 °C before analysis. TCOD, SCOD, NH_4^+ and NO_3^- were measured under HACH method with help of HACH Odyssey DR/2800. For DO and pH, Thermo Orion (810 A+) meter and pH-11 series pH/(mV°C) meter (Oakton, Singapore) were used for measurement. The samples of effluent VSS, suspended VSS and attached VSS were analyzed according to standard method. Specifically, approximately 2 g bioparticles were taken from each

column at three heights, suspended in a 50 ml vial, and sonicated for 3 h at 30°C in a sonicator (Model 75HT, ETL Laboratory Testing, Inc., New York). Then prepared VSS was evaporated to dryness in a drying oven at 103 to 105°C, then put in a muffle furnace and ignite the contents at 550°C. The VSS was calculated by the mass difference. Alkalinity was measured by titration with 0.02 N H_2SO_4 with standard method No. 2320. The specific procedures of measurement are presented in appendix A.

Chapter 3

3   Results and discussion

3.1   Startup tests

For inverse fluidized bed bioreactor, regular startup method which was increasing liquid flowrate gradually, did not work all the time, due to the shear force in the aerobic zone. To optimize the startup process, especially for aerobic column starting up, there were a series of tests at different HRTs, support medium and organic concentrations to be set in aerobic column. The startup performances of particles were shown under various conditions.

3.1.1   Effect of HRT on effluent COD and attached biomass

As described in literature review, the great effects of hydraulic retention time on biofilm formation were tested in previous work (Zhou et al., 1998). As shown in Figure 3.1, with an influent COD of 300 mg/L, effluent COD decreased to relatively stable value about 40 mg/L for PE at 12h HRT. For 8h and 4h HRT, effluent COD were 45 mg/L and 48 mg/L respectively. Similarly, for PP, the effluent COD for 12h, 8h and 4h HRT were 34 mg/L, 55 mg/L and 42 mg/L respectively. For PEC, the effluent COD for 12h, 8h and 4h HRT were 42 mg/L, 50 mg/L and 46 mg/L respectively. High organic loading with large flow rate required more time to acquire stable effluent COD.
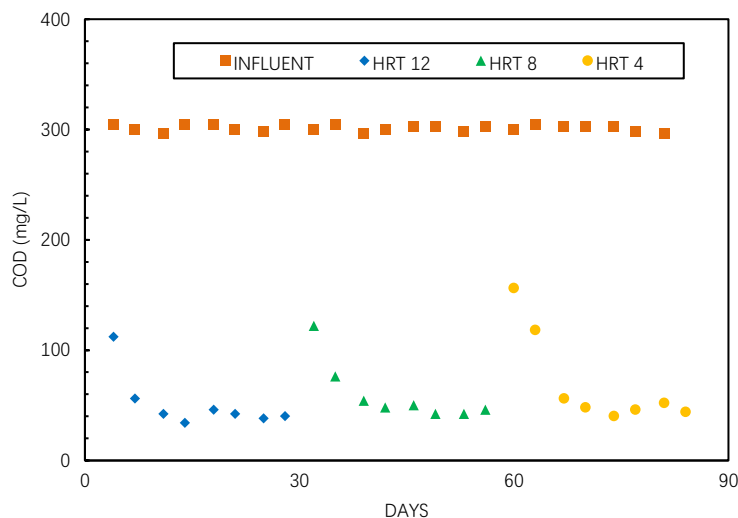
(a)
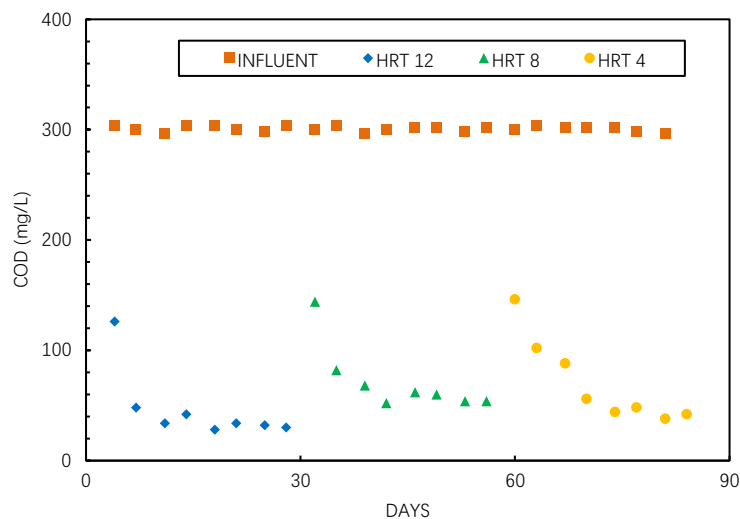
(b)
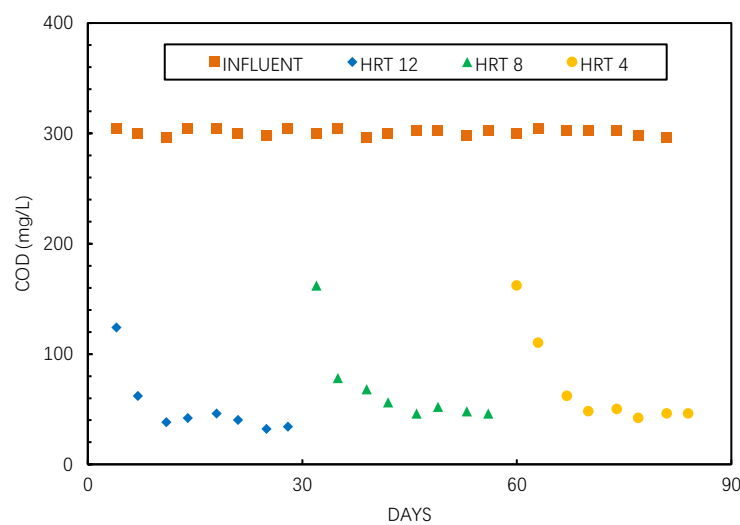
(c)

Figure 3.1 Influent and effluent COD over various HRT, (a) for PE; (b) for PP; (c) for PEC.

For biomass attachment, less than 1 mg VSS/g media was acquired under HRT of 12h and 8h for both PP, PE and PEC. However, a huge contrast appeared under HRT of 4h, that attached biomass for PE and PEC reached 9 mg VSS/g media and 5.5 mg VSS/g media respectively at the end of tests. But for PP, the attached biomass still remained at about 0.5 mg VSS/g media.

The theory that the only condition for biofilm attachment on particles is that hydraulic retention time is smaller than the inverse of maximum growth rate, could be used to explain these phenomena (Heijnen, 1984). As shown in Figure 3.3, fraction of attached biomass (X_A/X), in which X_A is attached biomass and X is the sum of attached biomass and suspended biomass, increased from 6% initially to 76% finally and from 11% initially to 57% finally for PE and PEC respectively under 4h HRT. That meant under high flow rate, the fraction of suspended biomass decreased obviously. A large proportion of suspended biomass was washed out with effluent, so that attached biomass had opportunity to be competitive with suspended biomass and attained dominant position in nutrient competition. Specifically, HRT was 4h and calculated maximum growth rate was 5 d^{-1} which was the average of 2.7 d^{-1} which was calculated by 6×0.45 (typical value of k and Y) (Tchobanoglous et al., 2014) and 7.2 d^{-1} which was reported in previous work (Wiesmann, 1994). Consequently, dilution rate for 4h HRT was larger than the maximum growth rate (6 $d^{-1}>$5 d^{-1}), while for 8h and 12h HRT, dilution rate was smaller than the maximum growth rate.
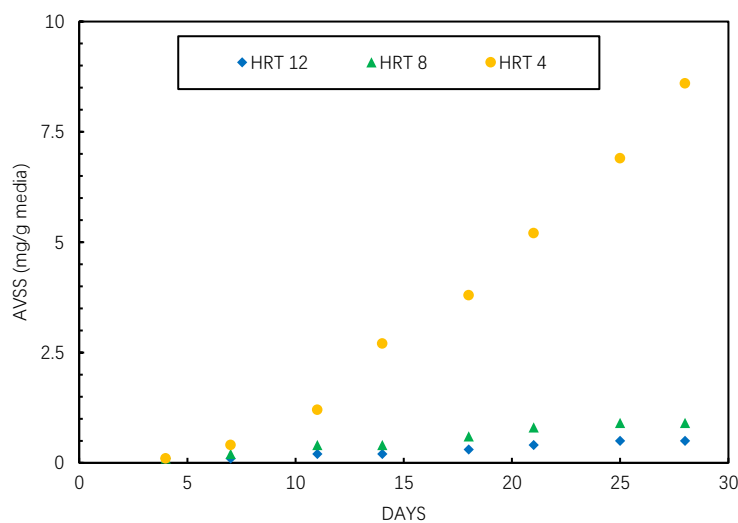
(a)
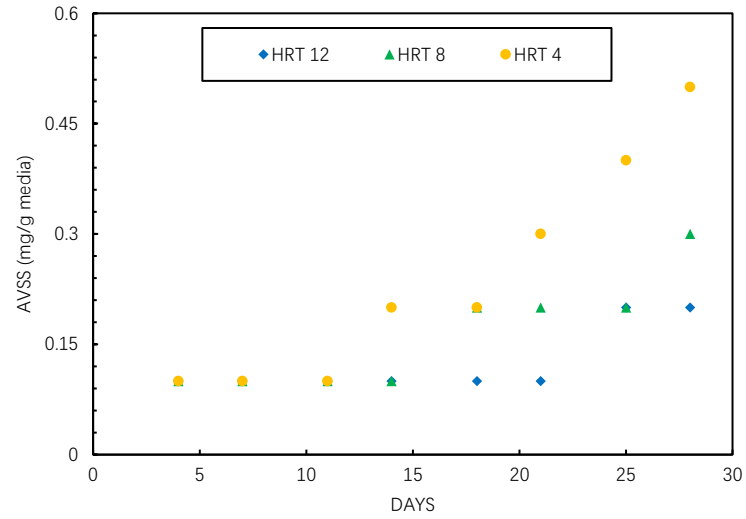
(b)
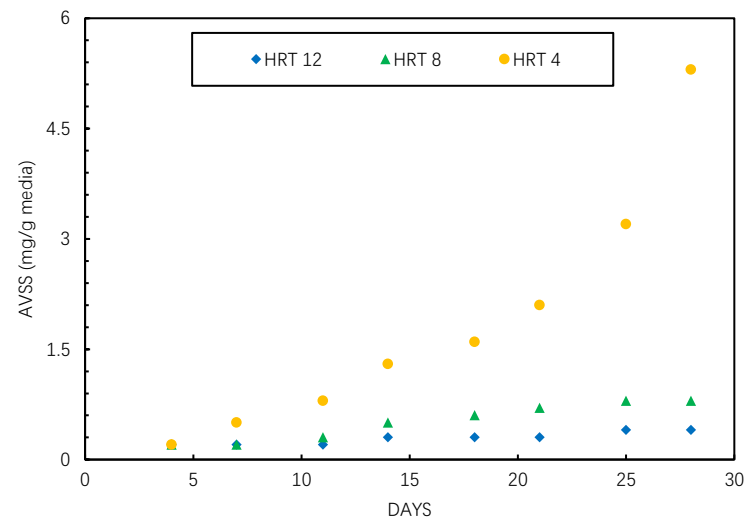
(c)

Figure 3.2 Attached VSS over various HRT, (a) for PE; (b) for PP; (c) for PEC.
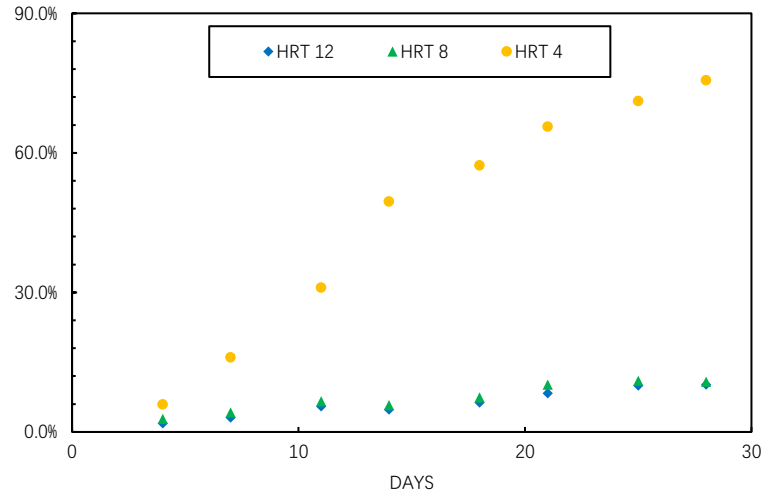
(a)
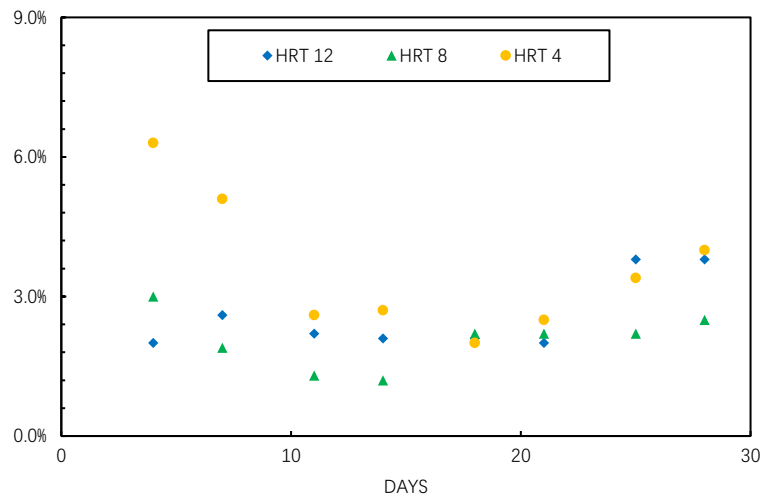
(b)
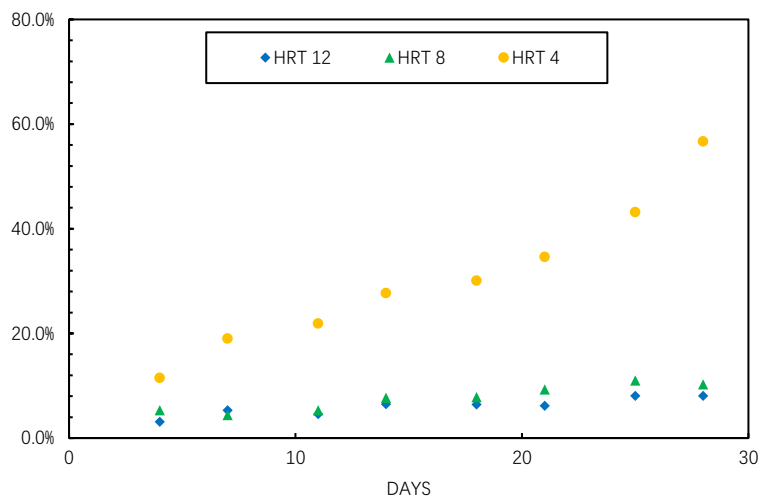
(c)

Figure 3.3 Fraction of attached VSS over various HRT, (a) for PE; (b) for PP; (c) for PEC.

3.1.2 Effect of particle properties on effluent COD and attached biomass

As described in Figure 3.5, no visible biofilm was observed at the end of the tests under 12h HRT. Only suspended biomass could be observed clearly. However, under 8h HRT, a thin transparent biofilm was observed at the end of tests. Under 4h HRT, obvious biofilm for PE was firstly observed at 15 days. Later then biofilm was observed on surface of PEC at 20 days. Generally, PEC had rougher surface and less negative potentials than PE (Matsumoto et al., 2012). However, PE was more hydrophobic than PEC which was closely associated with microbial adhesion (Liu et al., 2004). That could be the reason of the phenomenon that biofilm attachment for PEC was several days later than PE.

For PE, biomass including attached and suspended was in form of filamentous with fluff, and that usually trapped bioparticles. Biomass was accumulated as a flocculent mass in PEC. For PP, suspended biomass was observed in form of firm organic sphere. The reasons for different forms were shear force and material properties. PP was the lightest one of three particles, so that the largest air flow which caused the most serious shear force compared with the others, was demanded to fluidize particles. To bear that shear stress, biofilm had to be tight and smooth to reduce the influence of shear force.

PE belonged to polymer plastic which had smooth surface originally. Though PE was ground to make surface rough, the scale of roughness was larger than PEC. Nature micropores of activated carbon was the main reason of surface roughness for PEC. Hence, initial attached biomass at first measurement on day 3 for PEC (0.2 mg/g media) was double of PE and PP (0.1 mg/g media).
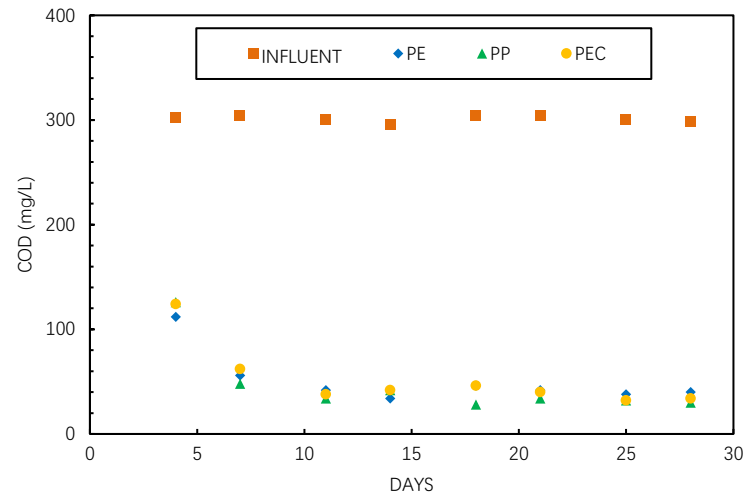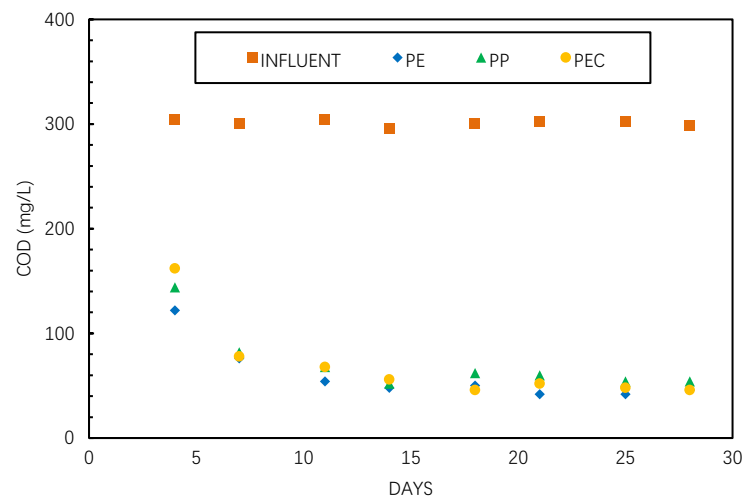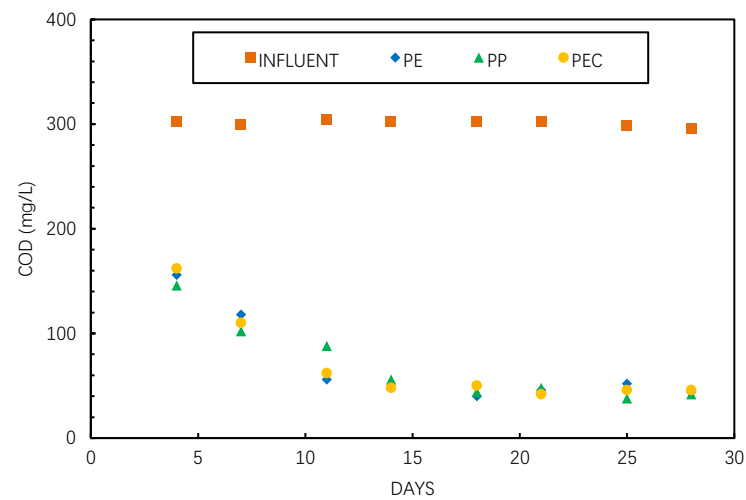
Figure 3.4 Influent and effluent COD for three particles, (a) under 12h HRT; (b) under 8h HRT; (c) under 4h HRT.
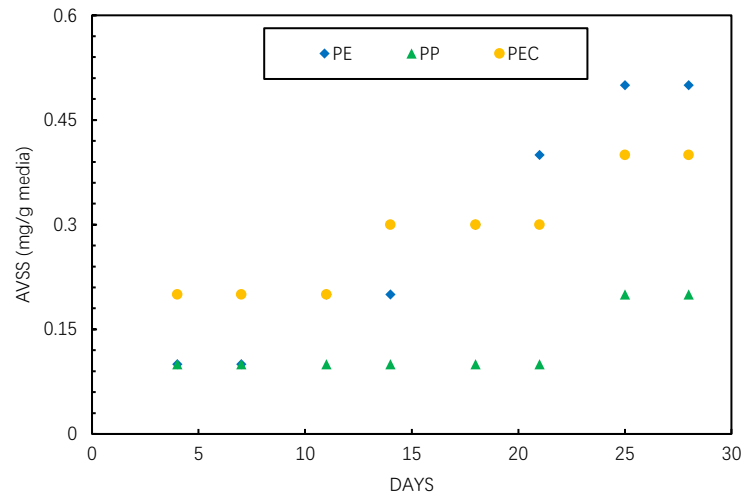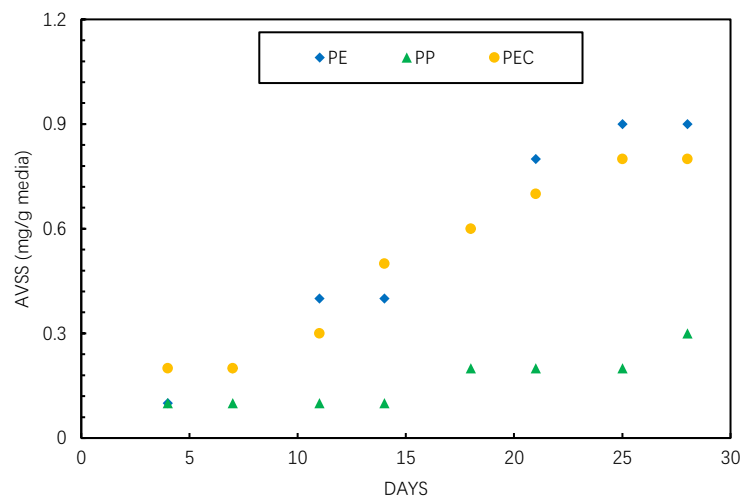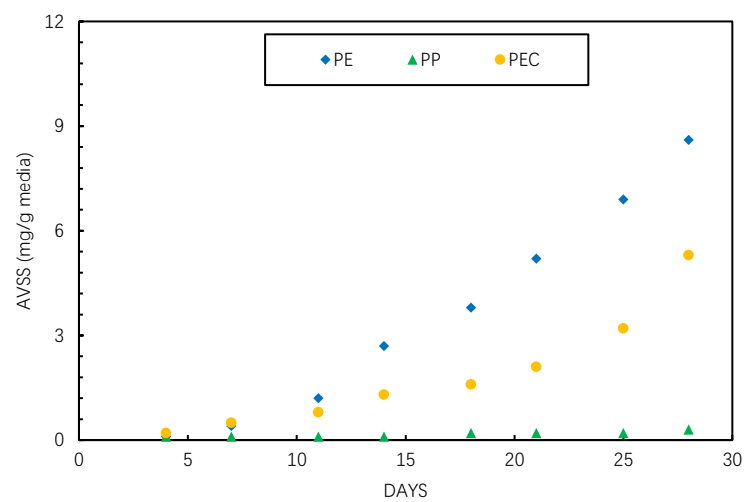
Figure 3.5 Attached VSS for three particles, (a) under 12h HRT; (b) under 8h HRT; (c) under 4h HRT.

3.1.3   Other factors

Shear force

Even though D $> \mu_{max}$ existed, little biomass got attached on the surface of PP. Air shear force was chief 'culprit' of bed attachment performance and it could be found from the biomass morphology of PP, firm organic sphere. Particles in PP column were turbulently fluidized. As a result of flow rate increasing, that serious strike was remitted a little, because less gas was required at high flow rate which could provide more drag force to fluidize particles.

Influent concentration

Organic loading was merely affected by HRT and influent concentration. In another word, for startup test, organic loading was not an isolated factor but reflected the influence of HRT at constant influent concentration or reflected the influence of influent concentration at constant HRT. Therefore, influent concentration rather than organic loading should be considered as another factor in startup test, because it could provide higher growth rate which means less startup time directly.

An extra test for PEC was designed with low influent concentration (150 mg/L) under 4h HRT. To discover the influence of influent concentration, this set should compare with the set of high influent concentration (300 mg/L), same HRT (4h) and particle (PEC). From Figure 3.7, particles for high COD had more attached biomass compared with low COD. In first three weeks, fraction of attached biomass under low COD kept increasing, though the rate of increase was relatively slow. Whereas in final week, fraction tended to flat at 19% with bits of increase. That could be explained by the structure of system. Not so as real inverse fluidized bed, there was no circulating in this case. Therefore, seed sludge which was added initially could washout without a hinderance, so the high COD would be favourable to hold as much as possible seed sludge in system because high growth rate could stimulate biomass growth to offset losing amount partly.
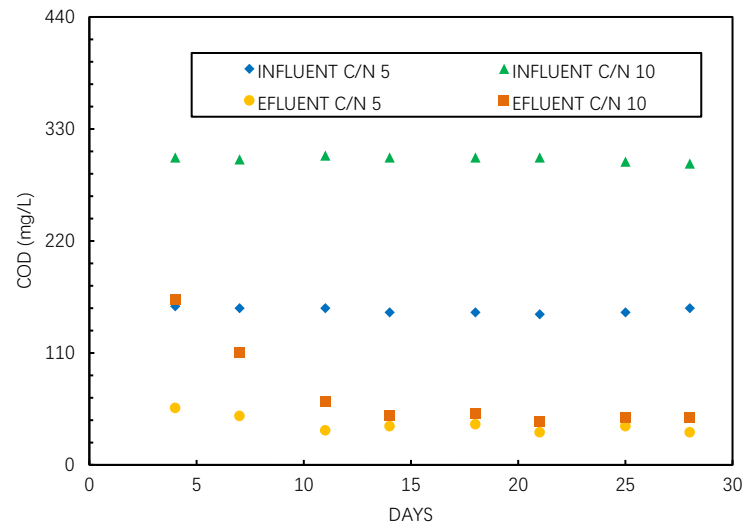
Figure 3.6 Influent and effluent COD with various COD concentration (for PEC over 4h HRT).
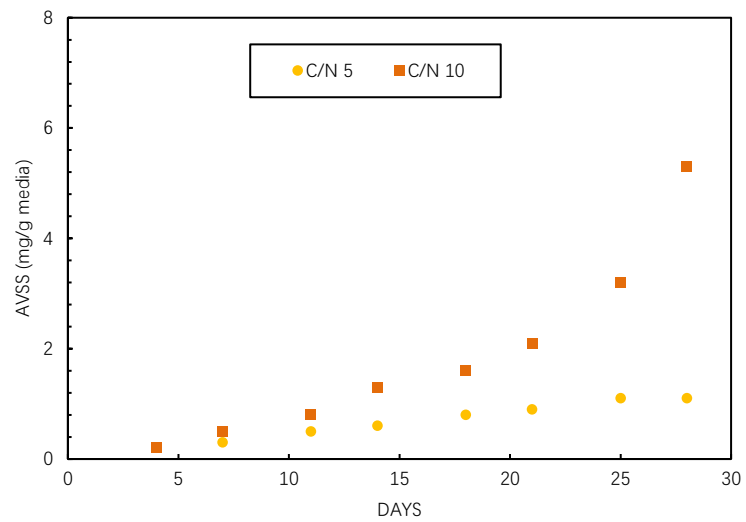
Figure 3.7 Attached VSS with various COD concentration (for PEC over 4h HRT).
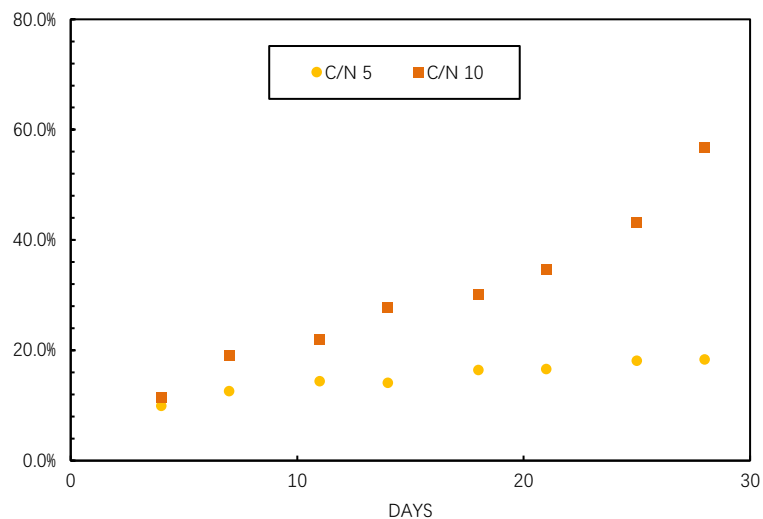
Figure 3.8 Fraction of attached VSS with various COD concentration (for PEC over 4h HRT).

As described above, short HRT which could impede suspended biomass growth and high COD which could accelerate growth process, can promote biofilm formation. A couple of tests were set to investigate the significance of this two factors, HRT and COD concentration as Table 3.1. Form Figure 3.9, low COD set had more attached biomass than high COD set. The fraction of attached biomass under high COD started to drop in the end. There was no chance for attached biomass to accumulate, because suspended biomass became dominant. When looking at the fraction of low COD, a low increase indicated that attached biomass could grow continuously, and the only problem was more time required. In conclusion, two factors all can influence the attachment process, but short HRT assured the possibility of attachment and COD concentration influenced the time of attached process.

Table 3.1 Operational conditions for identifying significance of HRT and COD concentration.

Material	HRT (h)	Influent COD (mg/L)	C/N
PEC	4	150	5
PEC	8	300	10
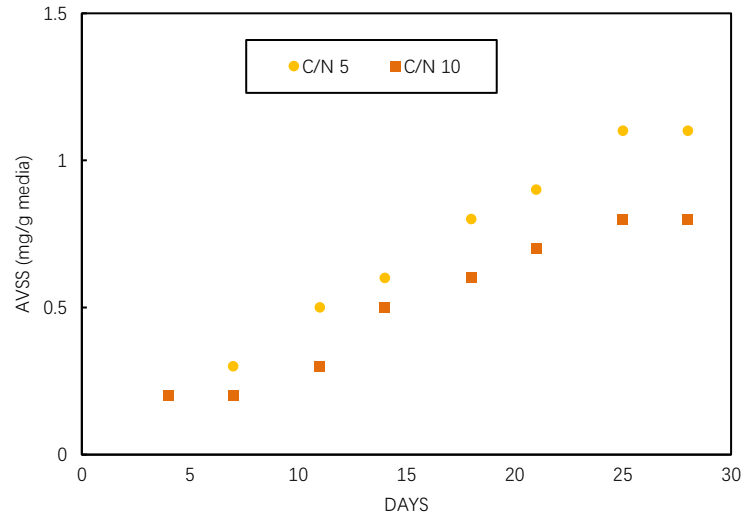
Figure 3.9 Attached VSS at same OL (various HRT and COD concentration for PEC).
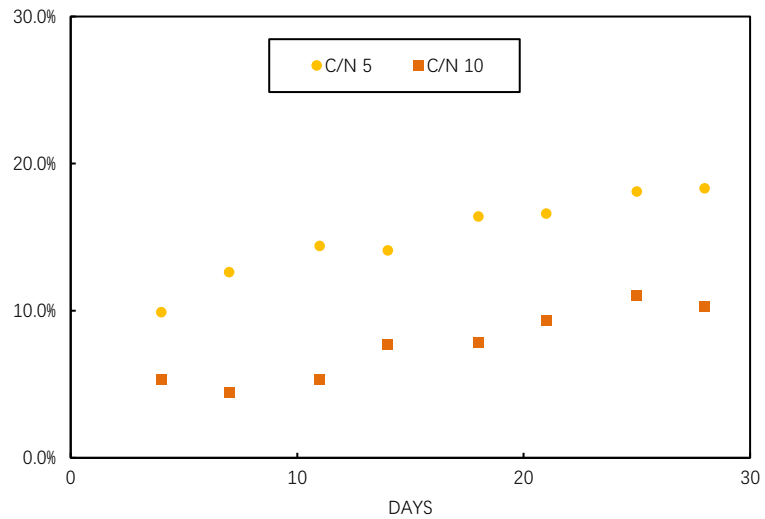
Figure 3.10 Fraction of attached VSS at same OL (various HRT and COD concentration for PEC).

3.2   Steady state

Three particles, PP, PE and PEC were tested in steady state under different HRT and C/N ratios. Influent and effluent characteristics for different media and operational conditions were listed in following tables. Biofilm characteristics and nutrient removal

efficiency were used to evaluate the performance of these medium. Statistic T-tests about COD and ammonia removal efficiency and attached VSS were done to confirm the difference between PE and PEC (Appendix C).

Table 3.2 Influent and effluent characteristics for different particles, (a) 9.2h HRT and C/N=10; (b) 6.1h HRT and C/N=10; (c) 4.1h HRT and C/N=10; (d) 4.1h HRT and C/N=5.

* a number of samples 4 with a frequency of a sample each week.

	Influent	PE	PP	PEC
DO (mg/L)		4.62	7.12	4.43
PH	8.57	7.65	8.01	7.77
TCOD (mg/L)	300±2	53±4	75±4	66±5
SCOD (mg/L)	300±2	31±3	28±2	38±2
NH_4-N (mg/L)	30.3±0.3	1.9±0.3	8.8±0.4	0.9±0.3
NO_3-N (mg/L)	0	21.6±0.4	14±0.4	23.2±0.4
ALK (mg/L as $CaCO_3$)	309±3	149±5	204±4	134±3
EVSS (mg/L)		22±3	40±3	26±3
AVSS (mg VSS/g media)		4.8±0.3	0.5±0.1	6.6±0.2
C:N:P	100:10:1.3			

(a)

	Influent	PE	PP	PEC
DO (mg/L)		3.44	6.63	3.28
PH	8.46	7.93	8.42	7.88
TCOD (mg/L)	298±3	81±3	110±5	74±4
SCOD (mg/L)	298±3	39±2	34±2	43±3
NH_4-N (mg/L)	30.4±0.2	11±0.5	20.6±0.2	8.4±0.6
NO_3-N (mg/L)	0	12.6±0.6	0.7±0.1	15±0.6
ALK (mg/L as $CaCO_3$)	308±4	210±7	295±2	192±6
EVSS (mg/L)		38±4	65±3	35±3
AVSS (mg VSS/g media)		6.5±0.3	0.6±0.1	8.2±0.4
C:N:P	100:10:1.3			

(b)

	Influent	PE	PP	PEC
DO (mg/L)		2.63		1.98
PH	8.51	8.34		8.16
TCOD (mg/L)	302±2	107±4		101±6
SCOD (mg/L)	302±2	42±2		49±3
NH_4-N (mg/L)	30.6±0.3	19.5±0.9		13.1±0.5
NO_3-N (mg/L)	0	2.5±0.5		9.2±0.3
ALK (mg/L as $CaCO_3$)	305±4	282±3.9		233±3
EVSS (mg/L)		48±3		41±4
AVSS (mg VSS/g media)		9.4±0.4		10.7±0.6
C:N:P	100:10:1.3			

(c)

	Influent	PE	PP	PEC
DO (mg/L)		3.53		2.87
PH	8.26	7.89		7.53
TCOD (mg/L)	148±2	47±2		44±2
SCOD (mg/L)	148±2	18±2		26±2
NH$_4$-N (mg/L)	30.5±0.2	14.3±0.4		2.5±0.5
NO$_3$-N (mg/L)	0	11.7±0.5		23.7±0.3
ALK (mg/L as CaCO$_3$)	304±2	216±3		131±2
EVSS (mg/L)		20±2		12±2
AVSS (mg VSS/g media)		6.1±0.4		7.4±0.5
C:N:P	50:10:1.3			

(d)

Table 3.3 Specific operational conditions for different particles, (a) 9.2h HRT and C/N=10; (b) 6.1h HRT and C/N=10; (c) 4.1h HRT and C/N=10; (d) 4.1h HRT and C/N=5.

	PE	PP	PEC
Influent flow (L/d)	8.6	8.6	8.6
Organic loading (g COD/L·d)	0.78	0.78	0.78
Nitrogen loading (g N/·d)	0.08	0.08	0.08
HRT (h)	9.2	9.2	9.2
Liquid velocity (cm/s)	2.6×10^{-3}	2.6×10^{-3}	2.6×10^{-3}
Gas flow (L/min)	0.5	0.9	0.4
Superficial gas velocity (cm/s)	0.22	0.39	0.17
AVSS (mg VSS/g media)	4.8	0.5	6.6
SVSS (mg/L)	995	1410	760
TVSS (g)	6.1	4.9	6.5
F/M (g COD/g VSS·d)	0.42	0.53	0.4
Detachment rate (d^{-1})	0.031	0.070	0.034
SRT (d)	32	14.3	29

(a)

	PE	PP	PEC
Influent flow (L/d)	13	13	13
Organic loading (g COD/L·d)	1.2	1.2	1.2
Nitrogen loading (g N/L·d)	0.12	0.12	0.12
HRT (h)	6.1	6.1	6.1
Liquid velocity (cm/s)	3.9×10^{-3}	3.9×10^{-3}	3.9×10^{-3}
Gas flow (L/min)	0.3	0.7	0.3
Superficial gas velocity (cm/s)	0.12	0.30	0.13
AVSS (mg VSS/g media)	6.5	0.6	8.2
SVSS (mg/L)	845	1570	715
TVSS (g)	6.7	5.5	7.3
F/M (g COD/g VSS·d)	0.59	0.73	0.53
Detachment rate (d^{-1})	0.074	0.154	0.063
SRT (d)	13.5	6.5	16

(b)

	PE	PP	PEC
Influent flow (L/d)	20		20
Organic loading (g COD/L·d)	1.8		1.8
Nitrogen loading (g N/L·d)	0.18		0.18
HRT (h)	4.1		4.1
Liquid velocity (cm/s)	6.0×10^{-3}		6.0×10^{-3}
Gas flow (L/min)	0.5		0.4
Superficial gas velocity (cm/s)	0.22		0.17
AVSS (mg VSS/g media)	9.4		10.7
SVSS (mg/L)	660		565
TVSS (g)	7.9		8.4
F/M (g COD/g VSS·d)	0.75		0.71
Detachment rate (d^{-1})	0.122		0.095
SRT (d)	8.2		10.5

(c)

	PE	PP	PEC
Influent flow (L/d)	20		20
Organic loading (g COD/L·d)	0.91		0.91
Nitrogen loading (g N/L·d)	0.18		0.18
HRT (h)	4.1		4.1
Liquid velocity (cm/s)	6.0×10^{-3}		6.0×10^{-3}
Gas flow (L/min)	0.3		0.2
Superficial gas velocity (cm/s)	0.13		0.09
AVSS (mg VSS/g media)	6.1		7.4
SVSS (mg /L)	410		460
TVSS (g)	5.0		5.9
F/M (g COD/g VSS·d)	0.6		0.51
Detachment rate (d^{-1})	0.080		0.041
SRT (d)	12.5		24.6

(d)

3.2.1 Biofilm characteristics

Attached biomass

Biofilm characteristics including quantity of biofilm and morphology were various for each particle under every operating condition. For PE, biomass including attached and suspended was filamentous with fluff, and that usually partially trapped bioparticle. For PEC, biomass was accumulated as flocculent mass. For PP, biomass was observed in form of firm organic sphere. The reasons of different shapes for each media were mentioned above. PEC had roughest surface from activated carbon natural structure and beneficial material properties, such as potentials. PP and PEC belonged to polymer

without features as activated carbon, while they had advantages on mechanical and chemical stability and more hydrophobic. With influence by shear force, weak surface support would lead to reduced biofilm and higher detachment.

With flow rate increasing, total biomass increased obviously due to overall organic loading rate increase. Attached biomass increase was not only because of incremental organic loading but also enhanced loss of suspended biomass with larger flow rate. Attached VSS for PE, PP and PEC under 9.2h HRT were 4.8, 0.5 and 6.6 mg VSS/g media respectively. Attached VSS for PE, PP and PEC under 6.1h HRT were 6.5, 0.6 and 8.2 mg VSS/g media respectively. When C/N ratio was altered, attached biomass decayed from 9.4 and 10.7 mg/g media under 4.1h HRT to 6.1 and 7.4 mg/g media for PE and PEC. That acute detachment came from decreasing C/N ratio. Furthermore, 9.4 and 10.7 mg/g media were the peak of attached biomass in this case. In general, PE and PEC had a larger amount of attached biomass compared with PP with below 1.0 mg/g media, and that disappointing performance of PP lasted for two HRT tests, so the PP column was shut down in rest of tests.

With attached VSS data, the estimated biofilm thickness in this case using Eq. 37 with biofilm wet density of 1.002 g/cm^3 (Zhang & Bishop, 1994) is shown in Table 3.4. Biofilm thicknesses for PP under 9h and 6h HRT were 13 and 16 μm respectively, while for PE under the same conditions, biofilm thickness were 130 and 179 μm respectively. Similarly, biofilm thickness for PEC were 179 and 222 μm respectively. Meanwhile, when C/N decreased from 10 to 5, biofilm thickness for PE and PEC under 4h HRT decreased from 255 and 290 μm to 165 and 200 μm respectively.

$$\delta = \frac{M_{attached}}{\rho_{biofilm} \times A_{surface}} \tag{37}$$

$$A_{surface} = N \times \pi d^2 \tag{38}$$

N = number of particle in the column calculated by dividing the total particles mass by the mass of each particle, 2923 for PEC, 2754 for PP and 2875 for PEC.

Figure 3.11 shows the relationship between biofilm thickness and organic loading rate for each particle. Obviously, for PE and PEC the biofilm thickness increase with organic loading rate increase. Specifically, the biofilm thickness for PE increased from 130 to 255 μm with organic loading rate increasing from 0.78 to 1.8 g COD/L d with a slope of 150.7. Similarly, for PEC, the biofilm thickness for PE increase from 179 to 290 μm with organic loading rate increasing from 0.78 to 1.8 g COD/L d with a slope of 181.5. However, biofilm thickness for PP remain at low level, 13 and 16 μm for 0.78 and 1.2 g COD/L d respectively. It is evident from Figure 3.11 that the biofilm thickness did not increase linearly with organic loading rate.

Table 3.4 Biofilm thickness for three different particles.

Particles	HRT (h)	Organic loading (g COD/L·d)	Attached VSS (mg VSS/g media)	Biofilm thickness (μm)
PP	9	0.78	0.5	13
PP	6	1.2	0.6	16
PE	9	0.78	4.8	130
PE	6	1.2	6.5	176
PE	4 (high C/N)	1.8	9.4	255
PE	4 (low C/N)	0.91	6.1	165
PEC	9	0.78	6.6	179
PEC	6	1.2	8.2	222
PEC	4 (high C/N)	1.8	10.7	290
PEC	4 (low C/N)	0.91	7.4	200
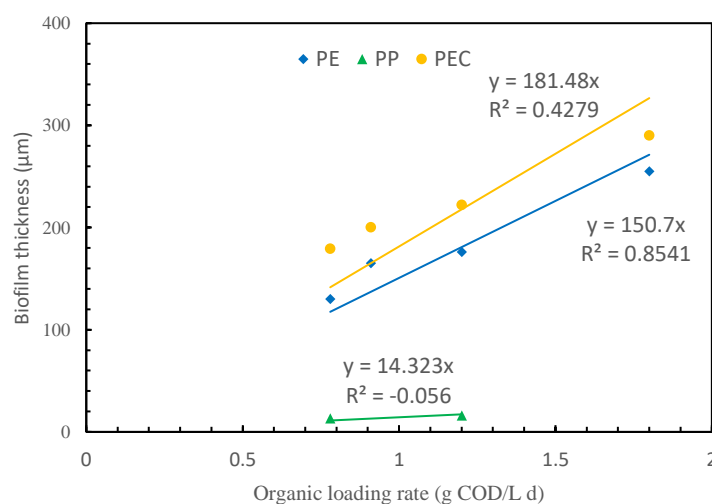
Figure 3.11 Correlations between organic loading rate and biofilm thickness.
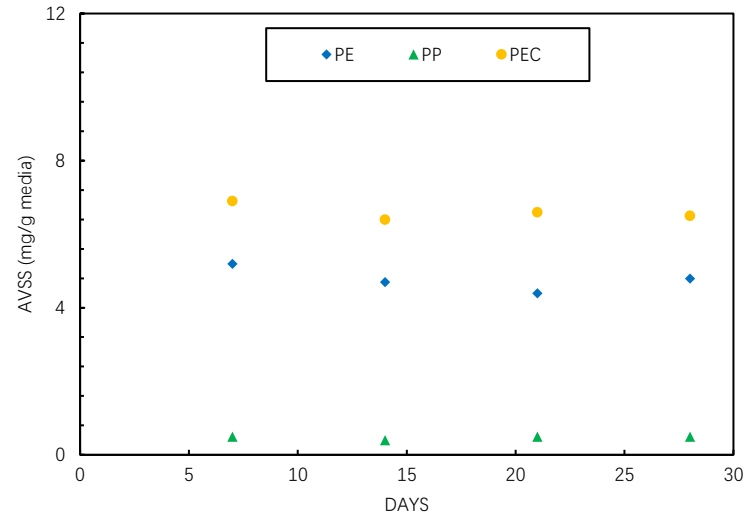
(a)
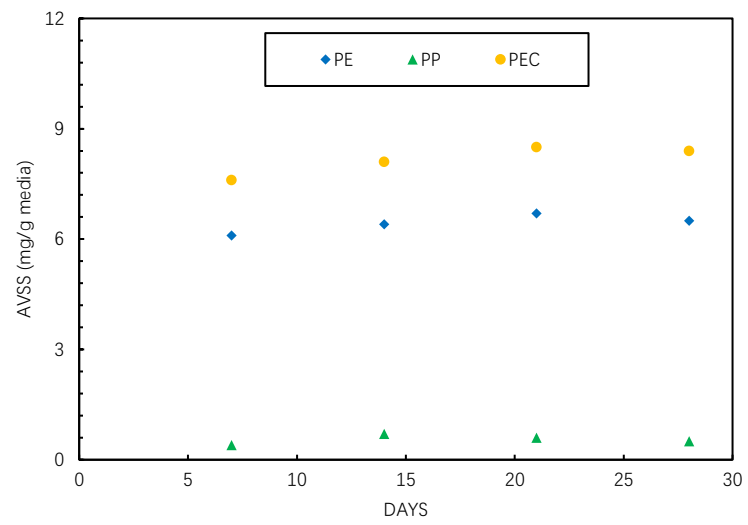
(b)
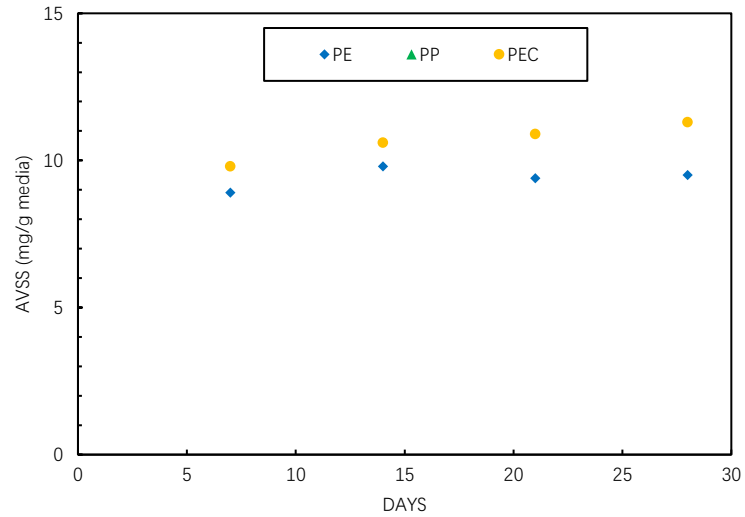
(c)
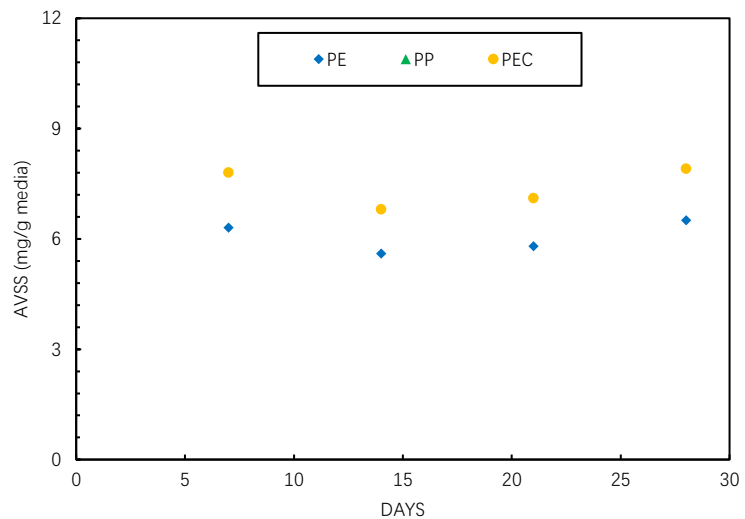
(d)

Figure 3.12 Attached VSS for different particles, (a) 9.2h HRT and C/N=10; (b) 6.1h HRT and C/N=10; (c) 4.1h HRT and C/N=10; (d) 4.1h HRT and C/N=5.

Biomass yield

Biomass yield was calculated by total VSS produced divided by COD consumed in system when the system is in steady state. In this case, biomass yield was calculated as the sum of the net change in attached biomass and effluent VSS divided by the total COD consumed.

The biomass yields for PP, PE and PEC under 9h HRT were 0.15, 0.08 and 0.08 g VSS/g COD respectively. For 6h HRT, the biomass yields were 0.25, 0.15 and 0.14 g

VSS/g COD respectively. Also, under 4 HRT (high C/N) and 4 HRT (low C/N), the biomass yields were 0.19, 0.15 for PE and 0.18 and 0.09 g VSS/g COD for PEC respectively. As a result of organic loading increasing from 0.78 to 1.8 g COD/L·d, biomass yield increased as well. True yield could be calculated by observed yield and SRT. Using typical value of b (0.12 g VSS/g VSS·d) and f_d (0.1 g VSS/g VSS), true yield for all medium under each operation conditions were listed in Table 3.5.
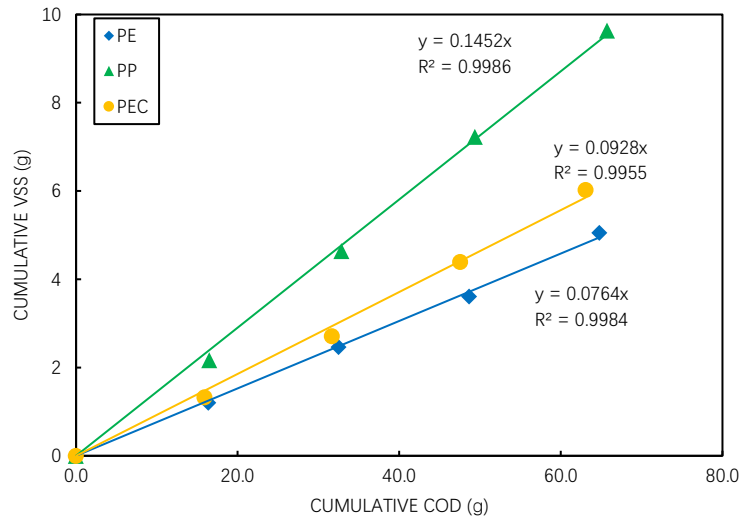
(a)
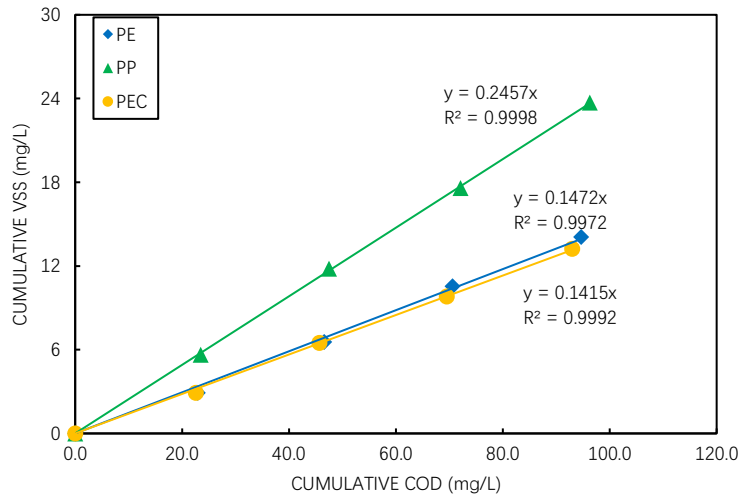
(b)
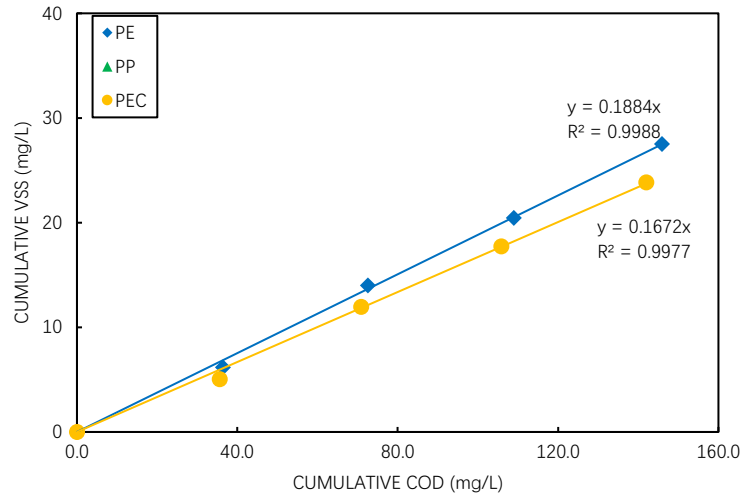
(c)
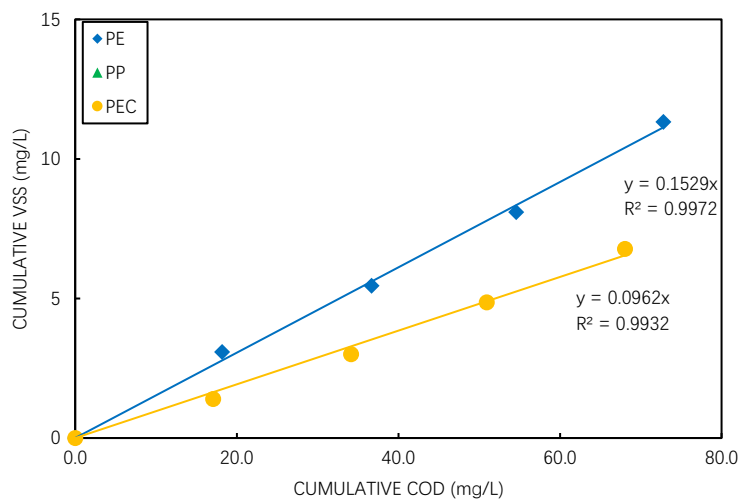
(d)

Figure 3.13 Biomass yield for different particles, (a) 9.2h HRT and C/N=10; (b) 6.1h HRT and C/N=10; (c) 4.1h HRT and C/N=10; (d) 4.1h HRT and C/N=5.

Table 3.5 True yield for three particles over various operational conditions.

Particles	HRT (h)	Observed yield (g VSS/g COD)	True yield (g VSS/g COD)	SRT (d)
PP	9	0.15	0.35	14.3
PP	6	0.25	0.41	6.5
PE	9	0.08	0.28	32
PE	6	0.15	0.34	13.5
PE	4 (high C/N)	0.19	0.34	8.2
PE	4 (low C/N)	0.15	0.33	12.5
PEC	9	0.09	0.30	29
PEC	6	0.15	0.36	16
PEC	4 (high C/N)	0.17	0.34	10.5
PEC	4 (low C/N)	0.10	0.30	24.6

Detachment rate

Specific biofilm detachment rate was calculated through total biomass detachment per day divided by total attached biomass on particles as Eq. 39. As previous anaerobic fluidized bed bioreactor research, main factors of detachment were the fraction solids, the hydrodynamic shear force and the Reynold number of the flow (Turan, 2000). Detachment rate increased with the fraction solids and the hydrodynamic shear force increasing and the Reynold number decreasing. In a word, shear force including attrition between particles and hydrodynamic shear force, was the dominant reason for biofilm detachment. In this case, gas was introduced to replace liquid flow to fluidize particles. Unfortunately, there was no accurate relations between gas shear force and gas flow rate in three phase fluidized bed. However, detachment rate influenced by gas shear force was 10 to 100 times than only influenced by liquid solid shear force (Trinet et al., 1991).

$$r_b = \frac{X_E Q}{M X_A} \tag{39}$$

r_b = specific biofilm detachment rate, d^{-1}

X_E = the amount of biomass (as VSS) leaving the reactor with effluent, mg/L

Q = flow rate, L/d

X_A = the amount of attached biomass, mg/g media

M = total mass of particles, g

Detachment rates for the three particles under each operational condition are listed in Table 3.6. Based on Table 3.6, a multi-variable linear regression analysis was completed for detachment rate with factors including biofilm thickness, liquid velocity, superficial gas velocity and superficial gas velocity to liquid velocity ratio. A linear model was developed as Eq. 40. In the model, Y is detachment rate and x_1 to x_4 are liquid velocity, superficial gas velocity and superficial gas velocity to liquid velocity ratio and biofilm thickness respectively. The multiple R is 0.98 which means that the combination of independent variables (x) are significantly relative to dependent variable

(y). R Square for this model is 0.97 which means that the independent variables (x) could illustrate about 97% of dependent variable (y).

0.06183693, -8.9760255, 1.12189644, -0.0027351 and -0.0001033 are coefficients for each factor. Besides that, T-Tests for each factor were completed to evaluate the dependency with the detachment rate. The P value for superficial gas velocity and superficial gas velocity and liquid velocity ratio are 0.00024 and 0.00058 which are much smaller than 0.05, meaning that these two factors are highly significant to detachment rate. However, for biofilm and liquid velocity, the P value are higher than 0.05, and that means they do not significantly affect the detachment rate.

$$Y = 0.06183693 - 8.9760255x_1 + 1.12189644x_2 - 0.0027351x_3 - 0.0001033x_4$$

$$(40)$$

Figures 3.14 to 3.17 show the individual relationship between the detachment rate and each of the aforementioned variables. After excluding outliers (red points), relations for each factor are described by linear equations. R^2 for superficial gas velocity and superficial gas to liquid velocity ratio are 0.94 and 0.70 respectively, meaning that they are more relative to detachment rate. However, for biofilm thickness and liquid velocity, R^2 are 0.52 and 0.39 meaning they do not significantly affect the detachment rate.

There were several conclusions, based on models and Table 3.6:

1. At same organic loading, detachment rate increased with the increase of superficial gas velocity. For example, PP and PE with organic loading of 0.78 g COD/L·d, detachment rates were 0.07 and 0.03 d^{-1} with superficial gas velocity as 0.39 and 0.22 cm/s.

2. Increased organic loading could aggravate detachment rate, due to high organic loading leading to thicker biofilm which was unstable.

3. As mentioned above in the literature review, although particle properties could influence detachment rate, there was no obvious evidence to prove that in this case.

4. Liquid shear force could influence the detachment rate, but it was not dominant compared with gas shear force.

Table 3.6 Detachment rate for three particles over various operational conditions.

Particles	Biofilm thickness (μm)	Liquid velocity (cm/s)	Superficial gas velocity (cm/s)	Detachment rate (d^{-1})
PP	13	2.6×10^{-3}	0.39	0.07
PP	16	3.9×10^{-3}	0.30	0.15
PE	130	2.6×10^{-3}	0.22	0.03
PE	176	3.9×10^{-3}	0.12	0.07
PE	255	6.0×10^{-3}	0.22	0.12
PE	165	6.0×10^{-3}	0.13	0.08
PEC	179	2.6×10^{-3}	0.17	0.03
PEC	222	3.9×10^{-3}	0.13	0.06
PEC	290	6.0×10^{-3}	0.17	0.10
PEC	200	6.0×10^{-3}	0.09	0.04

Table 3.7 Multi-variable linear regression analysis for detachment rate.

		Coefficients	t Stat	P-value
Intercept		0.06183693	2.49436693	0.05486697
Liquid velocity (cm/s)	x_1	-8.9760255	-1.9411401	0.10991022
Superficial gas velocity (cm/s)	x_2	1.12189644	9.28147009	0.00024416
Superficial gas velocity/Liquid velocity	x_3	-0.0027351	-7.7302927	0.00057869
Biofilm thickness (μm)	x_4	-0.0001033	-1.7947273	0.13265507
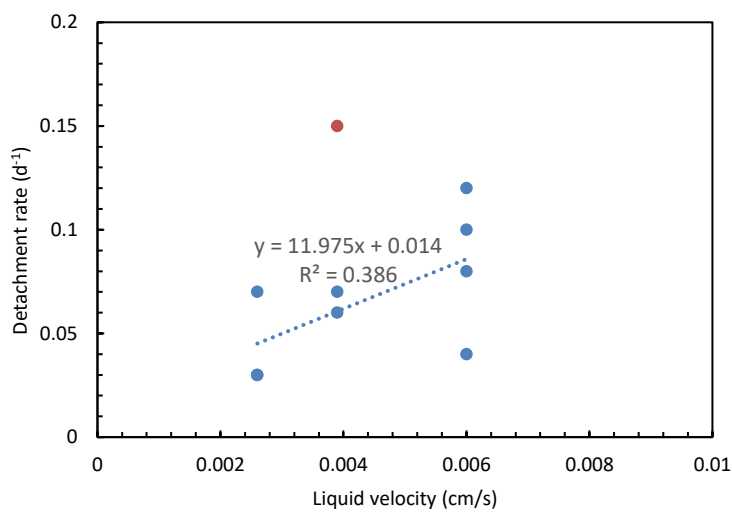
Figure 3.14 Detachment rate under different liquid velocity.
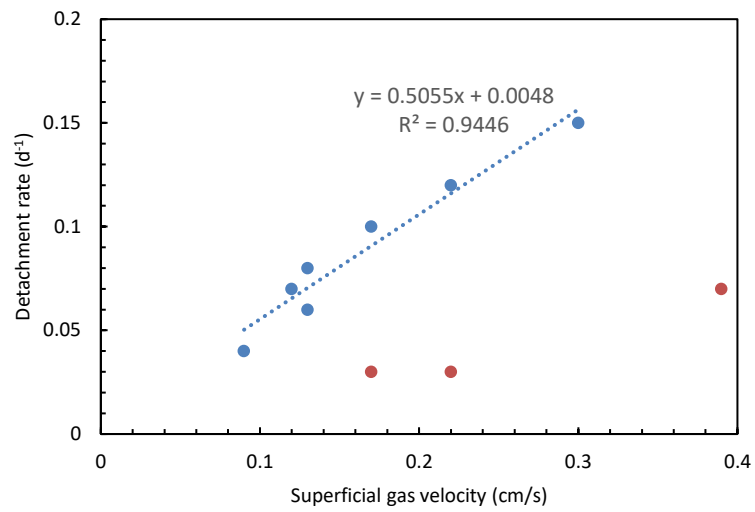
Figure 3.15 Detachment rate under different superficial gas velocity.
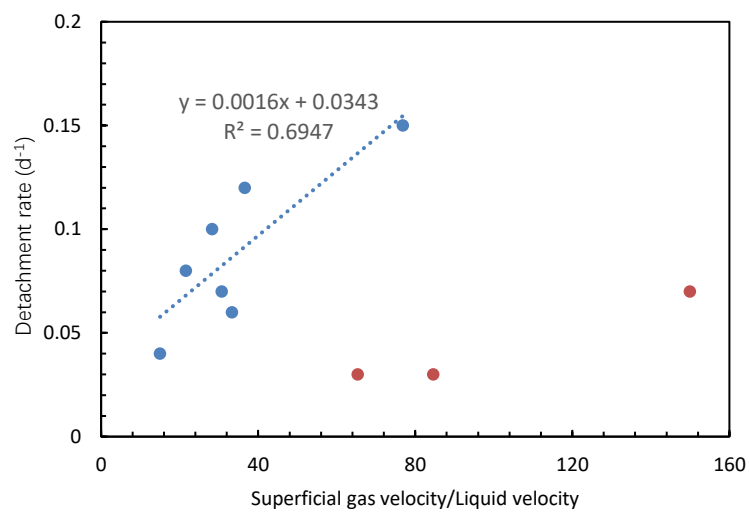
Figure 3.16 Detachment rate under different superficial gas to liquid velocity ratio.
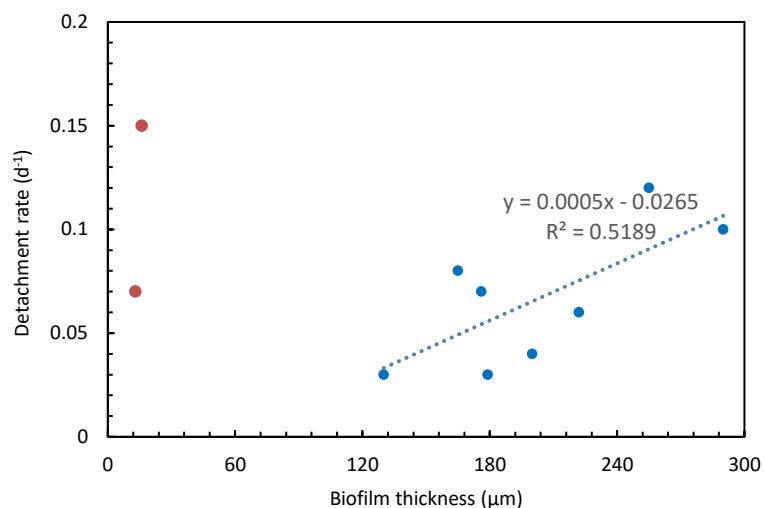
Figure 3.17 Detachment rate under different biofilm thickness.

Except for indicating the biofilm stability, detachment rate also related to SRT which could influence bioreactions, like nitrification, thereby influencing nutrient removal efficiency and system performance. Generic detachment rate in aerobic column in circulating fluidized bioreactor was reported in range of 0.017 to 0.026 d^{-1}, while nitrifier detachment rate in aerobic column was reported from 0.15 to 0.23 d^{-1} (Patel et al., 2005). The difference between previous work and result of this case was engendered by different system structure. For circulating fluidized bioreactor, liquid was applied to fluidize particles rather than gas. Because of existing aerobic and anaerobic column, most of COD was consumed in anaerobic column so that biofilm in circulating fluidized bed was not as thick as the biofilm in this case. Therefore, detachment rate of previous works was definitely lower than this work.
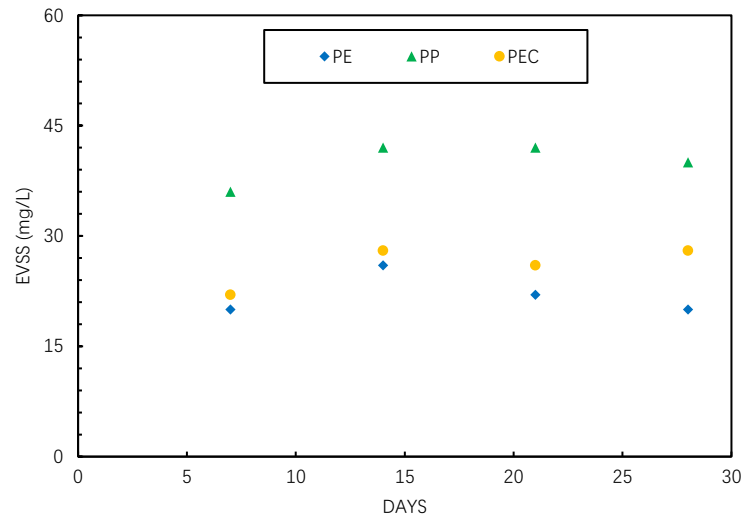
(a)
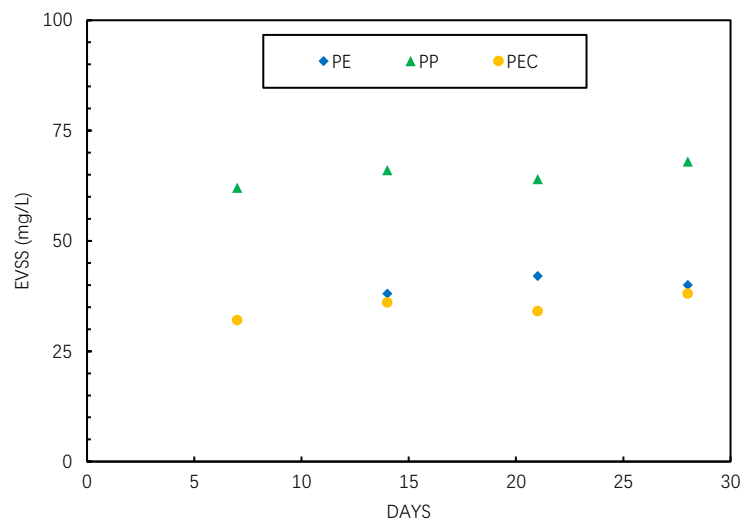
(b)
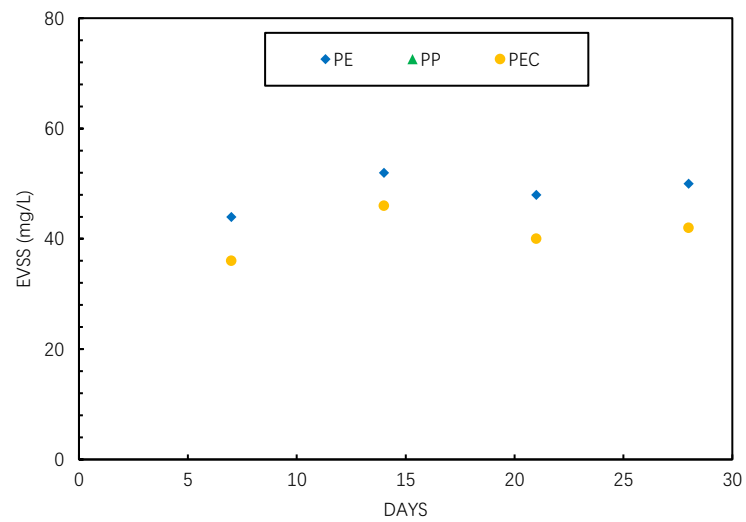
(c)
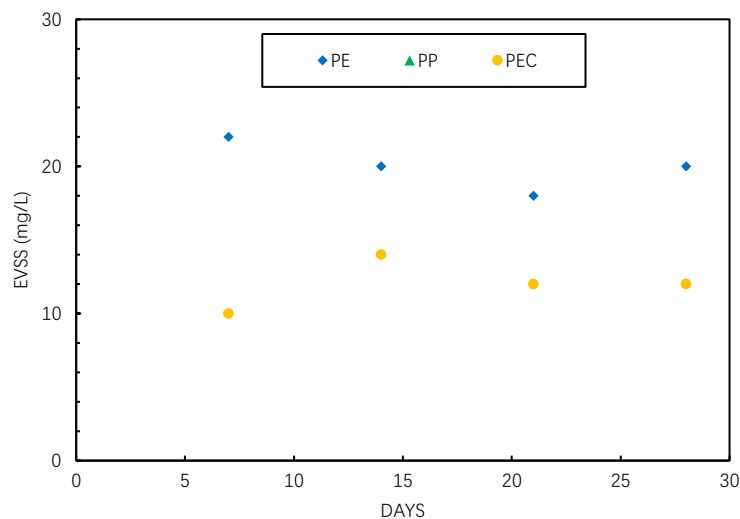
(d)

Figure 3.18 Effluent VSS for different particles, (a) 9.2h HRT and C/N=10; (b) 6.1h HRT and C/N=10; (c) 4.1h HRT and C/N=10; (d) 4.1h HRT and C/N=5.

3.2.2   Organic and nutrient removal efficiencies

Organic removal

Influent and effluent soluble COD were presented in following figures. Effluent SCOD for three particles under various conditions were all within the range of 20 to 50 mg/L. COD removal efficiencies of PP, PE and PEC with organic loading as 0.78 g COD/L·d were 90.7%, 89.7% and 87.3% respectively. With organic loading increasing, efficiencies slightly decreased to 88.6%, 86.9% and 85.6% of PP, PE and PEC with organic loading as 1.2 g COD/L·d. Meanwhile, efficiencies for PE and PEC with organic loading as 1.8 and 0.91 g COD/L·d, were 86.1%, 83.8%, 87.8% and 82.4% respectively.

When considering total COD as remained COD, COD removal efficiencies of PP, PE and PEC with organic loading as 0.78 g COD/L·d, were 75%, 82.3% and 78% respectively. Efficiencies of PP, PE and PEC with organic loading as 1.2g COD/L·d, were 63.1%, 72.8% and 75.2% respectively. Efficiencies for PE and PEC with organic loading as 1.8 and 0.91 g COD/L·d, were 64.6%, 66.6%, 68.2% and 70.3% respectively.
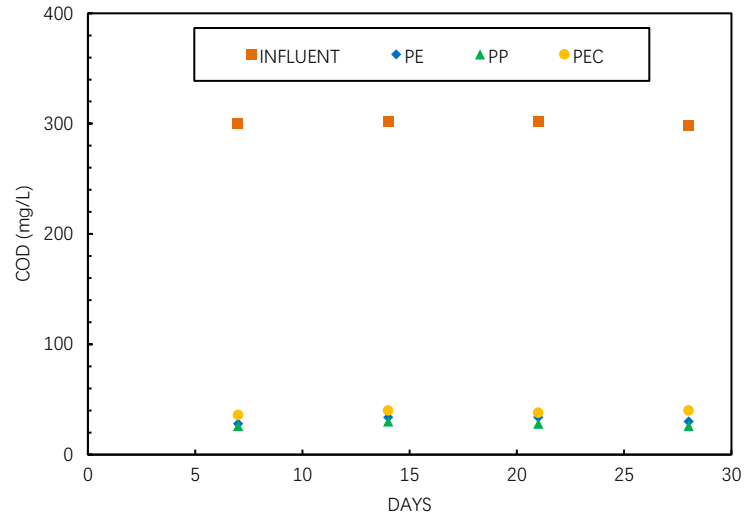
(a)
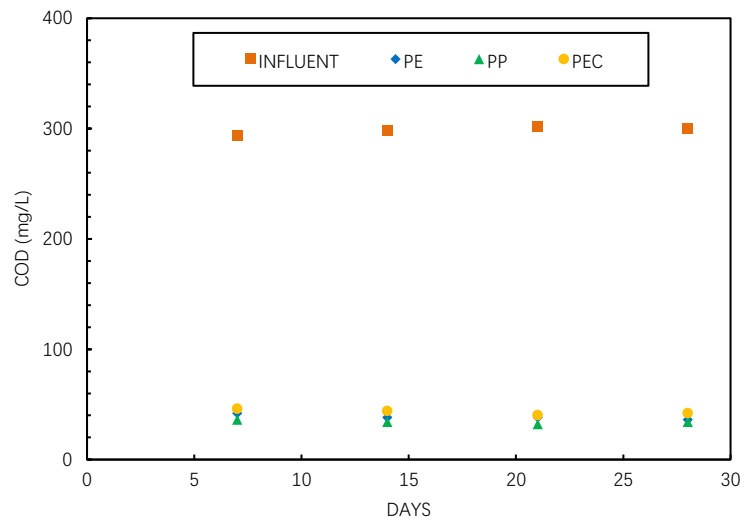
(b)
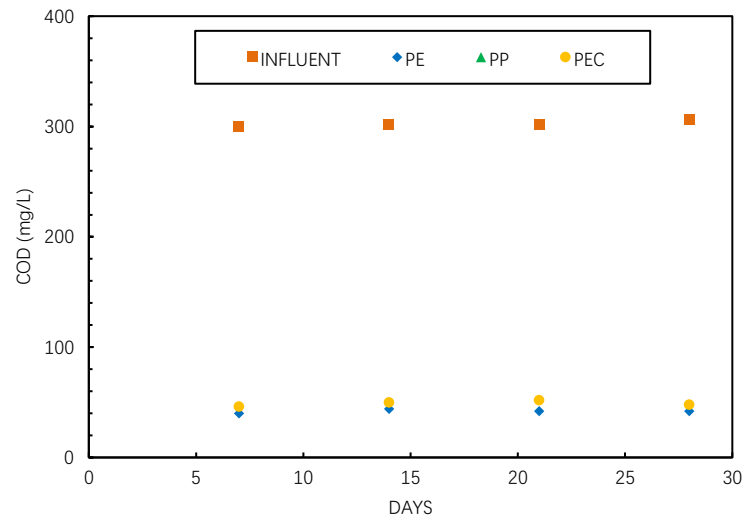
(c)
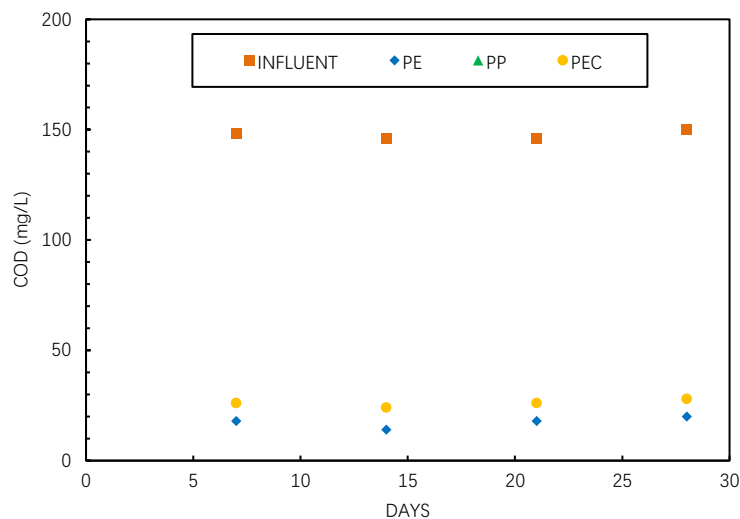
(d)

Figure 3.19 Influent and effluent SCOD for different particles, (a) 9.2h HRT and C/N=10; (b) 6.1h HRT and C/N=10; (c) 4.1h HRT and C/N=10; (d) 4.1h HRT and C/N=5.

The sequence of removal efficiency was PP, PE and PEC which corresponded to the amount of suspended biomass and condition of biofilm. Suspended biomass accessed nutrients and oxygen more easily than attached biomass (Bassin et al., 2016). PP had the most suspended biomass and the least attached biomass. PE had fewer attached biomass and loose structure than the biofilm on PEC. Besides, COD removal efficiency decreased with HRT decreasing was explained by decreasing fraction of suspended biomass. TCOD removal efficiency supported same theory, because PP became the worst media due to high effluent VSS and high fraction of suspended biomass. Furthermore, the performance of PP showed that more COD was stored in biomass rather than oxidized to H_2O and CO_2 which agreed with high true yield. On the contrary, PEC had relatively low yield which performed as the highest removal efficiency of TCOD. In another word, more COD was utilized for energy rather than synthesizing biomass.
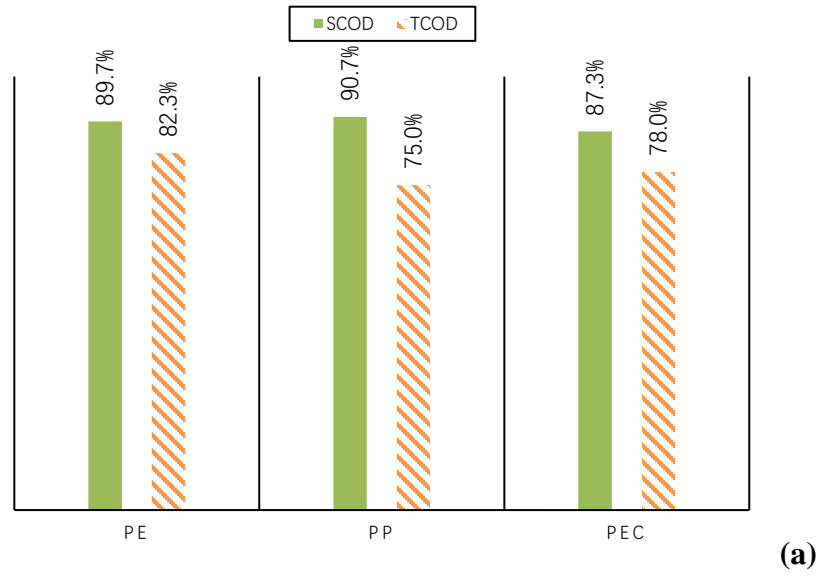
(a)
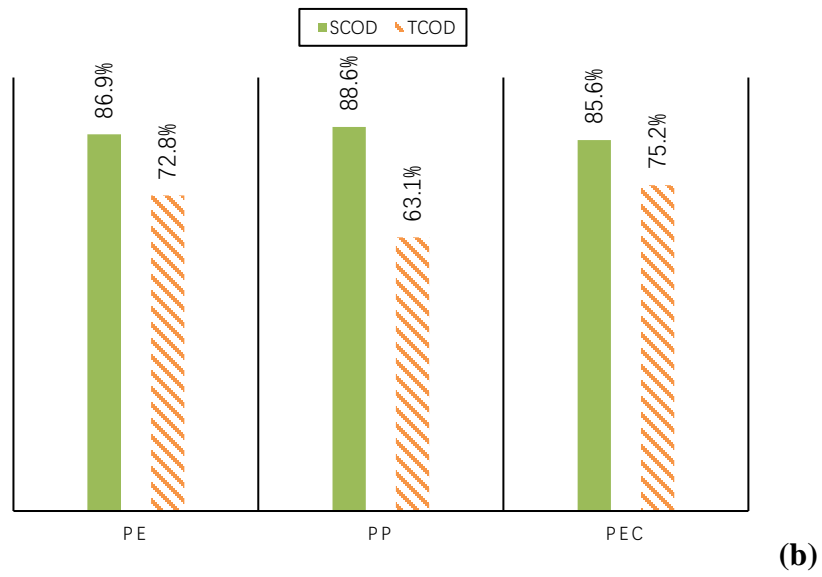
(b)
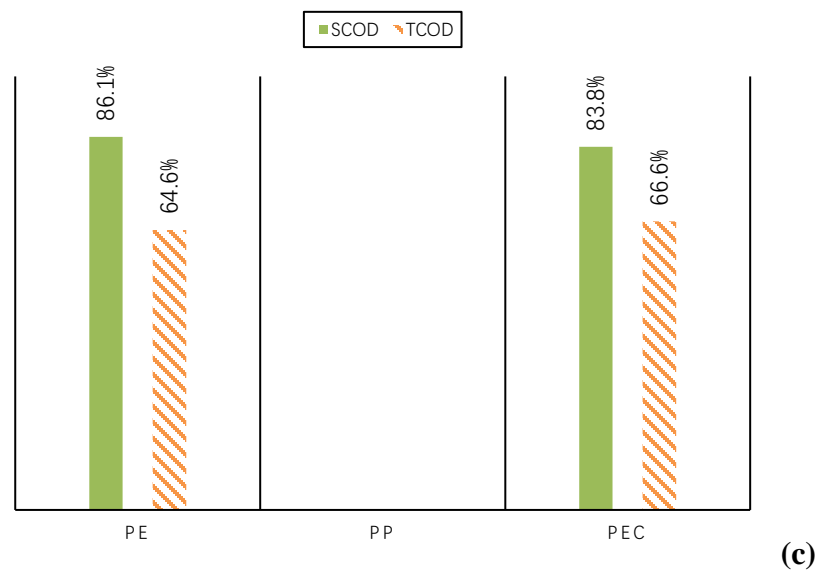
(c)
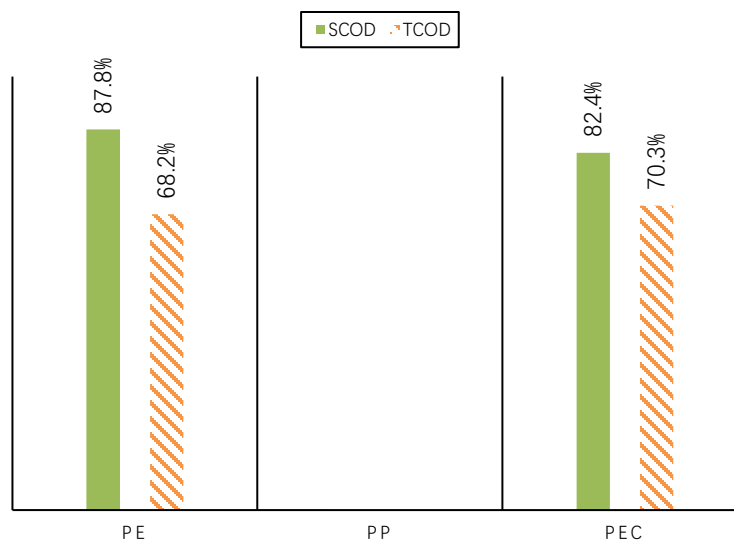
(d)

Figure 3.20 COD removal efficiency for different particles, (a) 9.2h HRT and C/N=10; (b) 6.1h HRT and C/N=10; (c) 4.1h HRT and C/N=10; (d) 4.1h HRT and C/N=5.

Nitrogen removal

As shown in following figures, effluent ammonia varied exaggeratively from 0.9 (9h HRT) to 21 mg/L (4h HRT) with flow rate increase. Ammonia removal efficiencies for PP, PE and PEC with nitrogen loading as 0.08 g N/L·d, were 71.0%, 93.7% and 97.0% respectively. Among removed nitrogen, 46.2%, 71.3% and 76.6% of influent ammonia was removed by nitrification of PP, PE and PEC, which was calculated by alkalinity. For nitrogen loading as 0.12 g N/L·d, PP, PE and PEC had influent ammonia removal efficiencies as 32.2%, 63.8% and 72.4%, thereinto 2.3%, 41.5% and 49.3% of influent ammonia were removed by nitrification respectively. For nitrogen loading as 0.18 g N/L·d, PE and PEC had ammonia removal efficiencies as 36.3% and 57.2%, thereinto 8.2% and 30.1% of influent ammonia were removed by nitrification respectively. From figures, most ammonia was removed through nitrification, though a part of nitrogen was utilized by microorganisms to synthesis themselves.

The minimum generation time for nitrifier was about 3d (Soliman & Eldyasti, 2018). Theoretically, if minimum generation time was smaller than SRT, nitrifier could reproduce in the systems. But practically SRT should be equal to three times of minimum generation time which was 10d to guarantee that nitrifier could exist successfully (Guo et

al., 2014; Soliman & Eldyasti, 2018). Besides, when COD was in high level, longer SRT should be set to keep nitrifiers in system. SRTs at 4h HRT were only 8.2d for PE and 10.5d for PEC and for PP at 6h HRT is just 6.5d. It was reported that most of N was removed by suspended biomass (Bassin et al., 2016). Within short SRT, few portions of nitrifier could existed in liquid.

The maximum specific growth rate of nitrifier was 0.77 d^{-1}, while for aerobic organic degeneration microorganisms was 7.2 d^{-1} which was 10 times than nitrifier's (Wiesmann, 1994). On the condition that nutrients were sufficient, fraction of nitrifier would continue decreasing close to zero which meant nitrifier was rare in system. Furthermore, nitrification species had higher detachment rate of 0.15 to 0.23 d^{-1} than maximum value of generic bacteria in this work (Patel et al., 2005). That would enhance nitrifier loss.

As calculated above, under condition of sufficient carbon and nitrogen source, nitrifier required more oxygen to reach same μ/μ_{max} for aerobic organic oxidation microorganisms (Wiesmann, 1994). Hence, on condition of limited resources, nitrifier would fail the competition with generic microorganisms. Accounting for low growth rate, nitrifiers usually occupied the inside layer of biofilm. Though it was impossible to calculate accurate oxygen concentration distribution inside biofilm, mass transfer efficiency could be limited when the thickness of biofilm was around 100 μm (Karamanev & Nikolov, 1996). The biofilm thickness in this case was estimated in Table 3.4.

$$\delta = \frac{M_{attached}}{\rho_{biofilm} \times A_{surface}} \tag{41}$$

Table 3.8 Micro-environment data at different depths in biofilms (Zhou et al., 2011).

	Superficial biofilm	Deep biofilm	Reference
Fraction of active biomass	72% ~ 91%	31% ~ 39%	Zhang & Bishop, 1994
Biofilm density (g/cm^{-3})	8 ~ 18	91 ~ 108	Yu, 2008
Porosity	84% ~ 93%	58% ~ 67%	Zhang & Bishop, 1994
DO (mg/L)	5.8	Close to 0	Zhou, 2007
Oxygen diffusion coefficient compared with bulk liquid coefficient	90%	25%	Zhang & Bishop, 1994

Owing to high COD concentration impeding growth of nitrifier and enhancing biomass loss, a low C/N ratio test was set with C/N equal to 5. PE and PEC had total N removal efficiencies as 53.1% and 91.8%, thereinto 38.4% and 77.7% of total nitrogen is removed by nitrification respectively.
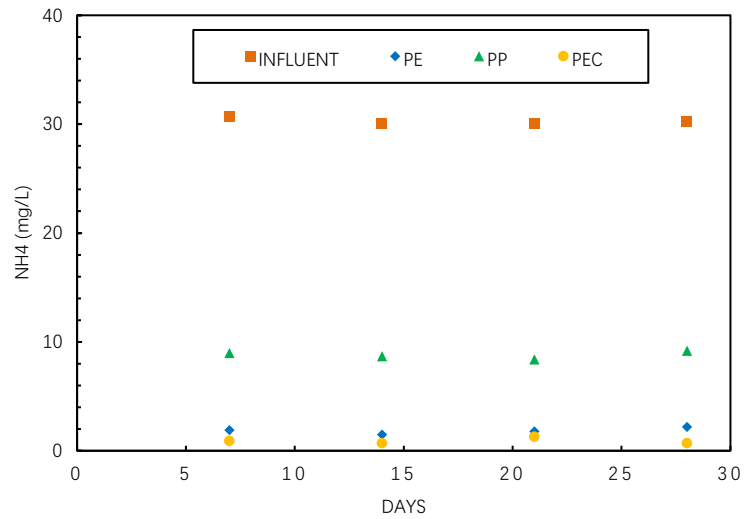
(a)
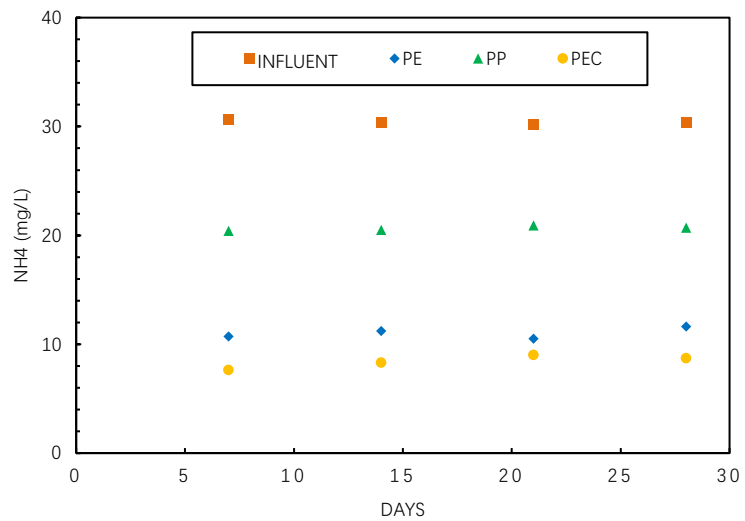
(b)
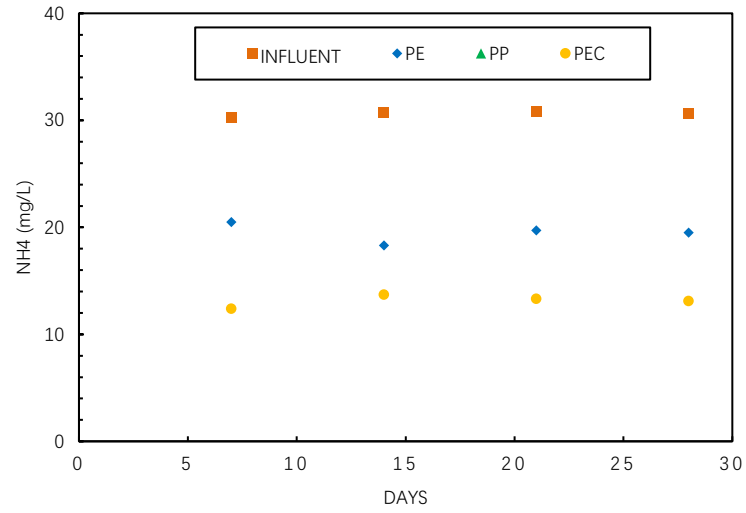
(c)
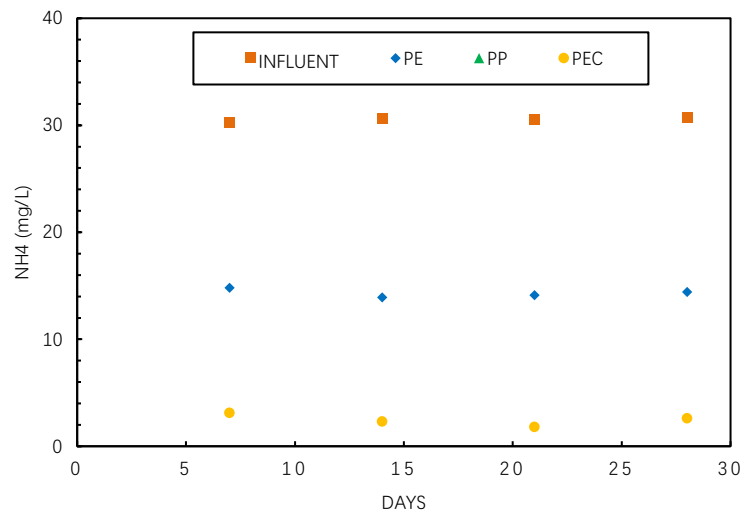
(d)

Figure 3.21 Influent and effluent ammonia for different particles, (a) 9.2h HRT and C/N=10; (b) 6.1h HRT and C/N=10; (c) 4.1h HRT and C/N=10; (d) 4.1h HRT and C/N=5.
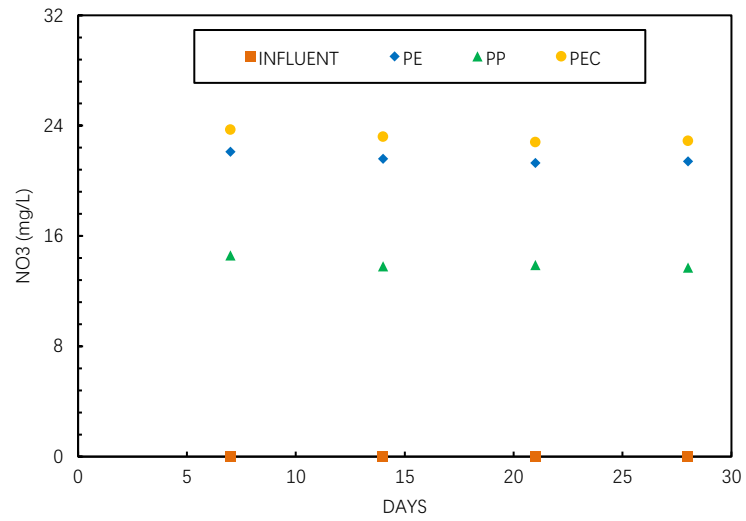
(a)
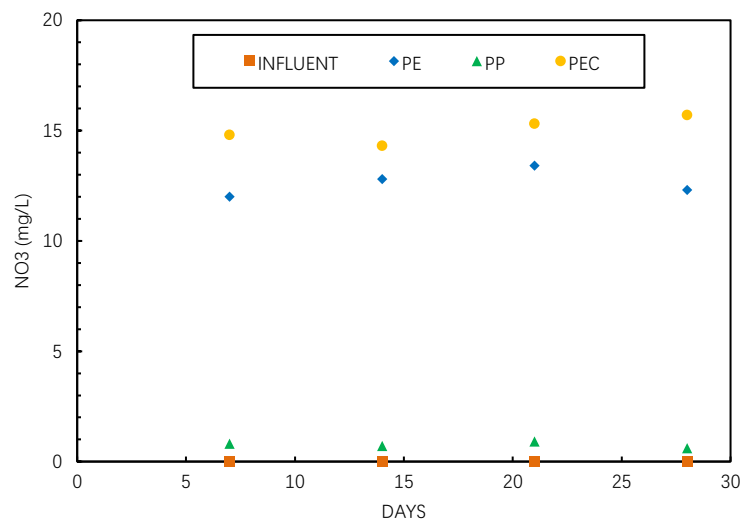
(b)
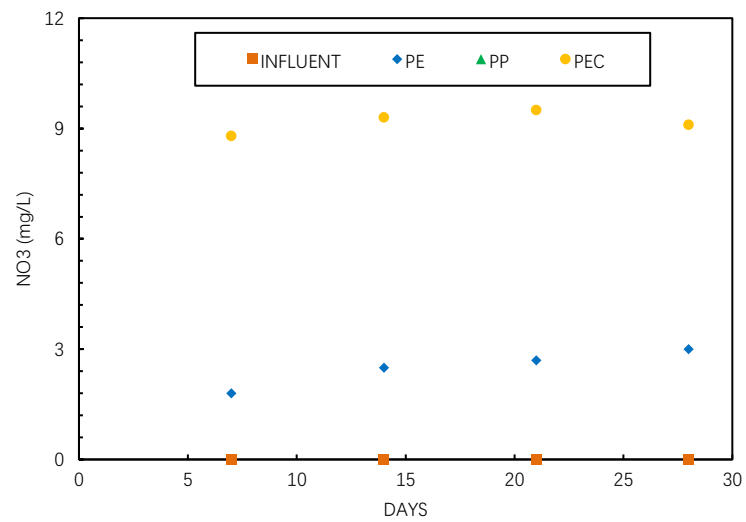
(c)
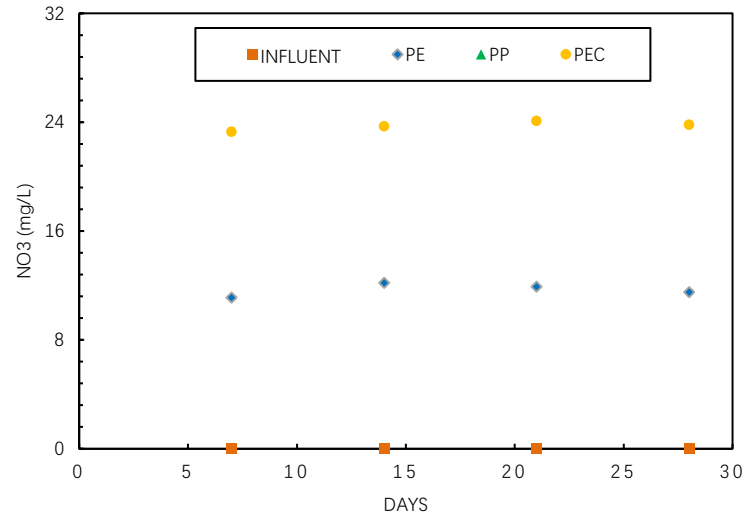
(d)

Figure 3.22 Influent and effluent nitrate for different particles, (a) 9.2h HRT and C/N=10; (b) 6.1h HRT and C/N=10; (c) 4.1h HRT and C/N=10; (d) 4.1h HRT and C/N=5.
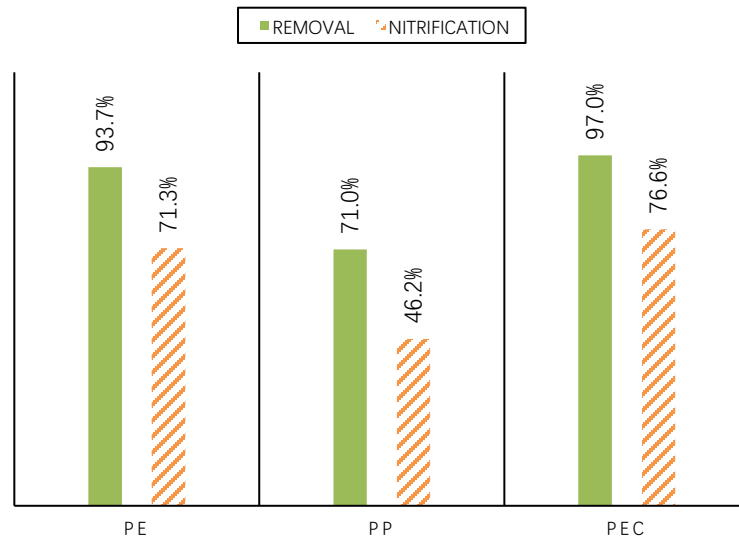
(a)
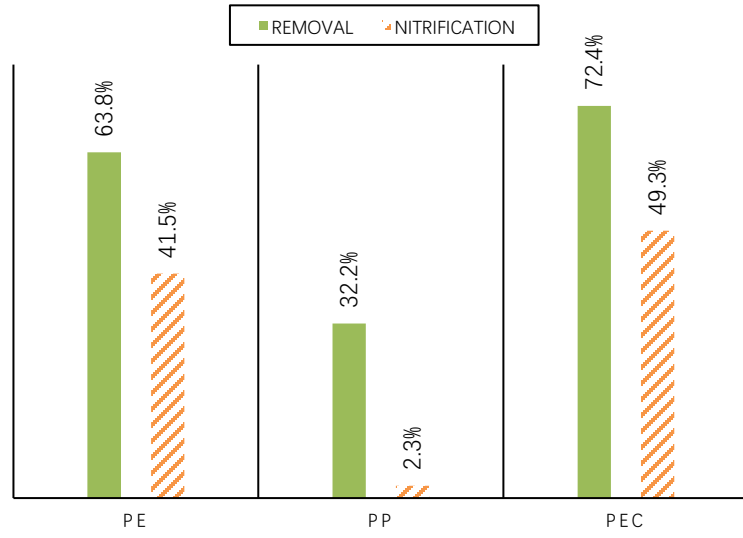
(b)
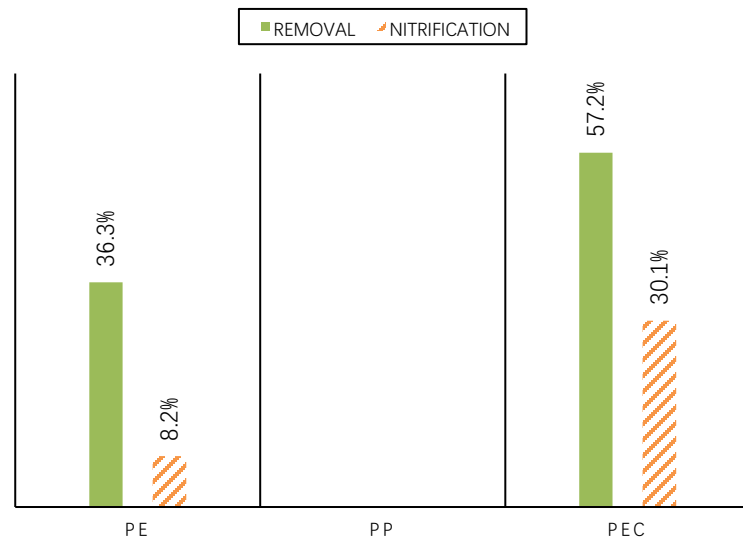
(c)
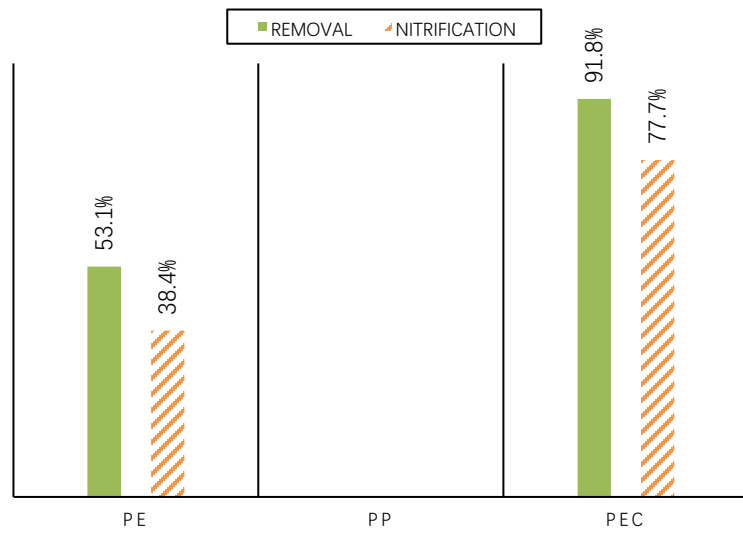
(d)

Figure 3.23 N removal efficiency for different particles, (a) 9.2h HRT and C/N=10; (b) 6.1h HRT and C/N=10; (c) 4.1h HRT and C/N=10; (d) 4.1h HRT and C/N=5.

3.2.3 Overall nutrient mass balance

Nitrogen balance

The treatment pathway of nitrogen in aerobic column were effluent ammonia, oxidized ammonia and nitrogen as component of organism ($C_5H_7NO_2$) in effluent biomass.

$$N - Nitrification = NO_{3_{eff}} - NO_{3_{in}} \tag{42}$$

$$\%N\ closure = \frac{Ammonia_{ntrification} + Ammonia_{eff} + N_{biomass}}{Ammonia_{in}} \tag{43}$$

For PE under 9h HRT, 6.3% of influent nitrogen flowed away as untreated ammonia; 9.0% of total nitrogen was used to synthesize biomass; 71.3% of total nitrogen was oxidized to NO_3. Similarly, the untreated ammonia, nitrogen of synthesizing biomass and oxidized ammonia were 29.0%, 16.4%, 46.2% for PP and 3.0%, 76.6%, 6.5% for PEC under 9h HRT. Therefore, the nitrogen closure of PE, PP and PEC were calculated by sum of three parts as 86.6%, 91.6% and 86.1% respectively.

For 6h HRT, the nitrogen closure of PE, PP and PEC were 93.2%, 96.6% and 91.2% respectively. Also, under 4 HRT (high C/N) and 4 HRT (low C/N), the nitrogen closure of PE and PEC were 91.3%, 89.5%, 93.4% and 90.8% respectively. PP had highest closure due to nitrification being so weak that most nitrogen was left untreated.
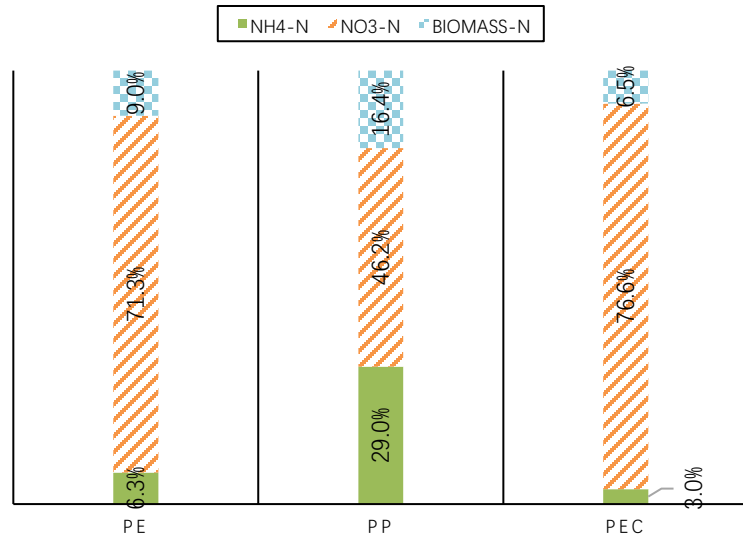
(a)
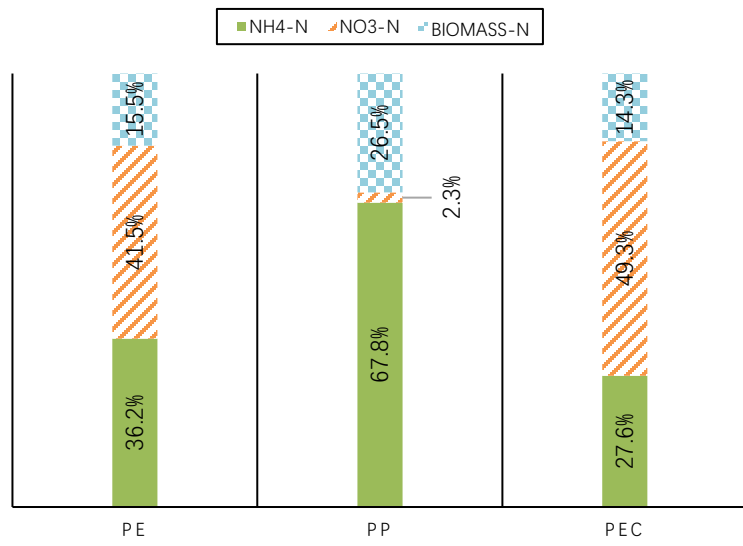
(b)
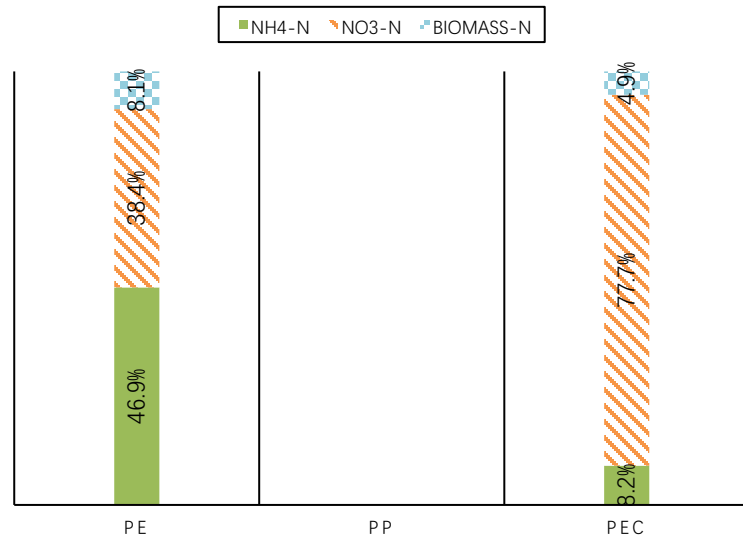
(c)
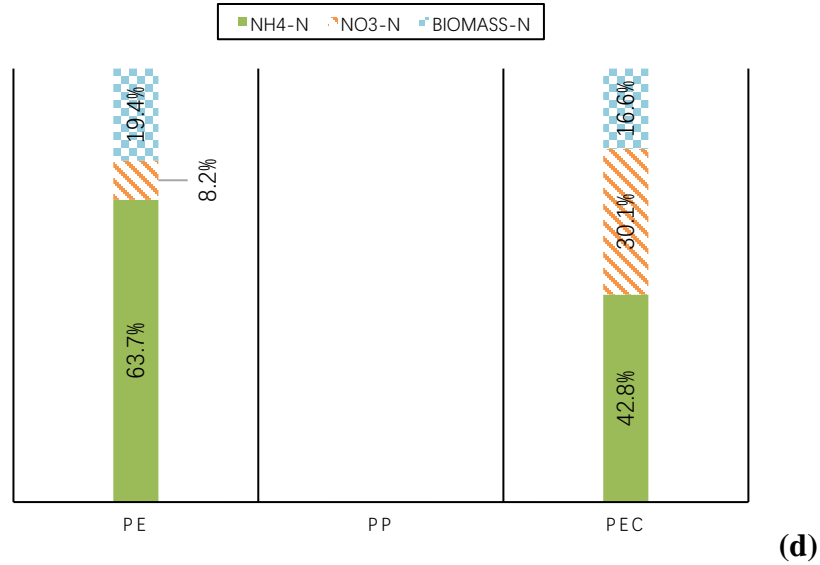
Figure 3.24 N balance for different particles, (a) 9.2h HRT and C/N=10; (b) 6.1h HRT and C/N=10; (c) 4.1h HRT and C/N=10; (d) 4.1h HRT and C/N=5.

Alkalinity balance

Corresponding to nitrogen balance, alkalinity balance was calculated by surplus alkalinity in effluent and theoretically consumed alkalinity which equals to $7.14 \times NO_3$.

$$ALK_{consumed} = 7.14(NO_{3_{eff}} - NO_{3_{in}}) \tag{44}$$

$$\%ALK\ closure = \frac{ALK_{consumed} + ALK_{eff}}{ALK_{in}} \tag{45}$$

For PE under 9h HRT, 48.2% of influent alkalinity was still left in effluent and the value of theoretically consumed alkalinity divided by influent alkalinity was 49.9%. For other two particles, PP and PEC, percentages of alkalinity loss and theoretically consumed alkalinity were 66%, 32.3%, 43.3% and 53.6% respectively. Therefore, the alkalinity closure of PE, PP and PEC were 98.1%, 98.3% and 97% respectively.

Furthermore, for 6h HRT, the alkalinity closure of PE, PP and PEC were 97.4%, 97.4% and 97.1% respectively. Also, under 4 HRT (high C/N) and 4 HRT (low C/N), the nitrogen closure of PE and PEC were 98.4%, 97.9%, 98.6% and 98.8% respectively.

(a)

(b)
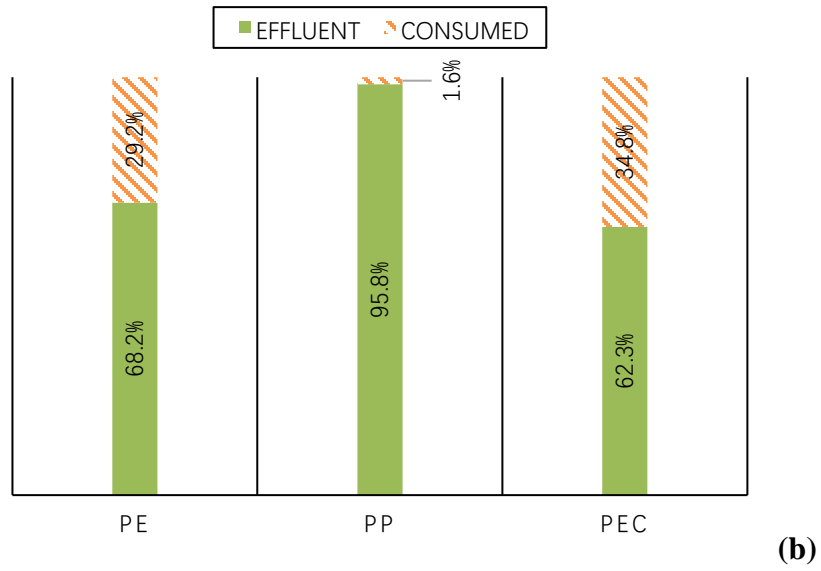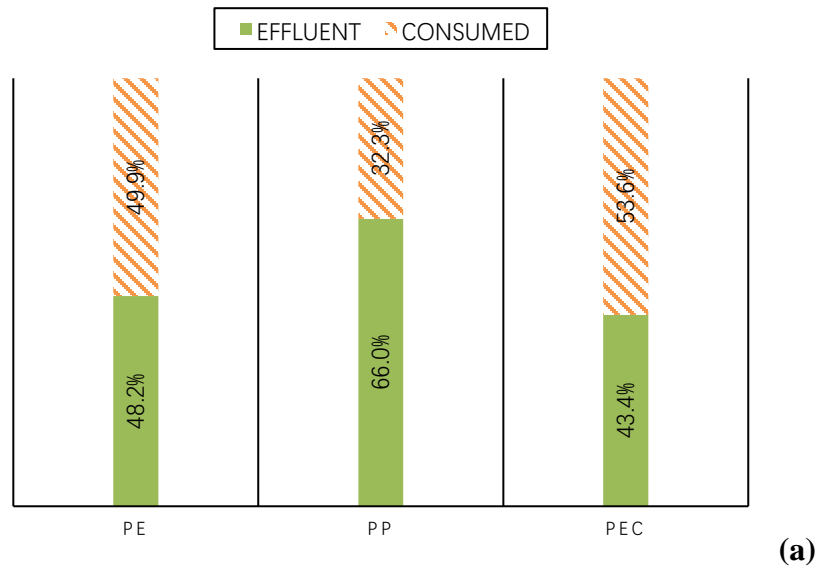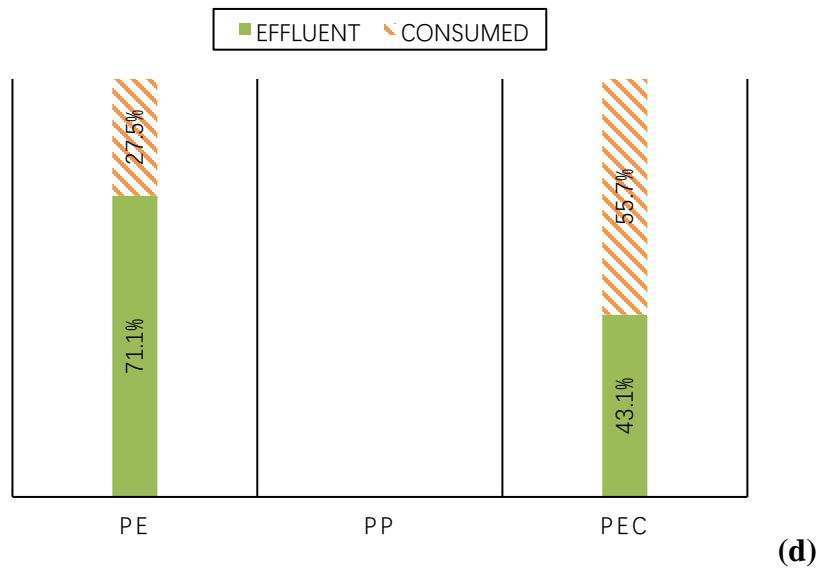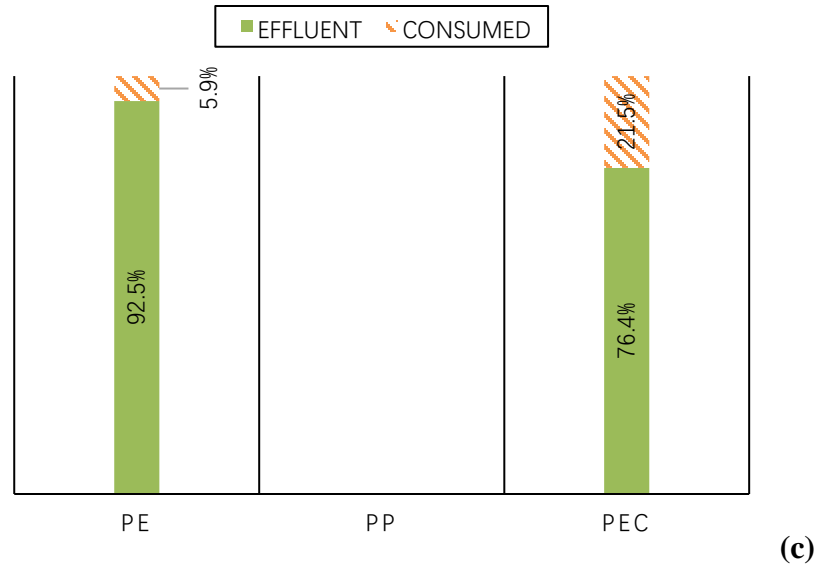
Figure 3.25 Alkalinity balance for different particles, (a) 9.2h HRT and C/N=10; (b) 6.1h HRT and C/N=10; (c) 4.1h HRT and C/N=10; (d) 4.1h HRT and C/N=5.

Chapter 4

4 Conclusions and recommendations

4.1 Conclusions

Attachment rate and biofilm quantity in the startup stage and biofilm characteristics and nutrient removal efficiency in steady state were analyzed to evaluate three different particles in three parallel aerobic fluidized bed bioreactors under various operational conditions. There were several conclusions:

1. For startup stage, HRT and COD concentration both can influence attachment process. Short HRT assured the possibility of attachment and COD concentration decided the time of attached process. Optimized conditions should have short HRT, and high influent COD, such as 4h and 300 mg/L.

2. Under best startup conditions, PE got attached in 15 days with 9 mg VSS/g media in the end. PEC got attached in 20 days with 5.5 mg VSS/g media in the end. PP had below 1.0 mg VSS/g media in the end. In steady state, peak attached biomasses were 9.4 and 10.7 mg VSS/g media for PE and PEC respectively. Plus, PEC had lowest suspended biomass fraction and detachment rate. Those phenomena could be explained by surface roughness and material properties, such as hydrophobic and zeta potentials.

3. The morphology for the three types of particles: For PE, biomass was filamentous with fluff; for PEC, biomass was accumulated as flocculent mass; for PP, biomass was observed in form of firm organic sphere.

4. The three types of particles had similar COD removal efficiency, about 85% ~ 90%. For nitrogen removal, PEC had highest efficiency of 91.8% (4h HRT, 5 C/N).

5. Shear force has great influence on attachment process, because it could enhance detachment to shorten SRT then to influence system performance. A model based on experimental model was developed to estimate detachment rate.

4.2　　Recommendations

For inverse fluidized bed bioreactor, carrier particles must be lighter than water. So, generally carrier particles are plastic particles which have similar properties. Therefore, modification is the only choice to produce particles with outstanding performance. In this case, PE is modified to produce PEC. There are two directions of modification, shape and property. For surface modification, several examples are listed in introduction, such as oxidation etching method.

For inverse fluidized bed bioreactor, one of the advantages is energy economy, because it uses gas to fluidize particles. However, the price for saving the cost from liquid circulating is a huge increase of gas flow rate. Large gas flow rate could increase air shear force. Thus, the balance between cost and system performance should be considered. The way of gas distribution should be researched in future.

Future work

1. Enriching the surface properties profile for three particles, such as surface roughness, zeta potentials and water contact angle.

2. Testing more particles to broaden the theories in this case.

3. Doing microbial community analyzing to identify influence of particle properties on microcosmic level.

Reference

Adelaide Wastewater Treatment Plant. (2018). Adelaide Wastewater Treatment Plant - 2017 Annual Report. Environmental & Engineering Services Department Wastewater Treatment Operations, city of London, Canada.

Ahmed, E., Shahrom, Z., Fatihah, S., & Pramanik, B. K. (2012). Biological aerated filters (BAFs) for carbon and nitrogen removal: A review. Journal of Engineering Science and Technology, 7(4), 428-446.

AL-Mashhadani, M. K. H., Wilkinson, S. J., & Zimmerman, W. B. (2015). Airlift bioreactor for biological applications with microbubble mediated transport processes. Chemical Engineering Science, 137, 243-253.

Andalib, M., Nakhla, G., & Zhu, J. (2010). Dynamic testing of the twin circulating fluidized bed bioreactor (TCFBBR) for nutrient removal from municipal wastewater. Chemical Engineering Journal, 162(2), 616-625.

Anderson-Glenna, M. J., Bakkestuen, V., and Clipson, N. J. W. (2008). Spatial and temporal variability in epilithic biofilm bacterial communities along an upland river gradient. Microb. Ecol. 64,407-418

Andrews, G. F. (1993). The yield equations in the modeling and control of bioprocesses. Biotechnology and Bioengineering, 42(5), 549-556.

Balaguer, M. D., Vicent, M. T., & Parfs, J. M. (1997). A comparison of different support materials in anaerobic fluidized bed reactors for the treatment of vinasse. Environmental Technology, 18(5), 539-544.

Barwal, A., & Chaudhary, R. (2014). To study the performance of biocarriers in moving bed biofilm reactor (MBBR) technology and kinetics of biofilm for retrofitting the existing aerobic treatment systems: A review. Reviews in Environmental Science and Bio/Technology, 13(3), 285-299.

Bassin, J. P., Dias, I. N., Cao, S. M. S., Senra, E., Laranjeira, Y., & Dezotti, M. (2016). Effect of increasing organic loading rates on the performance of moving-bed biofilm reactors filled with different support media: Assessing the activity of suspended and attached biomass fractions. Process Safety and Environmental Protection, 100, 131-141.

Birou, B., Marison, I. W., & Stockar, U. V. (1987). Calorimetric investigation of aerobic fermentations. Biotechnology and Bioengineering, 30(5), 650-660.

Bishop, P. L. (1997). Biofilm structire and kinetics. Water Science and Technology, 36(1), 287.

Boaventura, T. P., Miranda-Filho, K. C., Oréfice, R. L., & Luz, R. K. (2018). Influence of porosity of low-density polyethylene media on the maturation process of biofilters used in recirculating aquaculture systems. Aquaculture International, 26(4), 1035-1049.

Capdeville, B., & Nguyen, K. M. (1990). Kinetics and modeling of aerobic and anaerobic film growth. Water Science Technology, 22(1-2): 147-170.

Cerca, N., Pier, G. B., Vilanova, M., Oliveira, R., & Azeredo, J. (2005). Quantitative analysis of adhesion and biofilm formation on hydrophilic and hydrophobic surfaces of clinical isolates of staphylococcus epidermidis. Research in Microbiology, 156(4), 506-514.

Chang, C., Kolewe, K. W., Li, Y., Kosif, I., Freeman, B. D., Carter, K. R., . . . Emrick, T. (2016). Underwater superoleophobic surfaces prepared from polymer Zwitterion/Dopamine composite coatings. Advanced Materials Interfaces, 3(6), 1500521-n/a.

Chang, H. T., Rittmann, B. E., Amar, D., Heim, R., Ehlinger, O., & Lesty, Y. (1991). Biofilm detachment mechanisms in a liquid-fluidized bed. Biotechnology and Bioengineering, 38(5), 499-506.

Chowdhury, N., Nakhla, G., Zhu, J., & Islam, M. (2010). Pilot-scale experience with biological nutrient removal and biomass yield reduction in a liquid-solid circulating fluidized bed bioreactor. Water Environment Research, 82(9), 772-781.

Colasanti, R. (1992). Cellular automata models of microbial colonies. Binary, 4: 191-193.

Corapcioglu, M. O., & Huang, C. P. (1987). The surface acidity and characterization of some commercial activated carbons. Carbon, 25(4), 569-578.

Cui, Y., Nakhla, G., Zhu, J., & Patel, A. (2004). Simultaneous carbon and nitrogen removal in anoxic-aerobic circulating fluidized bed biological reactor (CFBBR). Environmental Technology, 25(6), 699-712.

Davey, M. E., and O'Toole, G. A. (2000). Microbial biofilms from ecology to molecular genetics. Microbiol. Mol. Biol. Rev. 64,847–867

Decho, A. W. (2000). Microbial biofilms in intertidal systems an overview. Cont. Shelf Res. 20,1257–1273

Dimitrov, D., Hadjiev, D., & Nikov, I. (2007). Optimisation of support medium for particle-based biofilm reactors. Biochemical Engineering Journal, 37(3), 238-245.

de Beer, D., Stoodley, P., Roe, F., & Lewandowski, Z. (1994). Effects of biofilm structures on oxygen distribution and mass transport. Biotechnology and Bioengineering, 43(11), 1131-1138.

Eldyasti, A., Nakhla, G., & Zhu, J. (2012). Influence of particles properties on biofilm structure and energy consumption in denitrifying fluidized bed bioreactors (DFBBRs). Bioresource Technology, 126, 162-171.

Feng, Q., Yu, A., Chu, L., & Xing, X. (2008). Performance study of the reduction of excess sludge and simultaneous removal of organic carbon and nitrogen by a combination of fluidized- and fixed-bed bioreactors with different structured macroporous carriers. Biochemical Engineering Journal, 39(2), 344-352.

Fu, Z., Yang, F., Zhou, F., & Xue, Y. (2009). Control of COD/N ratio for nutrient removal in a modified membrane bioreactor (MBR) treating high strength wastewater. Bioresource Technology, 100(1), 136-141.

G lli, R. (1987). Biodegradation of dichloromethane in waste water using a fluidized bed bioreactor. Applied Microbiology and Biotechnology, 27(2)

Gao, Y. (1999). Water pollution control engineering. Higher education press.

Gebara, F. (1999). Activated sludge biofilm wastewater treatment system. Water Research, 33(1), 230-238.

Gerbersdorf, S. U., Jancke, T., Westrich, B., and Paterson, D. M. (2008). Microbial stabilization of riverine sediments by extracellular polymeric substances. Geobiology 6,57–69

Gjaltema, A., Arts, P. A. M., Van Loosecht, M. C. M., Kuenen, J. G., & Heijnen, J. J. (1994). Heterogeneity of biofilms in rotating annular reactors: Occurrence, structure, and consequences. Biotechnology and Bioengineering 44(2), 194-204. (1994), 44(2), 194-204.

Gottenbos, B., van der Mei, H., & Busscher, H. (2000). Initial adhesion and surface growth of staphylococcus epidermidis and pseudomonas aeruginosa on biomedical polymers. Journal of Biomedical Materials Research, 50(2), 208-214.

Gottenbos, B., Van der Mei, H., Busscher, H., Grijpma, D., & Feijen, J. (1999). Initial adhesion and surface growth of pseudomonas aeruginosa on negatively and positively charged poly(methacrylates). Journal of Materials Science-Materials in Medicine, 10(12), 853-855.

Golladay, S. W., and Sinsabaugh, R. L. (1991). Biofilm development on leaf and wood surfaces in a boreal river. Freshwater Biol. 25,437–450

Guo, H., Zhang, Z., Sun, S., & Sun, D. (2014). Influencing factors of nitrous oxide production and emission in a/o process. Chinese Journal of Environmental Engineering, 8(6), 2515-2522.

Guo, Z., Sang, L., Wang, Z., Chen, Q., Yang, L., & Liu, Z. (2016). Deposition of copper thin films by plasma enhanced pulsed chemical vapor deposition for metallization of carbon fiber reinforced plastics. Surface & Coatings Technology, 307, 1059-1064.

Haribabu, K., & Sivasubramanian, V. (2016). Biodegradation of organic content in wastewater in fluidized bed bioreactor using low-density biosupport. Desalination and Water Treatment, 57(10), 4322-6.

Heijnen, J. J. (1984). Biological industrial waste-water treatment minimizing biomass production and maximizing biomass concentration. Ph.D. dissertation. Delft University of Technology. The Netherlands.

Heijnen, J. J., & Van Dijken, J. P. (1992). In search of a thermodynamic description of biomass yields for the chemotrophic growth of microorganisms. Biotechnology and Bioengineering, 39(8), 833-858.

Herbert, D., Elsworth, R., & Telling, R. C. (1956). The continuous culture of bacteria: a theoretical and experimental study. J. gen. Microbial, 14: 601-622.

Hoang, V., Delatolla, R., Abujamel, T., Mottawea, W., Gadbois, A., Laflamme, E., & Stintzi, A. (2014). Nitrifying moving bed biofilm reactor (MBBR) biofilm and biomass response to long term exposure to 1 °C. Water Research, 49, 215-224.

Hunt, S. M., Werner, E. M., Huang, B., Hamilton, M. A., & Stewart, P. S. (2004). Hypothesis for the role of nutrient starvation in biofilm detachment. Applied and Environmental Microbiology, 70(12), 7418-7425.

James, E. M. (1999). Polymer data handbook. Oxford university press.

Jackson, G., Beyenal, H., Rees, W. M., & Lewandowski, Z. (2001). Growing reproducible biofilms with respect to structure and viable cell counts. Journal of Microbiological Methods, 47(1), 1-10.

Jian, H., Zhang, X., Lo, X., Zhou, S., Cai, X., & Tso, W. (1983). Porous kaolinite bead: A novel but economical solid support material for biomass in fluidised bed technology. Biotechnology Letters, 5(2), 85-88.

Jiang, J., Yao, X., Xu, C., Su, Y., Zhou, L., & Deng, C. (2017). Influence of electrochemical oxidation of carbon fiber on the mechanical properties of carbon fiber/graphene oxide/epoxy composites. Composites Part A, 95, 248-256.

Jiang, X., Zhou, L., Liu, J., & Han, X. (2009). A model on attrition of quartzite particles as a bed material in fluidized beds. Powder Technology, 195(1), 44-49.

Jiang, Y., Wei, L., Zhang, H., Yang, K., & Wang, H. (2016). Removal performance and microbial communities in a sequencing batch reactor treating hypersaline phenol-laden wastewater. Bioresource Technology, 218, 146-152.

Karamanev, D. G., & Nikolov, L. N. (1996). Application of inverse fluidization in wastewater treatment: from laboratory to full-scale bioreactors. Environmental Progress & Sustainable Energy, 15(3), 194-196.

Kim, J., Kim, K., Ye, H., Lee, E., Shin, C., McCarty, P. L., & Bae, J. (2011). Anaerobic fluidized bed membrane bioreactor for wastewater treatment. Environmental Science & Technology, 45(2), 576-581.

Klausen, M., Gjermansen, M., Kreft, J., & Tolker-Nielsen, T. (2006). Dynamics of development and dispersal in sessile microbial communities: Examples from pseudomonas aeruginosa and pseudomonas putida model biofilms. FEMS Microbiology Letters, 261(1), 1.

Lee, C., Lee, E., Chun, Y., Han, C., & Lim, D. (2017). Effect of hydrogen plasma-mediated surface modification of carbon fibers on the mechanical properties of carbon-fiber-reinforced polyetherimide composites. Composites Part B, 116, 451-458.

Leenen, E. J. T. M., Dos Santos, V. A. P., Grolle, K. C. F., Tramper, J., & Wijffels, R. (1996). Characteristics of and selection criteria for support materials for cell immobilization in wastewater treatment. Water Research, 30(12), 2985-2996.

Leyva-Díaz, J. C., Martín-Pascual, J., & Poyatos, J. M. (2017). Moving bed biofilm reactor to treat wastewater. International Journal of Environmental Science and Technology, 14(4), 881-910.

Linton, J. D., & Stephenson, R. J. (1978). A preliminary study on growth yields in relation to the carbon and energy content of various organic growth substrates. FEMS Microbiology Letters, 3(2), 95-98.

Liu, Y., Yang, S., Li, Y., Xu, H., Qin, L., & Tay, J. (2004). The influence of cell and substratum surface hydrophobicities on microbial attachment. Journal of Biotechnology, 110(3), 251-256.

Lofrano, G., & Brown, J. (2010). Wastewater management through the ages: A history of mankind. Science of the Total Environment, 408(22), 5254-5264.

Lu, Y., Dagot, C., & Baudu, M. (2015). Nitrogen and phosphorus removal in a novel extra-loop fluidized bed bioreactor (EFBBR). Desalination and Water Treatment, 54(4-5), 1098-1108.

Luo, Y., Yang, H., Lu, L., & Qi, R. (2014). A review of the mathematical models for predicting the heat and mass transfer process in the liquid desiccant dehumidifier. Renewable and Sustainable Energy Reviews, 31, 587-599.

Mannina, G., Ekama, G. A., Capodici, M., Cosenza, A., Di Trapani, D., & Ødegaard, H. (2017). Moving bed membrane bioreactors for carbon and nutrient removal: The effect of C/N variation. Biochemical Engineering Journal, 125, 31-40.

Matsumoto, S., Ohtaki, A., & Hori, K. (2012). Carbon fiber as an excellent support material for wastewater treatment biofilms. Environmental Science & Technology, 46(18), 10175.

Mccarty, P. L. (1965). Thermodynamics of biological synthesis and growth. Air Water Pollut, 10: 621-39.

M C M van Loosdrecht, Eikelboom, D., Gjaltema, A., Mulder, A., Tijhuis, L., & Heijnen, J. J. (1995). Biofilm structures. Water Science and Technology, 32(8), 35.

Naz, I., Hodgson, D., Smith, A., Marchesi, J., Sehar, S., Ahmed, S., . . . Saroj, D. P. (2018). Investigation of the active biofilm communities on polypropylene filter media in a fixed biofilm reactor for wastewater treatment: Wastewater treating biofilms in polypropylene media reactors. Journal of Chemical Technology & Biotechnology, 93(11), 3264-3275.

Nelson, M. J., Nakhla, G., & Zhu, J. (2017). Fluidized-bed bioreactor applications for biological wastewater treatment: A review of research and developments. Engineering, 3(3), 330-342.

Noble, P. A., Park, H., Olson, B. H., Asvapathanagul, P., Hunter, M. C., Garrido-Baserba, M., . . . Rosso, D. (2016). A survey of biofilms on wastewater aeration diffusers suggests bacterial community composition and function vary by substrate type and time. Applied Microbiology and Biotechnology, 100(14), 6361-6373.

Park, S., Bae, W., Chung, J., & Baek, S. (2007). Empirical model of the pH dependence of the maximum specific nitrification rate. Process Biochemistry, 42(12), 1671-1676.

Passos da Silva, D., Schofield, M. C., Parsek, M. R., & Tseng, B. S. (2017). An update on the sociomicrobiology of quorum sensing in gram-negative biofilm development. Pathogens (Basel, Switzerland), 6(4), 51.

Patel, A., Nakhla, G., & Zhu, J. (2005). Detachment of multi species biofilm in circulating fluidized bed bioreactor. Biotechnology and Bioengineering, 92(4), 427-437.

Pernites, R. B., Santos, C. M., Maldonado, M., Ponnapati, R. R., Rodrigues, D. F., & Advincula, R. C. (2012). Tunable protein and bacterial cell adsorption on colloidally templated superhydrophobic polythiophene films. Chemistry of Materials, 24(5), 870-880.

Qiu, Y., Zhou, X., Shi, H. (2008). An approach to study bio-kinetic parameters in wastewater biofilms. China environmental science, 28(8), 679-682.

Rittman, B. E. (1982). The effect of shear stress on biofilm loss rate. Biotechnology and Bioengineering, 24(2), 501-506.

Rittmann, B. E., Rittmann, B. E., McCarty, P. L., & McCarty, P. L. (1980). Model of steady-state-biofilm kinetics. Biotechnology and Bioengineering, 22(11), 2343-2357.

Romaní i Cornet, Anna M, Guasch, H., & Balaguer, M. D. (2016). Aquatic biofilms: Ecology, water quality and wastewater treatment. Norfolk, UK: Caister Academic Press.

Rutgers, M. (1990). Control and thermodynamics of microbial growth. Ph.D. dissertation. University of Amsterdam. The Netherlands.

Saeidi, N., & Lotfollahi, M. N. (2016). Effects of powder activated carbon particle size on activated carbon monolith's properties. Materials and Manufacturing Processes, 31(12), 1634-1638.

Saucedo-Terán, R. A., Ramírez-Baca, N., Manzanares-Papayanopoulos, L., Bautista-Margulis, R., & Nevárez-Moorillón, G. V. (2004). Biofilm growth and bed fluidization in a fluidized bed reactor packed with support materials of low density. Engineering in Life Sciences, 4(2), 160-164.

Schügerl, K. (1997). Three-phase-biofluidization—Application of three-phase fluidization in the biotechnology—A review. Chemical Engineering Science, 52(21-22), 3661-3668.

Siegrist, H., & Gujer, W. (1987). Demonstration of mass transfer and pH effects in a nitrifying biofilm. Water Research, 21(12), 1481-1487.

Singh, A. V., Vyas, V., Patil, R., Sharma, V., Scopelliti, P. E., Bongiorno, G., . . . Milani, P. (2011). Quantitative characterization of the influence of the nanoscale morphology of nanostructured surfaces on bacterial adhesion and biofilm formation. PloS One, 6(9), e25029.

Stewart, P. S. (2002). Mechanisms of antibiotic resistance in bacterial biofilms. International Journal of Medical Microbiology, 292(2), 107-113.

Stoodley, P., Sauer, K., Davies, D. G., & Costerton, J. W. (2002). biofilms as complex differentiated communities. Annual Reviews in Microbiology, 56(1), 187-209.

Sokół, W., & Korpal, W. (2006). Aerobic treatment of wastewaters in the inverse fluidised bed biofilm reactor. Chemical Engineering Journal, 118(3), 199-205.

Sokół, W., Ambaw, A., & Woldeyes, B. (2009). Biological wastewater treatment in the inverse fluidised bed reactor. Chemical Engineering Journal, 150(1), 63-68.

Soni, K. A., Balasubramanian, A. K., Beskok, A., & Pillai, S. D. (2008). Zeta potential of selected bacteria in drinking water when dead, starved, or exposed to minimal and rich culture media. Current Microbiology, 56(1), 93-97.

Tavares, C. R. G., Sant'anna, G. L., & Capdeville, B. (1995). The effect of air superficial velocity on biofilm accumulation in a three-phase fluidized-bed reactor. Water Research, 29(10), 2293-2298.

Tavares, C. R. G., Sant'anna, G. L., & Capdeville, B. (1995). The effect of air superficial velocity on biofilm accumulation in a three-phase fluidized-bed reactor. Water Research, 29(10), 2293-2298.

Tchobanoglous, G., Stensel, H. D., Tsuchihashi, R., Burton, F. L., Abu-Orf, M., Bowden, G., . . . Metcalf & Eddy. (2014). Wastewater engineering: Treatment and resource recovery (Fifth ed.). New York, NY: McGraw-Hill Education.

Telgmann, U., Horn, H., & Morgenroth, E. (2004). Influence of growth history on sloughing and erosion from biofilms. Water Research, 38(17), 3671-3684.

Terada, A., Okuyama, K., Nishikawa, M., Tsuneda, S., & Hosomi, M. (2012). The effect of surface charge property on escherichia coli initial adhesion and subsequent biofilm formation. Biotechnology and Bioengineering, 109(7), 1745-1754.

Tijhuis, L., van Loosdrecht, M. C., & Heijnen, J. J. (1994). Formation and growth of heterotrophic aerobic biofilms on small suspended particles in airlift

Trinet, F., Heim, R., Amar, D., Chang, H. T., & Rittmann, B. (1991). Study of biofilm and fluidization of bioparticles in a three-phase liquid-fluidized-bed reactor. In Water Science and Technology (7-9 ed., Vol. 23, pp. 1347-1354)

Thomas, W. E., Nilsson, L. M., Forero, M., Sokurenko, E. V., & Vogel, V. (2004). Shear-dependent 'stick-and-roll' adhesion of type 1 fimbriated escherichia coli. Molecular Microbiology, 53(5), 1545-1557.

Turan, M. (2000). Mechanisms of biofilm detachment in anaerobic fluidized bed reactors. Environmental Technology, 21(2), 177-183.

Underwood, G. J. C., Perkins, R. G., Consalvey, M. C., A. R. M. Hanlon, Oxborough, K., Baker, N. R., & Paterson, D. M. (2005). Patterns in microphytobenthic primary productivity: Species-specific variation in migratory rhythms and photosynthetic efficiency in mixed-species biofilms. Limnology and Oceanography, 50(3), 755-767.

Verduyn, C., Stouthamer, A. H., Scheffers, W. A., & Van Dijken, J. P. (1991). A theoretical evaluation of growth yields of yeasts. Antonie Van Leeuwenhoek, 59.1991, Nr. 1, 59(1), 49-63.

von Stockar, U., & Liu, J. -. (1999). Does microbial life always feed on negative entropy? thermodynamic analysis of microbial growth Elsevier B.V.

Wang, H., Kim, M., Li, K., Shao, Y., Zhu, J., & Nakhla, G. (2019). Effective partial nitrification of ammonia in a fluidized bed bioreactor. Environmental Technology, 40(1), 94-101.

Wiesmann U. (1994) Biological nitrogen removal from wastewater. In: Biotechnics/Wastewater. Advances in Biochemical Engineering/Biotechnology, vol 51. Springer, Berlin, Heidelberg.

Wingender, J., and Flemming, H. C. (2011). Biofilms in drinking water and their role as reservoir for pathogens. Int. J. Hyg. Environ. Health. 214,417–423

Woodhead, A. L., de Souza, M. L., & Church, J. S. (2017). An investigation into the surface heterogeneity of nitric acid oxidized carbon fiber. Applied Surface Science, 401, 79-88.

Wright, P. C., & Raper, J. A. (1996). A review of some parameters involved in fluidized bed bioreactors. Chemical Engineering & Technology, 19(1), 50-64.

Xiao, J., & VanBriesen, J. M. (2008). Expanded thermodynamic true yield prediction model: Adjustments and limitations. Biodegradation, 19(1), 99-127.

Xiong, F., Zhao, X., Liao, Y., Wen, D., & Li, Q. (2018). Effects of surface properties on biofilm formation and the related applications. Microbiology China, 45(1): 155−165.

Xu, S., & Jiang, Q. (2018). Surface modification of carbon fiber support by ferrous oxalate for biofilm wastewater treatment system. Journal of Cleaner Production, 194, 416-424.

Yin, H., He, L., Lu, J., Gao, H., & Gao, D. (2014). Effect of hydraulic retention time on nitrogen and phosphorus removal by biofilm and granular coupling process. CIESC journal, 65(6): 2294.

Yu, G., Gao, C., Jia, C., & Chen, L. (2008). Fractal characteristics of density distribution in heterogeneous biofilms. Journal of Xinyang Normal University: Natural Science Edition, 21(1), 61-63.

Yu, Z., Wang, D., & Zhang, X. (2004). The reviewing and expectation of the development on urban sewage dispose technique. Journal of Guangxi normal university, 22(2).

Yusof, N., Ismail, A. F., Rana, D., & Matsuura, T. (2012). Effects of the activation temperature on the polyacrylonitrile/acrylamide-based activated carbon fibers. Materials Letters, 82, 16-18.

Zhang, T. C., & Bishop, P. L. (1994). Density, porosity, and pore structure of biofilms. Water Research, 28(11), 2267-2277.

Zhang, T. C., & Bishop, P. L. (1994). Structure,Activity and Composition of Biofilms. Water Sci Technol, 29 (7): 335-344.

Zhang, T. C., & Bishop, P. L. (1994). Experimental determination of the dissolved oxygen boundary layer and mass transfer resistance near the fluid-biofilm interface. Water Science and Technology, 30(11), 47-58.

Zhang, W., Tang, B., & Bin, L. (2017). Research progress in biofilm-membrane bioreactor: A critical review. Industrial & Engineering Chemistry Research, 56(24), 6900-6909.

Zhou, L., Li, H., Li, T., & Xing, L. (2011). Research progress on mass transfer in biofilm for wastewater treatment. Acta Scientiae Circumstantiae, 31(8), 1580-1586.

Zhou, P., He, H., & Qian, Y. (1998). Biofilm formation in internal loop biofluidised bed. ACTA SCIENTIAE CIRCUMSTANTIAE, 18(1).

Zhou, P., He, J., & Qian, Y. (2003). Biofilm airlift suspension reactor treatment of domestic wastewater. Water, Air, and Soil Pollution, 144(1), 81-100.

Zhou, X., Shi, H., & He, M. (2007). Measurement of the effective diffusion coefficient of dissolved oxygen by microelectrodes. Chinese Journal of Environmental Science, 28(3), 598- 602.

Zhu, J., Karamanev, D. G., Bassi, A. S., & Zheng, Y. (2000). (gas-)liquid-solid circulating fluidized beds and their potential applications to bioreactor engineering. The Canadian Journal of Chemical Engineering, 78(1), 82-94.

Appendices

Appendix A: Analyzing procedures

DO and pH

DO is measured by an installed Thermo Orion (810 A+) meter for every column.

pH is measured by pH-11 series pH/(mV°C) meter (Oakton, Singapore) and checked again when measuring alkalinity.

Alkalinity

1. Take 10 mL sample in a titration flask

2. Titrate against 0.02 N H_2SO_4 using pH meter to an end pH of 4.5.

3. Note the volume of 0.02 N H_2SO_4 used.

$$\text{alkalinity (mg}/L \text{ as CaCO}_3) = \frac{volume\ of\ H_2SO_4\ used\ (ml) \times 0.02 \times 1000 \times 50}{volume\ of\ sample} \qquad \text{(A)}$$

TCOD

1. Take 1mL of sample and 1mL of distilled water (2 mL total and dilution factor 1:1) and add them to COD vials and do the same for Blank and Standard. Based on sample concentration, dilution factor could be changed.

2. Digest it for 2 hours at 150°C in the COD digester and cool it to room temperature.

3. Perform similar procedure for blank by taking 2 mL of distilled water.

4. Measure the COD on Hach spectrophotometer (HACH Odyssey DR/2800).

$$\text{TCOD (mg/}L) = \text{reading (mg/}L) \times dilution\ factor \times \frac{standard\ (100\ mg/L)}{standard\ measurement} \quad \text{(B)}$$

SCOD

1. Filter the sample with 0.45μm filter papers.

2. Take 2 mL of sample and add it in a COD vial. Based on sample concentration, decide appropriate dilution factor. Do the same for Blank and Standard.

3. Digest it for 2 hours at 150°C cool it to room temperature.

4. Measure the COD on Hach spectrophotometer (HACH Odyssey DR/2800).

$$\text{SCOD (mg/}L) = \text{reading (mg/}L) \times dilution\ factor \times \frac{standard\ (100\ mg/L)}{standard\ measurement} \quad \text{(C)}$$

NH$_4$ -N (HACH method No. HR 342N, 0.4-50 mg/L NH$_4$ -N)

1. Add 0.1 mL filtered sample to HACH reagent vial (for NH$_4$ -N)

2. Add 0.1 mL distilled water to a HACH reagent vial (for NH$_4$ -N). This is blank.

3. Add one powder pillow of ammonium salicylate and ammonium cyanurate to each vial.

4. Cap the vials and mix thoroughly.

5. After 20 minutes set the instrument at zero with blank. And take reading of sample.

$$\text{NH}_4^+ - \text{N (mg/}L) = \text{reading (mg/}L) \times \frac{standard\ (100\ mg/L)}{standard\ measurement} \quad \text{(D)}$$

NO$_3$ -N (HACH method No. HR 344N, 0.2-30 mg/L NO$_3$ -N)

1. Add 1 mL filtered sample to a HACH reagent vial (for NO_3-N) and mix. This is

Blank.

2. Add 1 mL filtered sample followed by reagent powder pillow for NO_3-N to a HACH reagent vial. This is sample.

3. Cap the vials and mix thoroughly.

4. After 5 minutes set the instrument at zero with blank. Take reading of sample.

$$NO_3^- - N \ (mg/L) = reading \ (mg/L) \times \frac{standard \ (100 \ mg/L)}{standard \ measurement} \qquad (E)$$

VSS

1. Put a 1.2 μm filter paper in evaporating (aluminum) dish. Keep it in muffle furnace at 550°C for 15 minutes and weigh it after cooling to room temperature.

2. Stir the sample with magnetic stirrer and pipette out 10mL volume through the filtration assembly (using the weighed 1.2 μm filter paper) with applied vacuum.

3. Continue suction for about 3 minutes after filtration is complete.

4. Transfer the filter paper with TSS to the aluminum dish and evaporated to dryness in a drying oven at 103 to 105°C for 30 minutes.

5. Cool in a desiccator to room temperature, and weigh (w_1).

6. Keep the evaporating dish containing the filter paper with dried TSS in a muffle furnace and ignite the contents at 550°C for 15-20 mins.

7. Remove the dish from the furnace, cool it to room temperature in a desiccator and take its weight (w_2).

8. Calculate the VSS as follows:

$$\text{VSS (mg}/L) = \frac{w_1 - w_2}{10} \tag{F}$$

Effluent VSS

1. Take 20 ml sample from effluent pipes.

2. Follow VSS measurement procedures above to determine effluent VSS.

Suspended VSS

1. Take 10 ml sample form top, mid and bottom of each column, and mix them completely.

2. Follow VSS measurement procedures above to determine suspended VSS.

Attached VSS

1. Collect approximately 4 ~ 5 g of the support media samples with attached biomass.

2. Suspended in a 50 mL vial.

3. Sonicate with Aqua sonic sonicator (Model 75HT, ETL Laboratory Testing, Inc., NewYork) for 3 ~ 4 h at 30°C to detach the attached biomass from the support media.

4. After sonification, determine the volatile suspended solids (VSS) content of the detached biomass.

5. Collect sonicated particles and dry at 104°C for 1h and take weight of particle.

Appendix B: Original data

Startup tests

Days	4	7	11	14	18	21	25
Influent COD (mg/L)	302	304	300	296	304	304	300
HRT 12h/PE							
Effluent COD (mg/L)	112	56	42	34	46	42	38
Attached VSS (mg VSS/g media)	0.1	0.1	0.2	0.2	0.3	0.4	0.5
Suspended VSS (mg/L)	980	560	625	725	815	805	820
HRT 12h/PP							
Effluent COD (mg/L)	126	48	34	42	28	34	32
Attached VSS (mg VSS/g media)	0.1	0.1	0.1	0.1	0.1	0.1	0.2
Suspended VSS (mg/L)	845	615	705	785	805	815	855
HRT 12h/PEC							
Effluent COD (mg/L)	124	62	38	42	46	40	32
Attached VSS (mg VSS/g media)	0.2	0.2	0.2	0.3	0.3	0.3	0.4
Suspended VSS (mg/L)	1120	640	755	780	805	825	820

(a)

Days	4	7	11	14	18	21	25
Influent COD (mg/L)	304	300	304	296	300	302	302
HRT 8h/PE							
Effluent COD (mg/L)	122	76	54	48	50	42	42
Attached VSS (mg VSS/g media)	0.1	0.2	0.4	0.4	0.6	0.8	0.9
Suspended VSS (mg/L)	635	830	1030	1170	1360	1290	1320
HRT 8h/PP							
Effluent COD (mg/L)	144	82	68	52	62	60	54
Attached VSS (mg VSS/g media)	0.1	0.1	0.1	0.1	0.2	0.2	0.2
Suspended VSS (mg/L)	530	870	1255	1360	1510	1450	1545
HRT 8h/PEC							
Effluent COD (mg/L)	162	78	68	56	46	52	48
Attached VSS (mg VSS/g media)	0.2	0.2	0.3	0.5	0.6	0.7	0.8
Suspended VSS (mg/L)	650	795	980	1080	1285	1240	1185

(b)

Days	4	7	11	14	18	21	25
Influent COD (mg/L)	302	300	304	302	302	302	298
HRT 4h/PE							
Effluent COD (mg/L)	156	118	56	48	40	46	52
Attached VSS (mg VSS/g media)	0.1	0.4	1.2	2.7	3.8	5.2	6.9
Suspended VSS (mg/L)	290	380	485	500	515	495	510
HRT 4h/PP							
Effluent COD (mg/L)	146	102	88	56	44	48	38
Attached VSS (mg VSS/g media)	0.1	0.1	0.1	0.2	0.2	0.3	0.4
Suspended VSS (mg/L)	250	310	610	1185	1680	1945	1895
HRT 4h/PEC							
Effluent COD (mg/L)	162	110	62	48	50	42	46
Attached VSS (mg VSS/g media)	0.2	0.5	0.8	1.3	1.6	2.1	3.2
Suspended VSS (mg/L)	280	390	520	615	675	720	765

(c)

Days	4	7	11	14	18	21	25
Influent COD (mg/L)	156	154	154	150	150	148	150

HRT 4h/PE							
Effluent COD (mg/L)	56	48	34	38	40	32	38
Attached VSS (mg VSS/g media)	0.2	0.3	0.5	0.6	0.8	0.9	1.1
Suspended VSS (mg/L)	330	380	540	665	740	825	905

(d)

Steady state

Days	7	14	21	28
Influent NO3 (mg/L)	0	0	0	0
Influent NH4 (mg/L)	30.7	30.1	30.1	30.2
Influent COD (mg/L)	300	302	302	298
Influent ALK (mg/L)	308	312	305	310
HRT 9.2h/PE				
Effluent NO3 (mg/L)	22.1	21.6	21.3	21.4
Effluent NH4 (mg/L)	1.9	1.5	1.8	2.2
Effluent ALK (mg/L)	156	145	148	145
Effluent SCOD (mg/L)	28	34	34	30
Effluent TCOD (mg/L)	48	58	54	50
Attached VSS (mg VSS/g media)	5.2	4.7	4.4	4.8
Effluent VSS (mg/L)	20	26	22	20
HRT 9.2h/PP				
Effluent NO3 (mg/L)	14.6	13.8	13.9	13.7
Effluent NH4 (mg/L)	9	8.7	8.4	9.2
Effluent ALK (mg/L)	210	200	201	204
Effluent SCOD (mg/L)	26	30	28	26
Effluent TCOD (mg/L)	70	80	76	76
Attached VSS (mg VSS/g media)	0.5	0.4	0.5	0.5
Effluent VSS (mg/L)	36	42	42	40
HRT 9.2h/PEC				
Effluent NO3 (mg/L)	23.7	23.2	22.8	22.9
Effluent NH4 (mg/L)	0.9	0.7	1.3	0.7
Effluent ALK (mg/L)	130	133	137	136
Effluent SCOD (mg/L)	36	40	38	40
Effluent TCOD (mg/L)	60	66	64	58
Attached VSS (mg VSS/g media)	6.9	6.4	6.6	6.5
Effluent VSS (mg/L)	22	28	26	28

(a)

Days	7	14	21	28
Influent NO3 (mg/L)	0	0	0	0
Influent NH4 (mg/L)	30.6	30.3	30.2	30.3
Influent COD (mg/L)	294	298	302	300
Influent ALK (mg/L)	309	303	312	308
HRT 6.1h/PE				
Effluent NO3 (mg/L)	12	12.8	13.4	12.3
Effluent NH4 (mg/L)	10.7	11.2	10.5	11.6
Effluent ALK (mg/L)	220	208	204	208
Effluent SCOD (mg/L)	42	38	38	36
Effluent TCOD (mg/L)	78	82	84	80
Attached VSS (mg VSS/g media)	6.1	6.4	6.7	6.5

Effluent VSS (mg/L)	32	38	42	40
HRT 6.1h/PP				
Effluent NO3 (mg/L)	0.8	0.7	0.9	0.6
Effluent NH4 (mg/L)	20.4	20.5	20.9	20.7
Effluent ALK (mg/L)	296	295	292	296
Effluent SCOD (mg/L)	36	34	32	34
Effluent TCOD (mg/L)	104	112	108	116
Attached VSS (mg VSS/g media)	0.4	0.7	0.6	0.5
Effluent VSS (mg/L)	62	66	64	68
HRT 6.1h/PEC				
Effluent NO3 (mg/L)	14.8	14.3	15.3	15.7
Effluent NH4 (mg/L)	7.6	8.3	9	8.7
Effluent ALK (mg/L)	194	198	190	185
Effluent SCOD (mg/L)	46	44	40	42
Effluent TCOD (mg/L)	74	78	68	76
Attached VSS (mg VSS/g media)	7.6	8.1	8.5	8.4
Effluent VSS (mg/L)	32	36	34	38

(b)

Days	7	14	21	28
Influent NO3 (mg/L)	0	0	0	0
Influent NH4 (mg/L)	30.2	30.7	30.8	30.6
Influent COD (mg/L)	300	302	302	306
Influent ALK (mg/L)	302	301	305	311
HRT 4.1h/PE				
Effluent NO3 (mg/L)	1.8	2.5	2.7	3
Effluent NH4 (mg/L)	20.5	18.3	19.7	19.5
Effluent ALK (mg/L)	287	282	280	278
Effluent SCOD (mg/L)	40	44	42	42
Effluent TCOD (mg/L)	102	106	108	112
Attached VSS (mg VSS/g media)	8.9	9.8	9.4	9.5
Effluent VSS (mg/L)	44	52	48	50
HRT 4.1h/PEC				
Effluent NO3 (mg/L)	8.8	9.3	9.5	9.1
Effluent NH4 (mg/L)	12.4	13.7	13.3	13.1
Effluent ALK (mg/L)	237	234	232	230
Effluent SCOD (mg/L)	46	50	52	48
Effluent TCOD (mg/L)	94	108	98	102
Attached VSS (mg VSS/g media)	9.8	10.6	10.9	11.3
Effluent VSS (mg/L)	36	46	40	42

(c)

Days	7	14	21	28
Influent NO3 (mg/L)	0	0	0	0
Influent NH4 (mg/L)	30.2	30.6	30.5	30.7
Influent COD (mg/L)	148	146	146	150
Influent ALK (mg/L)	306	306	302	303
HRT 4.1h/PE				
Effluent NO3 (mg/L)	11.1	12.2	11.9	11.5
Effluent NH4 (mg/L)	14.8	13.9	14.1	14.4
Effluent ALK (mg/L)	220	213	215	218
Effluent SCOD (mg/L)	18	14	18	20
Effluent TCOD (mg/L)	50	46	44	46

Attached VSS (mg VSS/g media)	6.3	5.6	5.8	6.5
Effluent VSS (mg/L)	22	20	18	20
HRT 4.1h/PEC				
Effluent NO3 (mg/L)	23.3	23.7	24.1	23.8
Effluent NH4 (mg/L)	3.1	2.3	1.8	2.6
Effluent ALK (mg/L)	134	131	128	130
Effluent SCOD (mg/L)	26	24	26	28
Effluent TCOD (mg/L)	42	44	42	46
Attached VSS (mg VSS/g media)	7.6	7.0	7.3	7.7
Effluent VSS (mg/L)	10	14	12	12

Appendix C: T-test for PE and PEC

There are three hypothesizes to be tested in following. Those hypothesizes will estimate the difference between PE and PEC on COD removal efficiency, ammonia removal efficiency and attached biomass.

(a)

H_0: there is no difference between PE and PEC on COD removal.
H_A: there is obvious difference between PE and PEC on COD removal.

HRT 9.2h	Removal efficiency			
PE	0.91	0.89	0.89	0.90
PEC	0.88	0.87	0.87	0.87
P	$0.0106 < 0.05$			
HRT 6.1h	Removal efficiency			
PE	0.86	0.87	0.87	0.88
PEC	0.85	0.85	0.87	0.86
P	$0.0468 < 0.05$			
HRT 4.1h (high COD)	Removal efficiency			
PE	0.87	0.85	0.86	0.86
PEC	0.85	0.83	0.83	0.84
P	$0.0057 < 0.05$			
HRT 4.1h (low COD)	Removal efficiency			
PE	0.88	0.91	0.88	0.87
PEC	0.83	0.84	0.83	0.81
P	$0.0022 < 0.05$			

Because all P values are smaller than 0.05, H_A is valid.

(b)
H$_0$: there is no difference between PE and PEC on ammonia removal.
H$_A$: there is obvious difference between PE and PEC on ammonia removal.

HRT 9.2h	Removal efficiency			
PE	0.94	0.95	0.94	0.93
PEC	0.97	0.98	0.96	0.98
P	0.0034＜0.05			
HRT 6.1h	Removal efficiency			
PE	0.65	0.63	0.65	0.62
PEC	0.75	0.73	0.70	0.71
P	0.0009＜0.05			
HRT 4.1h (high COD)	Removal efficiency			
PE	0.32	0.40	0.36	0.36
PEC	0.59	0.55	0.57	0.57
P	0.0003＜0.05			
HRT 4.1h (low COD)	Removal efficiency			
PE	0.51	0.55	0.54	0.53
PEC	0.90	0.92	0.94	0.92
P	0.0000＜0.05			

Because all P values are smaller than 0.05, H$_A$ is valid.

(c)
H$_0$: there is no difference between PE and PEC on attached VSS.
H$_A$: there is obvious difference between PE and PEC on attached VSS.

HRT 9.2h	Removal efficiency			
PE	5.2	4.7	4.4	4.8
PEC	6.9	6.4	6.6	6.5
P	0.0002＜0.05			
HRT 6.1h	Removal efficiency			
PE	6.1	6.4	6.7	6.5
PEC	7.6	8.1	8.5	8.4
P	0.0008＜0.05			
HRT 4.1h (high COD)	Removal efficiency			
PE	8.9	9.8	9.4	9.5
PEC	9.8	10.6	10.9	11.3
P	0.0203＜0.05			
HRT 4.1h (low COD)	Removal efficiency			
PE	6.3	5.6	5.8	6.5
PEC	7.8	6.8	7.1	7.9
P	0.0083＜0.05			

Because all P values are smaller than 0.05, H$_A$ is valid.

Curriculum Vitae

Name: Haoran Xu

Post-secondary   Dalian University of Technology
Education and   Dalian, Liaoning, China
Degrees: 2012-2016 B.A.

                         The University of Western Ontario
                         London, Ontario, Canada
                         2017-2018 M.A.

Work experience Dalian Entry-Exit Inspection and Quarantine Bureau Technology
(internship):   Center
                    Dalian, Liaoning, China
                    2014-2016

                    Dalian Dongda Group Lvshun Sewage Plant
                    Lvshun, Liaoning, China
                    2014-2016

                    Dalian Power Generation Co., Ltd
                    Dalian, Liaoning, China
                    2014-2016